Analysis of Selective Laser Sintering Print Parameter Modelling Methodologies for Energy Input Minimisation

A thesis presented in partial fulfilment of the requirements for the degree of

Master of Engineering

in

Mechatronics

at Massey University, Albany,

New Zealand.

by

Cameron D. H. Mearns

2017

The author declares that this is his own work, except where due acknowledgement has been given. The thesis is submitted in fulfilment of the requirements of a Masters in Engineering at Massey University, New Zealand.

Cameron Mearns

Abstract

Additive Manufacturing (AM) is the name given to a series of processes used to create solids, layer upon layer, from 3 Dimensional (3D) models. As AM experiences rapid growth there exists an opportunity for Selective Laser Sintering (SLS) to expand into markets it has not previously accommodated. One of the ways SLS can accomplish this is by expanding the range of materials that can be processed into useful products, as currently only a small number of materials are available when compared to other AM technologies. One of the biggest barriers to the adoption of materials is the danger inherent to high-energy processes such as SLS. The aim of this research was to identify opportunities to improve current methods for modelling the relationship between material specifications, and printing parameters. This was achieved by identifying existing models used to determine printing parameters for a new material, identifying weaknesses in current modelling processes, conducting experimentation to explore the validity of these weaknesses, and exploring opportunities to improve the model to address these weaknesses. The current models to determine printer parameters to achieve successful sintering include both the Sintering Window (SW) and the Energy Melt Ratio (EMR). These two models are complementary, and both are required to establish all common print parameters. They include both thermal and physical powder properties, but do not include any optical properties. This is significant because the nature of the SLS printing process relies on concentrated delivery of laser energy to achieve successful sintering. Analysis of two similar polyamide powders, one black and one white, identified that the two powders were similar thermally and physically, which meant the models predicted that they should both sinter successfully utilizing the same set of print parameters. Results of the experimental trials showed that no trials involving the white powder sintered successfully, and trials involving the black powder suffered from issues with either insufficient energy to successfully remove parts without damage, or excessive energy causing excess powder to bond to the part. Further experimentation was carried out to investigate the differences in optical properties using Fourier Transform Infrared Spectroscopy (FTIR) and Spectrofluorophotometry. FTIR revealed that there was a difference in absorption as a material property, indicating that differences in laser energy absorption could explain the results seen in the trials. Spectrofluorophotometry revealed minimal differences in fluorescence of the powders, suggesting it an unlikely source of energy loss. Future work is recommended to research a standardised form of testing setup that can be used to categorize the reflectance of a material, as current work relies on proprietary experimental setups. Finding methods of classifying the laser absorption that is easily available to operators would enable refinement of the EMR equation to reflect the energy losses during printing, and remove another barrier for adoption of new materials.

Acknowledgements

As with all projects of this scale, I owe thanks to the many people who ensured that I was able to take advantage of the opportunities offered to me. Without them I would never had achieved as much as I have.

To the endless experience and patience of my mother, who went above and beyond to support me, and who pushed me to succeed. To my father, to whom I owe my persistence and confidence. To my darling Emma, for her love and encouragement despite the late nights, the weekends, and my eternally messy desk. To my sisters, for their perspective and humour after long days.

I would also like to offer my deepest gratitude to A/Prof Johan Potgieter, for his guidance and enthusiasm over many years now. Thank you to Dr. Steven Dirven for his attention to detail, and his drive for excellence. In addition to this, I must recognise all the staff and students at Massey University's School of Engineering and Advanced Technology for helping to create such a supportive environment to study in.

A special thanks to both Dr. Marie Joo Le Guen and Scion for contributing their invaluable expertise and support to this project.

Thank you to the Ministry of Business, Innovation and Enterprise for their assistance in funding this project through the Extrusion Plus program.

Thank you to Dr. John Harrison, for humouring my strange questions, and unusual requests.

Thank you to my friends, for keeping me from becoming a recluse, and ensuring my problems never felt like mine to bear alone.

To the staff and cadets of No. 6 (North Shore) Squadron Air Training Corps, for providing me with ample motivation to go outside.

Table of Contents

List of Figures

List of Tables

List of Publications

Mearns, C., Potgieter, J., Dirven, S. and Joo Le Guen, M. (2017). Experimental analysis of the effectiveness of current modelling methods for SLS parameter determination. In: *Mechatronics and Machine Vision in Practice*. Auckland: 2017 24th International Conference on Mechatronics and Machine Vision in Practice (M2VIP).

List of Abbreviations

2D	Two Dimensional
3D	Three Dimensional
AM	Additive Manufacturing
ATR	Attenuated Total Reflectance
AU	Absorbance Units
DFMC	Designing for Mass Customisation
DoE	Design of Experiment
DSC	Differential Scanning Calorimetry
EMR	Energy Melt Ratio
FDM	Fused Deposition Modelling
FTIR	Fourier Transform Infrared Spectroscopy
ISO	International Organisation for Standardisation
MPS	Mean Particle Size
PR	Packing Ratio
PSD	Particle Size Distribution
SE	Secondary Electron
SEM	Scanning Electron Microscope
SLA	Stereolithography
SLM	Selective Laser Melting
SLS	Selective Laser Sintering
SM	Subtractive Manufacturing
SW	Sintering Window
TPU	Thermoplastic Polyurethane

Chapter 1 Introduction

1.1 Chapter Overview

The purpose of this chapter is to introduce the project and establish the goals of the research undertaken. After a brief project background to establish the project motivations and context, the aims, and objectives of the project are identified. The scope of the project, and the layout of this thesis are then explained.

1.2 Project Background

Additive Manufacturing (AM) is the name given to a series of processes used to create solids, layer upon layer, from 3 Dimensional (3D) models [5]. It is also known as Free Form Modelling, and 3D Printing [6]. Initially AM was developed to produce solids using polymers [7], however as new technologies and methods have been developed this has expanded to include metals [8] and ceramics [2, 9]. One such technology is Selective Laser Sintering (SLS), a process that involves the progressive processing of thin "slices" of powder into formed solids by means of a heated chamber, and a focused laser beam [10].

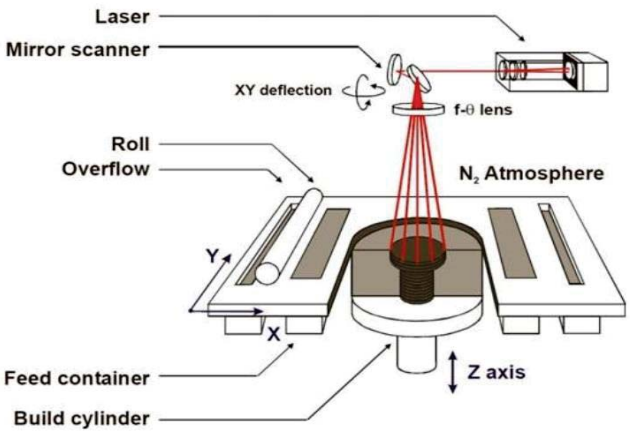

Figure 1.1: A typical SLS machine setup [1]

As AM processes, including SLS, increase in popularity one of the areas of growth identified is the diversification of printing materials [11]. Due to the elevated risk of combustion caused by the SLS machines, many operators are unwilling to test new powders unless it can be shown they can be processed safely by SLS. This means that the number of materials available is currently limited by the understanding of powder properties, and the ability to determine printing parameters from powder specifications [12]

1.3 Project Motivation

The thermal qualities of a material are particularly important for SLS printing. The elevated temperatures of the SLS process increase the risk of material combustion, which puts greater importance of the precise and controlled application on energy into the powder. This energy input can occur both in the form of convection, from the heated chamber of the printer, and in the form of radiation, from the laser. To be able to predict the energy required from the machine to successfully print a material it is important to understand the properties of the material, and how they correlate with printing parameters.

Current methods of determining print parameters utilize standardized laboratory tests to determine energy requirements of a material, but do not account for energy losses incurred during printing. This limits the ability of print parameter models to accurately predict the behaviour of materials during the printing process, which limits its usefulness in identifying parameters for new materials.

The aim of this research is to identify opportunities to improve current methods for modelling the relationship between material specifications, and printing parameters to account for losses occurred during printing.

1.4 Objectives

To achieve the stated aim of this research the following objectives are identified:

1. Identify the existing models used to determine printing parameters for a new material
2. Identify weaknesses in current modelling processes
3. Conduct experimentation to explore the validity of these weaknesses.
4. Explore opportunities to improve the print parameter models to address these weaknesses

1.5 Research Scope

This project focuses on the development of methods used in the selection of printing parameters for selective laser sintering. As such, research is limited to processes that use polymer powders, rather than other material families, such as metals, or ceramics. Discussion of the application of this research to the use of unknown materials is from an operator's perspective, someone who operates in a commercial context, as opposed to a more academic-based research-driven context.

While several sintering process parameters have effects on sintered parts, such as affecting warpage, or dimensional accuracy, this research focuses primarily on parameters which affect an operator's ability to safely process a material during sintering. Specifically, this means parameters which affect the maximum amount of energy present during the process of sintering, the point during a SLS printing process at which the risk of combustion is at its greatest.

This research will also focus solely on the process of determining printing parameters for a given material. This research will not cover pre-processing, post-processing of a material, or the use of additional additives to improve its suitability for printing by SLS process.

1.6 Thesis Layout

Chapter One of this research outlines the project motivations, processes, and objectives as detailed in the rest of this document. Chapter Two explores the state of AM, current technologies, and modelling processes specific to SLS. Opportunities for improvement of current models will be identified and discussed, and testing processes of powders to test the models will be identified.

To achieve the objectives of assessing the effectiveness of models used to determine printing parameters of new material, the models must first be demonstrated, and then tested experimentally. Chapter 3 focuses on the classification of powders using the models identified in Chapter 2 for the purposes of identifying print parameters. Chapter 4 contains an experimental trial for the purposes of evaluating the ability of the models to identify print parameters that lead to sintering successfully.

To meaningfully identify further opportunities for improvement the powders will then be assessed in further experimentation. In Chapter 5 new methods of classifying additional properties of the powders are explored, for the purposes of improving the ability of the models to predict print parameters.

Chapter 6 discusses the results of Chapters 3,4 and 5 with reference to both the aims and objectives of this study, and to existing literature. Chapter 7 explores the outcome of this dissertation, and whether objectives were achieved. In this chapter recommendations for further work are also made to advance the research conducted in this study.

1.7 Chapter Summary

With the project background, aim, objectives, scope, and thesis layout identified, the next step of research is to conduct a review of existing literature. Objectives 1 and 2 can be achieved during this process, which will occur during the literature review in Chapter 2. This will be conducted with the intent to assess the weakness identified in Objective 2 whilst completing Objective 3 in Chapter 3.

Chapter 2 Literature Review

2.1 Chapter Overview

Chapter 1 outlined the rationale and focus of the research project, which is to investigate methods for determining the relationship between material specifications, and printing parameters, to account for losses occurred during printing. In this chapter, the detailed literature review focuses on achieving objectives 1 and 2 set for this project.

This chapter begins by discussing Additive Manufacturing (AM) as a larger set of techniques, and identifying the specific processes involved in this research. Applications are discussed, as well as opportunities for development identified. Key properties of SLS polymer powders will be identified, including how those properties affect the parameters of the SLS printing process, and the current methods used to model the relationship between powder properties and print parameters. This then sets the context for the discussion of existing methods of modelling and optimizing processing parameters. Limitations to existing modelling methods are identified, with reference to previously mentioned properties. Potential solutions to these limitations are discussed, and experimental processes to confirm both the limitations and potential solutions are briefly explored. From the identification of these limitations a review of the effectiveness of current modelling methods will be discussed to ensure the validity of the identified limitations.

This review of testing processes will focus predominantly on the thermal characteristics of SLS composite powders and printing parameters relating to energy input, as these are most likely to cause unintended combustion or thermal damage to a machine. However, other characteristics of significance will be identified and discussed during the review, with references to where they have relevance for the subsequent design of testing methods.

2.2 Additive Manufacturing Processes

Processes for Additive Manufacturing (AM) has been around since the patent of Stereolithography (SLA) in 1986 [7]. Since that time, many new techniques and methods have been developed. These techniques will be discussed in greater detail in this chapter with comparison to one another. Each of these techniques has advantages and disadvantages when compared to each other, as well as traditional manufacturing techniques such as CNC machining, or injection moulding.

With the development of so many technologies there has been some ambiguity about the relationship between some of these technologies[13]. In response to this the ASTM International organisation published a document defining a number of these processes to lead industry standardisation of naming conventions [14]. This former ASTM document has since been withdrawn and superseded by a document produced in conjunction with the International Organisation for Standardisation (ISO) [5]. A number of these terms are repeated in the glossary of this document for clarity.

There are, however, commonalities that all AM processes share, such as a common architecture, seen in Figure 2.1, despite using different processes and materials [15]. Additive manufacturing processes produce a solid by depositing a layer of work material in a 2-Dimensional (2D) layer, or a "slice" [16]. The 2D layers are created by slicing the digital 3D model into the required number of layers for the part [6]. This slicing process mirrors the physical printing process, where these consecutive layers are then produced to manufacture the part. The number of layers can vary according to factors such as: the part; the orientation of the part; desired accuracy; the AM process used; and the file format [17]. In addition to the product itself, some machines may require additional removable support material to be able to produce the product [6, 18, 19].

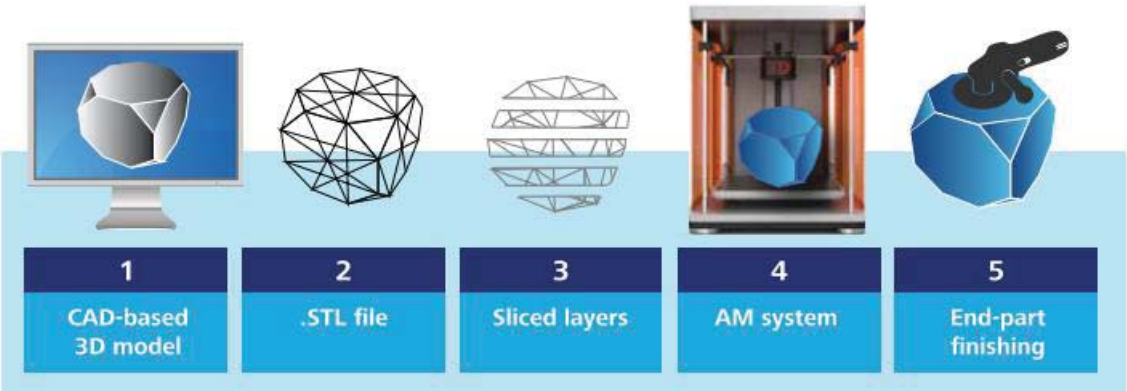

Figure 2.1: The process of AM from file to finished solid [20].

The forms of these printed materials have been expanded as well. From the original development using a vat photopolymerization processes [7] there has been significant expansion into material extrusion-based machines [2], as well as several powder bed fusion processes [19, 21]. These three technologies make up most AM machines in use today [22].

Techniques such as SLA utilise liquid-resin baths to solidify layers using ultra-violet light, to form a solid part in a bath one layer at a time [7], like in Figure 2.2 below. This uses a variety of materials, including biostructures and ceramics [23]. SLA is used in development applications where small, functional mechanisms with tight tolerances need to be tested [24]. However, the applications for SLA are limited by the mechanical properties of the materials. The printed products are often low-strength, and are best suited to prototyping, and non-structural uses [18].

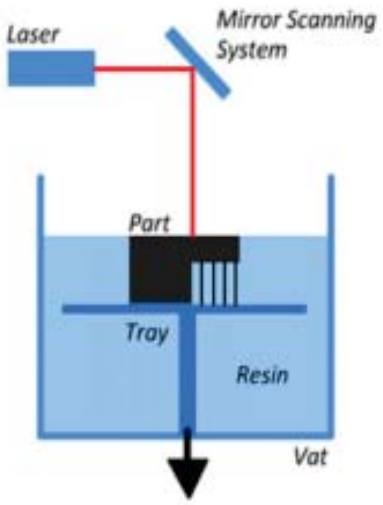

Figure 2.2: A stereolithographic system [2].

One of the most popular forms of AM is Fused-Deposition-Modelling (FDM). Initially, production of FDM machines was limited by the patenting of the pioneer machines. Since the expiry of the primary FDM patents, there has been a rise in the number of machines available [25], not just in the commercial market, but for hobbyists, and even for consumers in the home [19]. FDM machines use a heated extrusion nozzle to lay down a layer of molten filament in a 2D arrangement. There are a range of materials that can be used, most commonly in the form of filaments [16]. These filaments often contain thermoplastics, but there have been successful experiments with composites [26]. These composites enable the additional of material properties not feasible in historical polymer materials, such as ferromagnetism [27]

There are several printing techniques that fall under the powder bed fusion technology umbrella. These include Selective-Laser-Sintering (SLS), and Selective-Laser-Melting (SLM) [2]. These two technologies are similar as they use powder spread over the print bed, both to produce the layer, and to provide support to the material as it is printed [18, 28]. Another key similarity is the use of a laser to bond the powder in each layer together to form consecutive slices [2]. Key differences to these processes are the materials they use, the mechanisms they use to bond the powder particles, and the technologies they use to achieve these mechanisms. SLS processes generally produce thermoplastic-based products, whereas SLM processes typically produce metal-based products [16].

SLS and SLM use different mechanisms to print each slice due to the differences in behaviour of these two families of materials. SLS takes advantage of the glass transition phase of thermoplastics [21]. By heating the entire printing chamber up to only a few degrees below the glass transition temperature of the material, SLS machines use a laser to quickly heat the polymer into the glass-transition phase [6]. This is important, because it allows the machines to produce a slice where all sintered particles are fully bonded without taking the material into the melting phase. Fully melting particles would sacrifice accuracy by causing particles nearby to the melted material to bond unintentionally due to the relatively low energy required to melt thermoplastics at these elevated temperatures [1].

Unlike SLS, SLM parts are produced by taking powder particles into a fully molten state. However, the finished product is visually like one produced by SLS. The different layers of the product are uniformly bonded together, both within the layer, as well as between layers [21]. SLS and SLM products differ visually from processes such as FDM, where the layers are visually discernible since the melted material cools and begins to crystallize before the next layer is laid down [24].

2.3 Applications of Additive Manufacturing

As an augmentation of current capabilities, AM sees widespread use as a method of prototyping [10]. Production using AM is much faster for complex parts than Subtractive Manufacturing (SM) methods like drilling or milling. This is especially for designs with a lot of internal detail, which would increase the number of matching processes to produce [15]. The latter are sometimes still physically possible to produce with SM, especially with machines with a higher number of Degrees of Freedom such as a 5-Axis CNC machine. However, it would take many machining operations to achieve the same outcome as AM [16].

The ability for SLM machines to manufacture products with properties fit for use in functional high-stress environments has already been exploited in several ways. An example of this is high-performance parts, such as those made from titanium, which are in production using SLM machines [29]. As well as having a prohibitive cost associated with the material itself, Titanium is also incredibly hard, which increases the associated costs of machining and manufacture through SM methods. These parts often take advantage of the ability for AM to produce complex parts through design processes such as topology optimisation.

Topology Optimisation, seen in Figure 2.3, is the process of obtaining the best shape for a part without restrictions on the topology of the part [30]. It presents an opportunity for AM to produce parts that could not be feasibly mass manufactured using SM techniques. While these parts are still constrained in design by manufacturing considerations of AM, use of structures such as repeating lattice elements can be used to reduce requirements for support structures, reducing build times and post processing requirements [31]. Previous authors note the limitations of current software in both the modelling of forms for part optimisation [32] [33] as well as residual post-processing required of the design to ensure it fits AM limitations [31]. This process does show some potential for AM to add value to production process, by producing parts for the aviation industry that are lighter, with lower stresses, while retaining strength and stiffness [33].

Figure 2.3: An example of an engine nacelle hinge bracket before (top) and after (bottom) the part design was optimised using Topologic Optimisation [4].

Another advantage of AM over SM is the lower investment of material required to produce the product [15]. During prototyping, it is often important for parts to be produced and tested for dimensional clearance, as well as allowances for maintenance and assembly processes for a finished product. While these same parts could be produced by either AM or SM methods there is a lower cost associated with producing a part through AM methods [34], particularly when the part can be produced out of cheaper thermoplastics, such as Nylon [35]. Considering that these prototypes may end up being changed multiple times, often discarded and not reused, it can be beneficial to make the initial physical version using AM methods. Production methods can then switch to more traditional methods of manufacture later in the development cycle, once part dimensions and features have been finalized.

One aspect of AM that is undergoing increased attention in recent years it the ability for AM to integrate with the idea of Designing for Mass Customisation (DFMC). DFMC refers to the process of designing an end product so that it can be configured to better suit the individual end user [36]. Because AM does not require tooling for each variation of a part, it adds minimal cost when compared to traditional manufacturing methods, such injection moulding. This enables DFMC to become a much more attainable business model, with several industries already adopting it to enable products customized for their clients, such as orthotic inserts [37], hearing aids [38], dental and orthopaedic implants [39].

One of the disadvantages of the SLS printing process is that is has many parameters that can have significant impact on the ability to successfully process a part. The complexity of this process has been explored by in efforts to classify all parameters in the Laser Sintering Process Chain [40]. The SLS process has a spectrum of success, ranging at one end from a successful print, which produces a dimensionally accurate part, with physical properties at, or near, the optimal point for the powder used. At the other end of the spectrum is a failed printing attempt, which could be as significant as to lead to permanent damage to the machine, such as due to combustion [41]. In between these two ends there is the machine completing the printing process, but producing a part that is out of specification, either dimensionally or by its properties [28]. The last example given could be considered acceptable dependent on the circumstances, but as operators seek to maximize their rates of success these situations are still to be avoided.

The risks presented by this complexity are what make this understanding of properties, and their translation into print parameters, so critical. Minimising risk to operators requires a better understanding of the properties of the print materials, their performance during the printing process, and the managing of risk factors such as energy input with respect to requirements including part density or dimensional accuracy.

2.4 Powder Properties

Much of the research around understanding the printing process centres around classifying the effect of various parameters and characteristics on the powder itself. Numerous papers note that several properties each have important influence, rather than one sole property [1, 11, 12, 42-45]. Verbelen *et al.* (2016) discusses the importance of particle morphology and associated powder flow, melting and coalescence of powder particles into one another, and finally crystallization and solidification. They noted relationships between part quality markers, such as part porosity and density, with powder properties such as powder flow, and in turn powder bed density.

Whilst the topic has significant breadth, as visible in Figure 2.4, relevant properties related to the amount of energy required to sinter are discussed in greater detail below. These properties are of importance because they have direct impact on the amount of energy input required from the machine during the printing process, and thus have the greatest impact on the operator's ability to find an appropriate set of print parameters to successfully sinter unfamiliar powders.

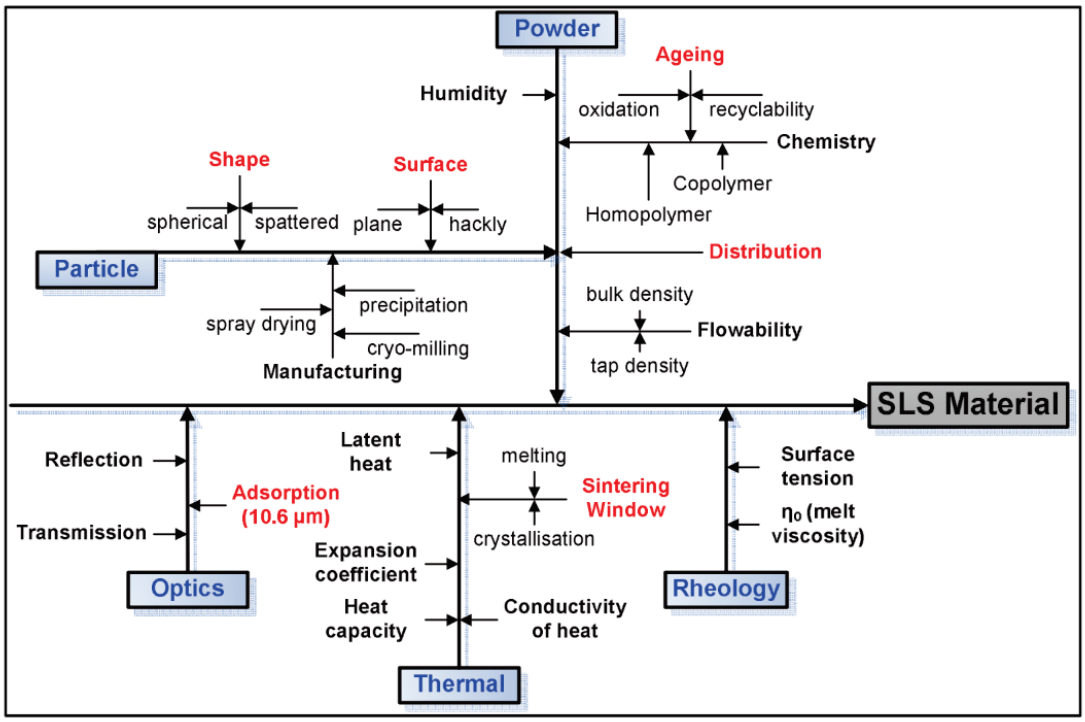

Figure 2.4: Powder property considerations for SLS powders [3].

2.4.1 Powder Spreading

In SLS printing there is an important relationship between flowability of powders and the quality of the resulting part. Powders that flow more easily are spread better during printing, which leads to parts with better density [46, 47]. Numerous attempts have been made at classifying how powder spreads [35, 46, 48-55], using different techniques. Krantz *et al.* (2009) identifies many standardized tests used across many disciplines, with good discussion about the importance of the results of each. However, as Schmid *et al.* (2013) and Ziegalmeier *et al.* (2013) note there is no specified method for expressing a powders' suitability for SLS printing. Van den Eynde *et al.* (2015) proposed a new method of classifying powder flow in a manner that more closely mimics many industry SLS machines than existing tests, however they do note that flow behaviours are subject to temperature and humidity variance.

Powder spreading has an effect on the amount of energy required for successful sintering as it has a direct impact on powder density [52], and thus the required energy density for sintering [12, 56]. Authors discussing laser energy density, such as Vasquez *et al.* (2013) utilize a combination of material and packing density for purposes of calculations. While these calculations do not represent the true mechanical behaviour of SLS powder spreading mechanisms they do offer the advantage of being comparatively easy to perform, requiring minimal specialist equipment unlike other methods which offer closer replication of the spreading process. In the context of an operator perspective this has significance as additional equipment required for characterisations represents a barrier, which could hinder adoption. Notably Schmid *et al.* (2013) found that simplified forms of density measurements, such as comparing bulk and tapped densities, were adequate for representing various SLS powders.

2.4.1.A **Particle size**

One of the key powder properties from a powder spreading perspective is the size of the polymer particles. Kruth *et al.* (2008) discusses the effect of particle size and morphology on the process ability of a powder. Typical Mean Particle Size (MPS) for successfully used plastics such as PA12 range from as low to 20µm to 100 µm[11, 12, 40]. Alongside MPS is Particle Size Distribution (PSD), both of which are obtainable using laser diffraction systems [11, 57], as well as image-processing software paired with conventional microscopes [12]. Given that SLS printers may have layer thicknesses as thin as 100µm particles that are too big will not be able to pack uniformly into a consolidated layer. Similarly, if PSD is too uniform, particles may not interlock leading to pore density, which can cause porosity and weakness in finished parts [58]. Alternatively, if the PSD is too great, an abundance of smaller particles can cause reductions in flowability due to greater proportional effect of van der Waals forces [55].

Particle size has also been demonstrated to have relevance in composite powder blends, particularly for non-polymer fillers. For example, depending on how a wood is processed may determine the size of saw dust particles [59]. Large differences in particle size between filler and matrix powders were not found to have made the powder blend unusable [60], provided polymer powders were able to flow around the larger particles, and fill in porous areas of the wood. However, when particles were more equally sized the more flow characteristics of the wood were noted to lead to degraded performance due to reduced particle interlocking [54].

2.4.1.B Particle Morphology

Another key factor of powder spreading is the morphology of the powder particles. Morphology importantly dictates both the friction particles experience as they move past one another, and their ability to interlock closely when spread into a thin layer. The morphology of the powders is observed using a Scanning Electron Microscope (SEM) [1, 10, 42, 46, 48, 61]. Spherical particles can be produced by co-extrusion processes, precipitation production processes result in powder particles with potato-like shapes, and cryogenic milling produces irregular, chip-like particles [11].

Spherical particles are better able to flow and form defect-free layers than potato-shaped particles, while cryogenic particles are less likely to flow successfully [11, 53]. It has been noted that material properties may on occasion have influence on powder flow, such as elastomers, like thermoplastic polyurethane (TPU) compressing under the force of the spreader blade [53].

These properties also have an effect when combining powders to form composites. Previous attempts at adding wood-based fillers have shown particles to be irregular and rough [49], or elongated and covered in burrs [54, 62] which are noted to flow poorly. Additives have been added in the past in order to try and compensate for these characteristics [49, 62]. These properties pose a severe problem in spreading powders, which can lead to porous parts, or even failed prints. Conversely, filled powder composites, such as Alumide, exhibit good flow characteristics consistent with other raw polymers with similar morphologies [44].

2.4.2 Temperature Considerations

Two final considerations of powder spreading are glass transition and crystallisation temperatures. During the sintering process the build chamber of the SLS machine is kept above the crystallisation temperature of the material in order to allow layers to coalesce properly, and allow layers to bond together while in the glass transition phase [56]. If the chamber temperature is too high the particles can begin to undergo glass transition, especially smaller particles. If this occurs the powder can begin to cake, at which point it becomes sticky and difficult to spread, as well as causing particles to melt unintentionally, which leads to a loss of detail [11]. If the chamber temperature is too low premature crystallisation can occur, which can cause distortion or curling [11].

By using a heated chamber, SLS machines keep sintered material above their crystallization temperature. This is beneficial for the bonding of consecutive layers of the printing process. By keeping material in the glass transition phase after each layer has been sintered, it allows the sintered material in the next layer to bond with the previous layer [6, 63]. This bonding between layers is important in the SLS process, as it gives it additional strength, as well as producing the continuous, uniform finish that is desirable with many applications [64].

This delicate balancing of glass transition between crystallisation and melting in SLS means it is critical that there is a uniform and accurate application of energy and mass in the process. Variables influencing this could be convection when heating the chamber and print beds [63], the accurate and controlled application of light energy from the laser assembly [64], as well as the uniform spreading of powdered material from the feed piston onto the print bed [46, 52]. If any one of these variables is not within a narrow margin, then the resulting product(s) may be of questionable strength or quality, if it successfully prints at all [43, 65, 66].

To achieve full coalescence, it is important to ensure that the polymer powder particles bond fully, both within and between layers. This bonding begins when polymer material reaches the Glass Transition (T_G) temperature, and they begin to soften, allowing necking between particles. Particles being formed into a slice do melt as they are sintered, but if large amounts of the material reach the melting temperature (T_M) at once it can lead to unintended bonding. This in turn can lead to a loss in dimensional accuracy and feature definition [28], as melting can occur in a far larger area than the focused spot of the laser.

2.4.3 Optical Properties

The ability for a powder to absorb laser energy is critical to its ability to be sintered. It must be able to transform the light energy to heat energy with a minimal of reflection, transmission, or re-emission of the light. Any energy reflected or re-emitted is simply lost back into the machine, but has the potential to cause damage to the machine if great enough. Laser energy transmitted by the powder has the potential to cause unintentional bonding with lower layers of powder [67].

Previous authors have used different methods to characterize these properties, including Fourier Transform Infrared Spectroscopy (FTIR) [44, 68, 69], and the use of integration spheres [67, 70]. FTIR enables the measurement of transmission of a light wavelength through the material, which can be used to find the complementing absorption. Machines are widely used in material testing laboratories, and also enable the use of identification of a material by its characteristic absorption bands [71]. This also enables any significant impurities in the material to be identified for quality control purposes. FTIR does not provide a truly representative method of measuring absorption for SLS printing, as the powder surface is not prepared in a manner that accurately represents the print bed surface during printing. This means that while FTIR provides a method of characterising material absorption characteristics, it does not provide an accurate means of quantifying the energy losses of the laser through reflection.

A more accurate method of characterising losses through reflection in the SLS process was demonstrated first using one [69, 70], and more recently two [67] integration spheres. Because these setups more accurately mimic the surface preparation of the powder bed in SLS printing they provide a more useful measure of quantifying the losses of laser energy through both reflection and transmission. The downside of this technique is that integration spheres are not a very common piece of laboratory equipment when compared to the likes of FTIR, and even then, the setup required is not common. This means that operators may struggle to find laboratories who will to conduct material classifications in this manner.

These difficulties have led to some studies being directed at finding other properties of the powder that affect the optical properties themselves. Seminal work on the topic found that absorption varies dependant on material and wavelength of the laser, and that powdered material is more absorbent than its bulk counterpart [70]. Subsequent work has found a relationship between the particle size and subsequent packing fraction and the absorption of the laser energy [69]. Laumer *et al.* (2016) noted that "the absorption behaviour of the basic polymer, and therefore the absorption behaviour of single particles in combination with occurring multiple reflections, determine the optical material characteristics of the powder in the case of similar particle geometries and size distributions." While this has been noted, the optical effects of common powder additives, such as graphite, dye, and agents used to improve powder flow properties has not been documented, despite their increasing usage in powder research, especially in composites [55, 72, 73].

2.5 Modelling Methods

For operators adopting new powders, initial testing is the greatest period of risk, as the initial behaviour of powders can be unpredictable. It is essential for them that they be able to determine print parameters for a new material, to reduce the chance of damaging the machine during printing through excess energy input, and to reduce the process of testing to determine operating parameters.

There are several methods used to characterise the optimal thermal conditions, which all have similarities. However, they each have weaknesses when compared to each other, which must be discussed within the context of this project. There have been recent attempts to use multiple thermal characterisations to better define the energy requirements of powders.

2.5.1 Sintering Window

The Sintering Window (SW) identifies the thermal boundaries for which sintering occurs in by Different Scanning Calorimetry (DSC) [11, 35, 74]. It defines a thermodynamic boundary set below the polymer's melting temperature, but above the crystallisation temperature (T_c), identified in Figure 2.5 below. By using the melting temperature as an upper boundary, the Sintering Window reduces the chance of unintended melting. Bonding can still occur in the Tg phase, which occurs before a material melts, so Sintering can still occur below TM.

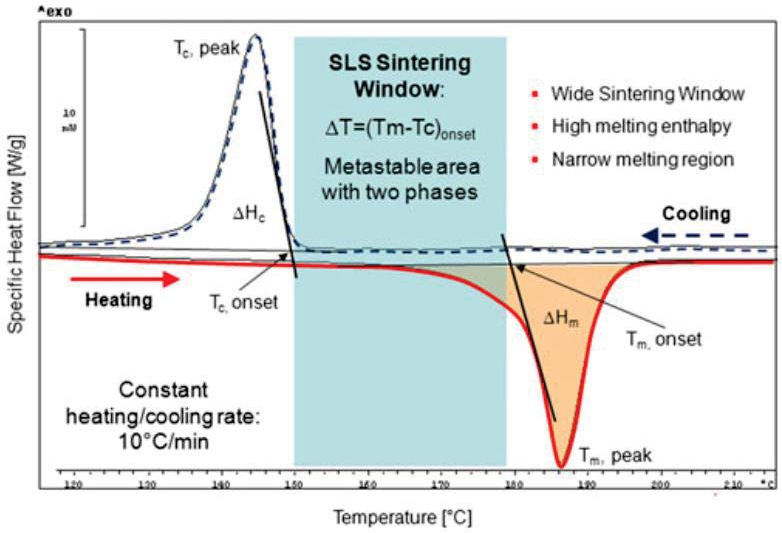

Figure 2.5: Sintering Window, overlaid on top of DSC Thermogram results [3].

Bounding the window on the lower side with the crystallisation temperature means that there should be adequate bonding between layers as the print progresses, as the sintered polymer does not have the opportunity to cool to a crystalline state before being introduced to the next layer.

The disadvantage of this approach is that it does not consider many factors, such as the energy requirements of the powder, or the layer thickness. This means that it does not allow accurate estimation of laser settings required to achieve successful sintering. Also, as the upper boundary is intentionally set before the TM the parts produced using the Sintering Windows as a process would be lower in strength that those produced with higher energy inputs to the powder [75]

The advantage of the Sintering Window is that it gives a succinct method of determining several important printing parameters, such as possible chamber and print bed temperatures. Knowing the crystallisation temperature allows for setting a chamber temperature high enough to prevent layers pre-emptively cooling and curling. Further, knowing the Tg enables selection of a chamber temperature that will not cause caking of the powder during spreading.

2.5.2 Stable Sintering Region

The Stable Sintering Region (SSR) is another concept at defining the thermal operating boundaries of an SLS. While the Sintering Window defines the upper boundary below that of the materials melting temperature, the Stable Sintering Region defines this temperature as the lower boundary. The upper boundary of the Stable Sintering Region is defined by the material's thermal degradation point [12, 42, 43, 45, 56, 75]. The advantage of this approach is that the material is more likely to be fully melted when sintered, leading to better bonding between particles. This in turn yields products with better yield strength [75].

However, like the Sintering Window, this approach has limitations. It does not include factor information such as the Tc, which is vital to ensure that prints coalesce into a strong final part.

2.5.3 Energy Melt Ratio

Vasquez et. al (2013) describes the Energy Melt Ratio (EMR) as "the ratio of the applied energy density relative to the theoretical energy to melt a single layer of material." As a unitless ratio it is a simple and effective representation of the energy inputs to a layer, and translates well between different variables such as material, temperature, and layer thickness. While it also relates thermal characteristics (such as enthalpy of melt, and specific heat capacity) EMR also considers physical factors such as powder and packing densities. This makes EMR a much more complete method of optimising parameters, in particular when compared to earlier methods to quantify energy, such as area energy density, or volume energy density [75]. As seen below in Equation 2.1, EMR includes laser power, scan count, scan spacing, beam speed, layer thickness, specific heat capacity, melting temperature, powder bed temperature, enthalpy of melt, material density, and packing density as P, V_C, V_S, V_B, z, C_P, T_M, T_B, h_f, δ_S, δ_D respectively

$$\textbf{Energy Melt Ratio} = \frac{\frac{P * V_C}{V_S * V_B * z}}{[C_P(T_M - T_B) + h_f] * (\delta_S)(\delta_D)} \quad (2.1)$$

2.5.4 Opportunities for improvement

Currently none of the models previously discussed account for any form of energy loss from the material during the printing process. This is significant because it makes it difficult for operators to gauge how effective these models will be in predicting the success of print parameters. Most printers currently account for the losses through thermal conduction by providing a constant heat source to the chamber during printing, and using sensors such as pyrometers to detect temperature levels. Energy losses from the laser source are not accounted for, in either the modelling methods discussed or in current machine designs. Existing literature has noted that the EMR models do not always provide accurate indications as to whether sintering will occur [43].

Experimentation in this work will explore these limitations in these models, especially at limited energy density levels. Firstly, testing will be conducted to characterise two polymer powders for SLS. After characterisation, trials will be conducted using parameters established in these characterisations to compare the effectiveness of these models in predicting successful printing parameters. Finally, further methods of characterisation will be explored, and discussed with reference to refinement of existing models.

To determine whether differing optical properties have an impact, powders will be chosen with the key difference between them being their optical properties. By ensuring that they are physically and thermally as similar as feasible, it can be evaluated whether the omission of optical properties from these models has a notable effect, and whether operators would benefit usefully from inclusion of these properties.

2.6 Chapter Summary

As mentioned, the EMR and SW are the most relevant methods of determining the energy requirements of SLS powders, and thus the print parameters with the minimum energy input. They combine both physical and thermal powder property considerations, as well as enabling operators to transform measurements of these properties into minimum print parameters required to achieve sintering, satisfying the first objective identified for this study.

As discussed, neither the SW or the EMR account for the possibility of energy losses during the printing process. These losses are somewhat understood in literature, with previous studies obtaining values for the energy losses incurred by a reflection of a laser off the powder. However, they have not even been introduced into this context, with the intent of using them to obtain a minimized energy input. The identification of losses absent from calculations satisfies the second objective identified for this study.

To satisfy the third objective identified for this study these losses must be confirmed to have validity within the context of the project, identifying minimum print parameters required for an unknown SLS powder. This will be done in two stages: firstly, the classification of the materials according to the two identified models, SW and EMR; secondly, a series of experimental trials will be conducted to establish whether the print parameters identified by the models do lead to successful sintering.

If the third objective is found to be achieved, then the fourth objective would be to investigate optical properties to improve the models. It is expected that this would be in the form of an improvement to the EMR equation.

Chapter 3 Characterisation by Existing Models

3.1 Chapter Overview

The aim of the initial powder classification tests is to use current common experimental methodologies to model and characterise powder behaviours. With these characterisations it is then possible to establish processing parameters for the Selective Laser Sintering (SLS) Design of Experiment (DoE) in Chapter 4.

As identified in Chapter 2, the most useful current method of modelling and characterising powder parameters is the Sintering Window (SW). The experimental process for determining the SW involves using Differential Scanning Calorimetry (DSC) to determine several critical thermal points of the material, including the crystallisation temperature (T_C) and melting temperature (T_M). DSC can also be used to determine several material properties needed to calculate the Energy Melt Ratio (EMR) for a material and parameter combination. These properties can be gathered through derivation of the results, and are commonly calculated by software packages that run the experimental trials themselves.

Furthermore, as discussed it is important to establish that the physical characteristics of the powder will not have undue influence on the validity of the SLS DoE. This will be established through examination of the powder under Scanning Electron Microscope (SEM) to establish the powder particle size and morphologies. In addition to analysis by SEM, the deposited density of the powder will be gathered for EMR calculations, in the manner identified during Chapter 2 [52].

Once these tests are conducted, the data will enable an assessment of the two powders, with reference to the SW models, and the ability for the two powders to successfully be processed under identical processing conditions.

3.2 Powder Selection

The two powders chosen for modelling and characterisation in this study are Precimid 1170 (Advanced Molding Solutions, USA), and Sintratec PA12 Black (Sintratec AG, Switzerland). Both powders are commercially available nylon powders marketed for using in SLS printing processes. The primary difference between these two powders is the colour of the material. The Precimid 1170 powder is white, while the Sintratec PA12 Black is black. The initial powder classification will determine if these two powders are classified as similar enough in other ways, to not matter according to the processes currently used. The manufacturer data sheets for both powders are available in Appendix A.

3.3 Differential Scanning Calorimetry

The objective of Differential Scanning Calorimetry is to determine the behaviours of the powder under a controlled heating and cooling cycle. By measuring the input of energy required to heat up a known mass of material, by a known temperature increase, several important material properties can be identified; such as the TM, and TC. Knowing the heat flow that occurs during the tests also allows for calculation of several material properties, such as Specific Heat Capacity (C_P), and Enthalpy of the Melt (Φ), which can be used to calculate the EMR of SLS printing parameters. During the trials, the powders are heated past the observed melting point, then allowed to cool and crystallise, and then heated again past melting point. Of interest are the first heating and cooling ramps, as this best matches the SLS printing conditions. While the second heating ramp is of interest for purposes of recycling unsintered powder, it is of less interest for initial classification of these unused 'virgin' powders.

3.3.1 Method of Differential Scanning Calorimetry Testing

All tests were conducted using a Discovery DSC (TA Instruments, USA). The testing procedure selected was ASTM 3418, with heating and cooling rates of 5°C/minute. The initial temperature before starting the test was 20°C, with samples being heated to a maximum of 250°C. After the heating ramp was completed, samples were cooled to 20°C, before being subjected to another heating ramp of 250°C. Two experimental thermogram test runs were conducted with fresh samples of each powder for the purposes of confirming the validity of the results. Previous works have indicated two trials is sufficient the have confidence in determining the EMR [12, 45].

Virgin powder was used for each of these experimental runs. Time, sample temperature, and heat flow were recorded using the Discovery TRIOS software package (TA Instruments, USA), along with heat flow normalized for sample weight. These recordings were exported from TRIOS as Excel spreadsheets. The data was then consolidated into a single file, converted to a Comma-Separated-Value file, and imported into MATLAB 2015 for further analysis. Sample sizes ranged from 3.10 - 4.10 grams. The full dataset of the experiments is available upon request.

3.3.2 Results of Differential Scanning Calorimetry Testing

The two-sequential heating-cooling cycles are illustrated in Figure 1. It is difficult to interpret the results when all values are included, as seen in Figure 6 below. One reason for this is that the second heating cycle is less relevant to determining the powder melting temperatures, so the results from that element of the experiment do not aid in determining the initial melting point of the powder. Melting points are indicated by troughs in the data, indicating a rapid input of heat as a phase change occurs. The value of this heat flow indicates the value of the enthalpy of the melt. The crystallisation temperature is indicated by the opposite, peaks in the data as heat is released by the material solidifying.

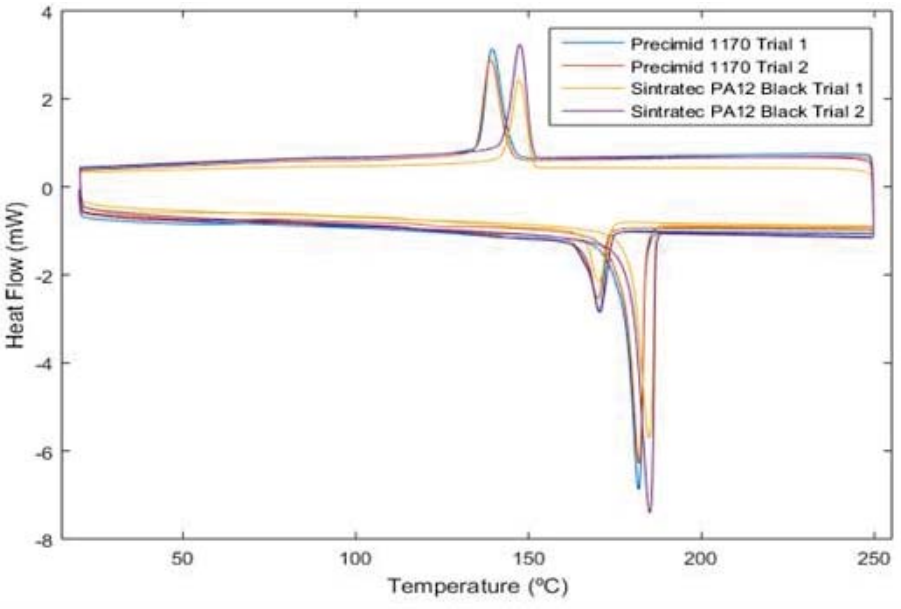

Figure 3.1: Raw data from all trials.

By truncating the data to remove the second heating cycle it becomes easier to see the common trends. While the magnitude of the peaks varies between trials, almost identical melting and crystallisation temperatures are present for the two trials of each powder, and the two powders have very similar melting temperatures, as seen in Figure 7 below. The crystallisation temperatures are more distant, but the powders are within a few degrees of each other in both trials.

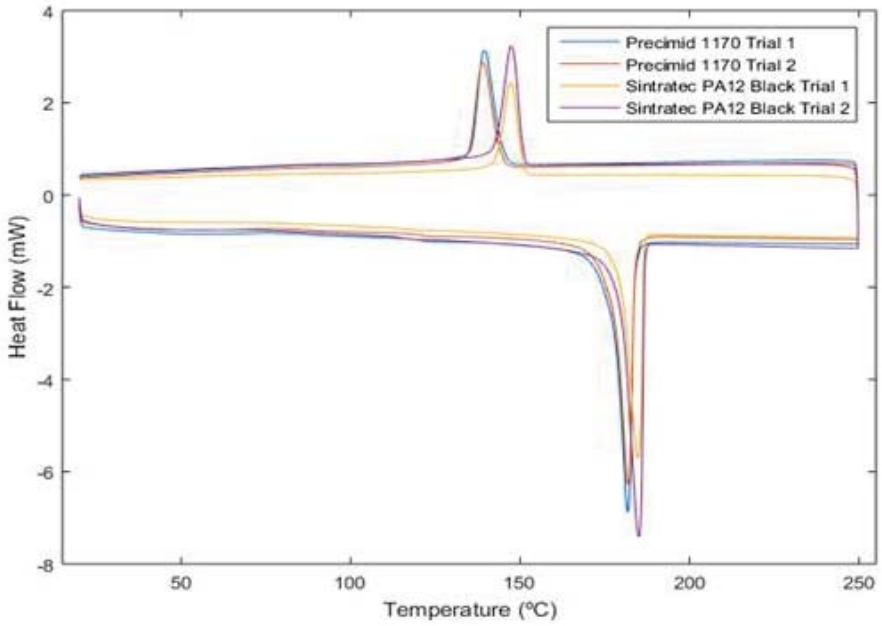

Figure 3.2: Truncated Thermogram results to include only first heating cycle.

The Discovery TRIOS software produces a table of exact values for each parameter, including onset and peak of melting and crystallisation temperatures, as seen below in Table 3.1 below. The Precimid powder has lower melting temperatures, and crystallisation temperatures in both trials when compared to the Sintratec powder.

Table 3.1 Onset and peak melting and crystallisation temperatures of powders

Parameter	Precimid 1170 Trial 1	Precimid 1170 Trial 2	Precimid 1170 Average	Sintratec PA12 Black Trial 1	Sintratec PA12 Black Trial 2	Sintratec PA12 Black Average
Temperature at onset of melting (ºC)	177.1	177.2	177.2	180.1	180.1	180.1
Temperature at melting (ºC)	181.8	181.9	181.9	184.6	184.7	184.7
Temperature at onset of crystallisation (ºC)	144.7	144.2	144.5	151.0	151.0	151.0
Temperature at crystallisation (ºC)	139.3	138.1	139.1	147.1	147.4	147.4

As well as the melting and crystallisation points of the material, DSC enables the classification of many other material properties, including Melt Enthalpy (Φ) and Specific Heat Capacity (C_P). These properties are not necessary for the identification of the SW, but for classifying the EMR of prints. Listed in Table 3.2, Melt Enthalpies are calculated by the Discovery TRIOS software for each trial, and Specific Heat Capacity is calculated by integrating all values before the onset of melting, using Equation 3.1 below. As shown, the Sintratec powder has a lower average Specific Heat Capacity, and a lower melt enthalpy.

Table 3.2: Melt enthalpy and specific heat capacity of the two powders

Parameter	Precimid 1170 Trial 1	Precimid 1170 Trial 2	Precimid 1170 Average	Sintratec PA12 Black Trial 1	Sintratec PA12 Black Trial 2	Sintratec PA12 Black Average
Melt Enthalpy (J/g)	101.31	111.76	111.0	103	108.1	105.6
Crystallisation Enthalpy (J/g)	49.82	52.48	51.2	49.4	52.8	51.1
Specific Heat Capacity (J/kg°C)	44007.240	49184.51	46595.876	40050.251	30281.896	35166.073

The heat flow results are adjusted to account for sample weight using the heat flow equation, as in Equation 3.1, giving Heat Flow Watts per gram (W/g) as shown in Figure 3. Here the results for the two powders overlap in many locations, with the only notable variances in melting and crystallisation temperatures. The agreement of the results indicates that additional trials are not required to establish the behaviour of the powders through DSC, which matches experience in previous literature [12, 45].

$$\Delta Q = C_P . m . \Delta T \qquad (3.1)$$

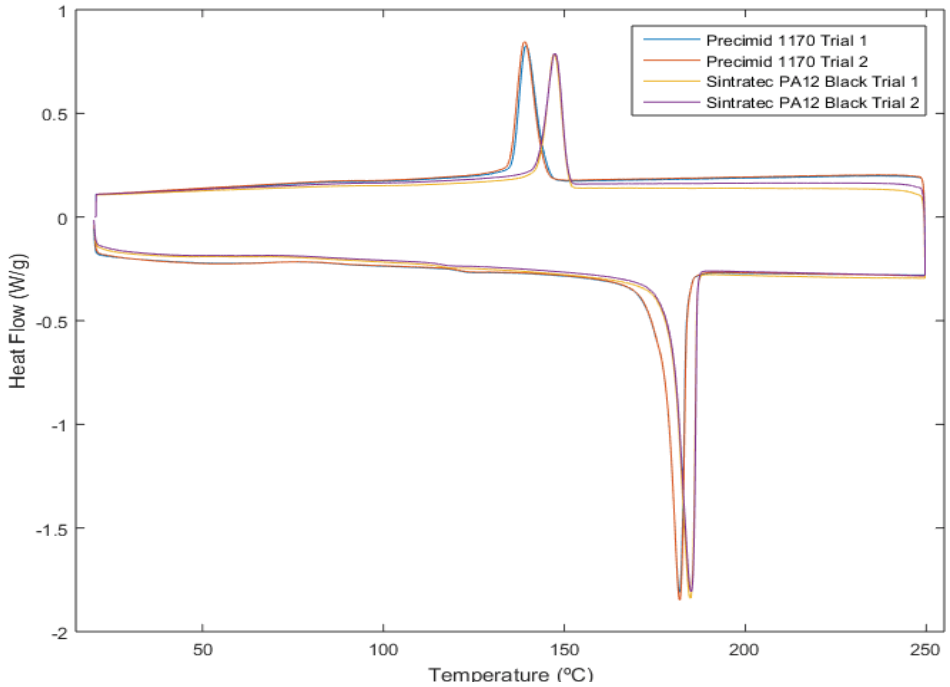

Figure 3.3: Heat Flow accounting for sample weight.

3.4 Scanning Electron Microscope

The benefit of the Scanning Electron Microscope (SEM) is that it allows for direct observation of interactions that have occurred on a particulate level. This means that powders can be compared visually to identify similarities and differences of particle size and morphology. While not a definitive method of comparing physical powder properties, it is useful for identifying broad similarities. This is useful in this case because although physical properties are not the primary property be investigated, they can affect the ability for a powder to be sintered, which could have an influence on the later SLS Design of Experiment.

3.4.1 Method of Imaging Using Scanning Electron Microscope

Samples were affixed to examination stubs by means of conductive tape. Clean stubs had the tape first affixed to them. Powder was poured into a small plastic vessel, and then agitated until the surface was roughly flattened. The tape-covered stub was then pressed against the powder surface firmly for 5 seconds before being removed. Filtered compressed air was then blown across the powder-covered tape to remove loose particles.

Despite a potential loss of image quality, samples were not sputter-coated prior to examination. Due to the nature of the sputter-coating process there is potential for heat transfer into the sample, which could affect smaller powder particles present, potentially causing necking between particles. Thus, samples could only be imaged for a period of up to ten minutes at a time before the charge build-up would lead to a loss of contrast in the images. All images were taken during this time-period, and samples were not re-examined after this initial exposure.

All samples were imaged using a TM3030Plus Desktop SEM (Hitachi, Japan), set to ‘Secondary Electron’ (SE) mode, with an accelerating voltage of 15, 000 Volts. When viewed under low magnification settings, such as 100 times magnification, comparisons about the average sizes of the powder particles can be drawn.

3.4.2 Results of Imaging Using Scanning Electron Microscope

Between the two powders, there appears to be a very similar distribution of powder particle sizes. There are few particles that are much larger than the rest of the particles. Several of these larger particles are visible in Figure 10 below. In the Precimid 1170 powder the largest particles appear to be much larger than those in the Sintratec PA12 powder, almost double the length. However, these particles also appear to be formed by multiple smaller particles, joined together, as indicated by their 'bubbly' geometry, whereas the large particles in the Sintratec PA12 Black do not exhibit this behaviour, and appear to be similar geometries to smaller particles. The size of the mean particle for both powders appears to be between 50 – 100 micrometres in size.

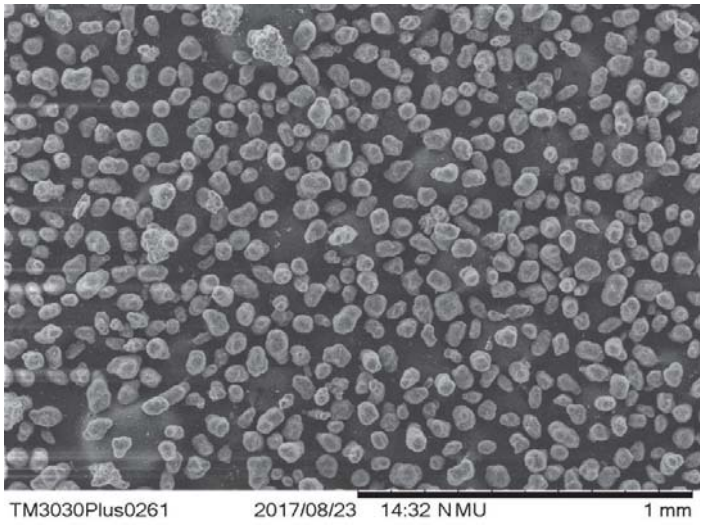

Figure 3.4: Image of Precimid 1170 powder taken at 100 x magnification.

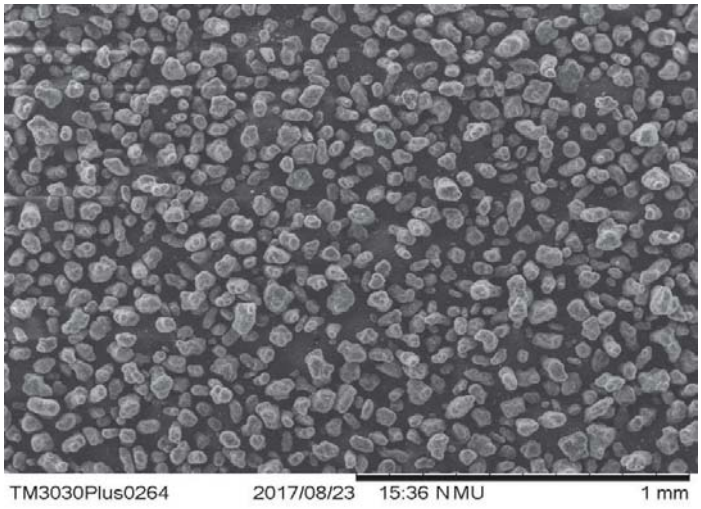

Figure 3.5: Image of Sintratec PA12 Black powder at 100 x magnification.

Increasing the magnification allows a more detailed examination. Figures 3.6 and 3.7, seen below, are taken at 500 times magnification, and the morphologies of individual particles are much more visible at this magnification. The Precimid particles appear to have a smoother morphology than the Sintratec powder.

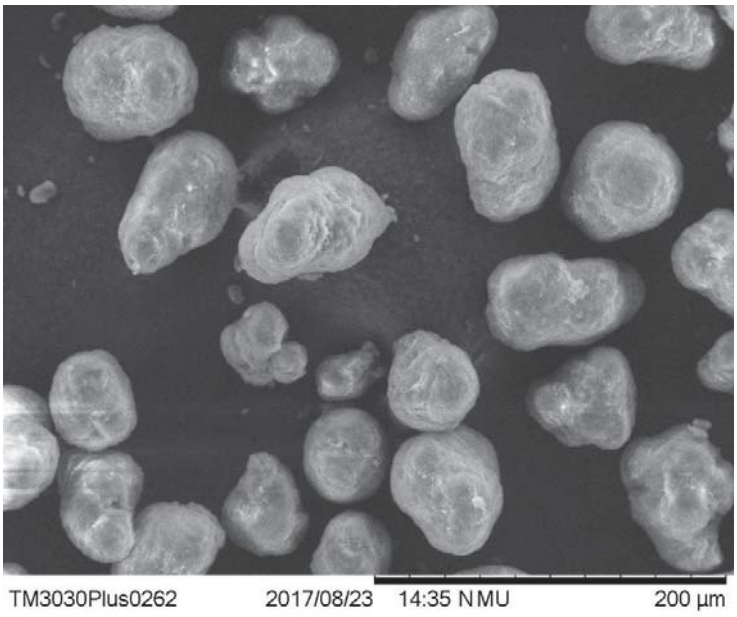

Figure 3.6: Image of Precimid 1170 powder taken at 500 x magnification.

Figure 3.7: Image of Sintratec PA12 Black powder taken at 500 times magnification.

At 1000 times magnification this differences in surface of the particles are much more apparent, as shown in Figures 8 and 9 below. At this magnification the surface of the Sintratec PA12 Black appears to have a rougher, less uniform surface when compared to the Precimid 1170. The Sintratec also has more irregular, less spherical particles.

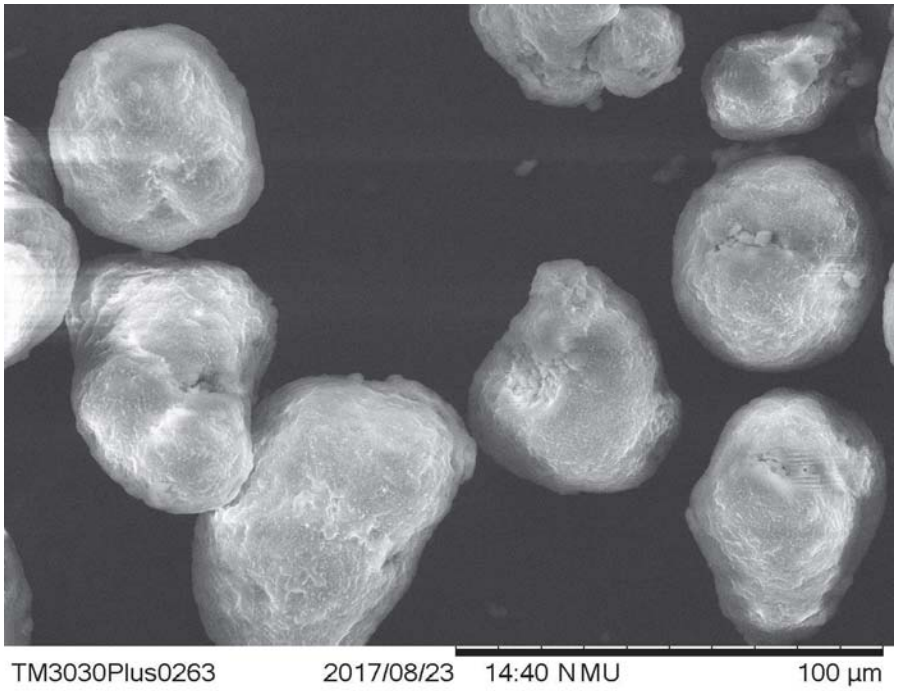

Figure 3.8: Image of Precimid 1170 powder taken at 1000 times magnification.

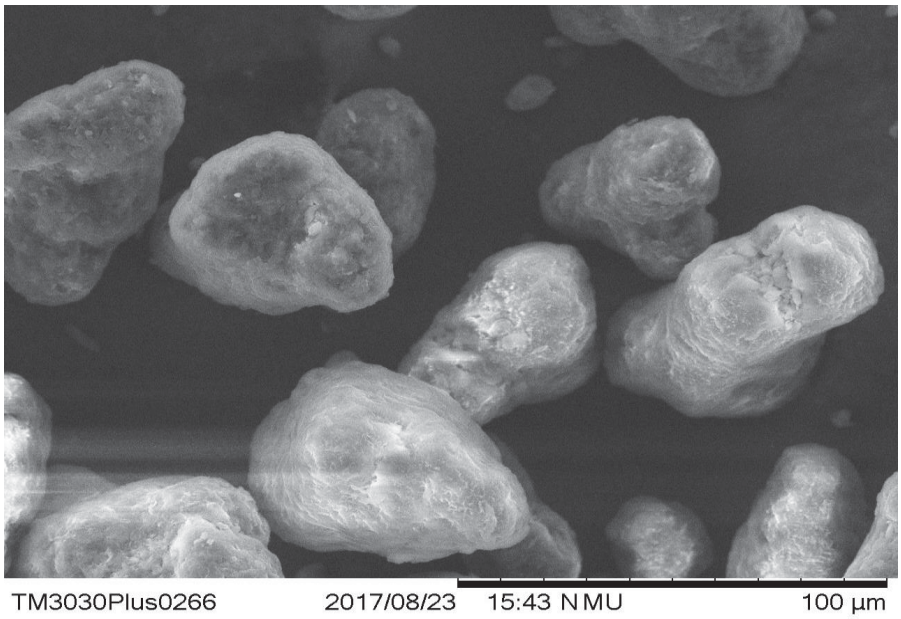

Figure 3.9: Image of Sintratec PA12 Black taken at 1000 times magnification.

3.5 Discussion

The purposes of the two methods of testing in this chapter was to use current common experimental methodologies to model and characterise powder behaviours. With these characterisations it is then possible to establish processing parameters for the SLS DoE in Chapter 4. The key parameters for processing are determined using the Sintering Window model, based on the results of the DSC tests. The suitability of the two powders to be processed using the same parameters was also assessed using their physical characteristics, identified using an SEM.

3.5.1 Differential Scanning Calorimetry

The Sintering Window is defined by the powder's melting point as a maximum upper boundary, and the crystallisation point as a minimum lower boundary. As per the DSC results, the SW for Precimid 1170 would exist between 139.1°C and 181.9°C, and for Sintratec PA12 Black it would exist between 147.4°C and 184.7°C. A common SW can exist for both powders, that would allow for processing of both powders between the highest of the two crystallisation points, and the lowest of the two melting points. This would give a common SW for both powders of between 147.4°C and 181.9°C. This window of 34.5°C is not dissimilar to the windows found for other powders[68, 74]

Comparatively the Precimid powder displays lower melting temperatures, meaning that it is more likely than the Sintratec powder to achieve melting in the SW identified for use with both powders. It also has a lower crystallisation temperature, meaning that it should be better able to form strong bonds between molten layers during the printing process. As per the EMR equation, the closer the powder surface temperature to the melting temperature, the higher the EMR value for identical laser parameters, and higher energy density settings have been linked to better mechanical characteristics of parts [75], indicating better bonding during the print process.

Furthermore, additional insight can be drawn from the DSC results in the form of melt enthalpies and specific heat capacities. These data points are useful for calculating EMR values during printing, which helps quantify the energy input from parameters in a more meaningful manner than simply using parameter values. While EMR values cannot be calculated at this stage as they require laser parameters, they do give more insight into the energy requirements of the two powders. These values do vary; however, the values are not magnitudes different, with CP varying by 32.5%, and Φ varying by 5.11%. These differences mean that identical sintering parameters will further vary the EMR values calculated for the DoE trials. However, in contrast to the melting and crystallisation temperatures, the Sintratec powder has lower values, giving more favourable printing parameters when trying to reduce maximum energy input during printing.

3.5.2 Scanning Electron Microscope

The objective of examination of both powders using SEM was to determine if the two powders were sufficiently similar physically as to enable the DoE experiment to be valid. The key factors that were to be examined were the particle morphology, and particle size, with reference to existing knowledge of the influence of these two factors as to their effect on SLS printing processes. While it is expected that no two powder samples will be identical, vastly physically different powder particle sizes and morphologies can invalidate the test by unintentionally impacting the outcome of the printing process.

As identified by the results, both powders have particles with spherical, or potato-shaped morphologies, and an average particle size of between 50-100 μm. The Sintratec powder was identified to have a rougher surface finish than the Precimid powder, and the Precimid powder was identified to have large particulate ‘clumps’ formed, that appeared to be formed from several smaller particles bonded together.

Ziegelmeier *et al.* (2015) identified that powders with either spherical and potato shaped particles demonstrated adequate powder flow characteristics for SLS printing. Fan *et al.* (2007) identified that the ability of a material to reflect laser energy is related to the wavelength of the laser, and the size of the particles in the powder. With that in mind it is expected that the physical characteristics of the powders will lead to their interactions with the laser being similar.

3.6 Chapter Summary

The aim of this chapter was to use existing experimental methodologies to model and characterise powder behaviours in order establish processing parameters for the Selective Laser Sintering (SLS) Design of Experiment (DoE) in Chapter 4. Both the Precimid 1170 and Sintratec PA12 Black powders were characterised using the SW and EMR models.

The results of the characterisation showed that the two powders have a number of similarities, including thermal and physical properties. They have similar melting and crystallisation points, similar specific heat capacities, and similar phase change enthalpies. In addition, the physical characteristics are similar, both in terms of particle size and morphology, as well as bulk and tapped densities.

These similarities lead the two models predicting that the same set of print parameters should lead to sintering of both powders during experimental trials. This will be tested in Chapter 4 during experimental trials, using the values gathered during characterisation in this chapter. Assessment of the parts produced during these trials will determine whether these models are sufficient to correctly predict minimum print parameters to successfully sinter the powder.

Chapter 4 Testing of Models Through Sintering Trials

4.1 Chapter Overview

The objective of this chapter is to conduct an experiment to assess whether the current methods of characterising Selective Laser Sintering (SLS) powders are sufficient. These methods (as identified in Chapter 2 and 3) are the sintering window (SW), energy melt ratio (EMR) and the packing ratio (PR). In Chapter 3, trials were conducted using Differential Scanning Calorimetry (DSC) to identify the Sintering Window (SW) and to determine values to be used in calculating the Energy Melt Ratio (EMR) of various print parameters. It was also established using Scanning Electron Microscope (SEM) imaging that the powders were physically similar enough in particulate size and morphology as to not affect required sintering parameters. This chapter explains the methods used to undertake testing of two different print powders under various processing conditions. It also details the methods used to assess the printed parts after the trials. The results are presented and then used to identify possible knowledge gaps within the existing methods. These are discussed within the context of current available literature and further avenues for testing identified.

4.2 Experimental Method

4.2.1 Selective Laser Sintering Machine

Calibration of the machine was carried out according to the manufacturer's procedure. Testing was carried out using a Sintratec Kit SLS Printer (Sintratec AG, Switzerland). The kit itself is equipped with a 2.3W 445 nm diode laser. Between each trial the printer was emptied, and the laser assembly was cleaned, including focusing lens, mirror galvanometers, and laser cover. The software used was the Sintratec Central Version 1.1.16 (Sintratec AG, Switzerland).

4.2.2 Printed Part Selection

The part selected for printing was the ANSI D638 Standard Type 5 Dog bone. Five parts were produced per print to provide a wider sample of results for each trial. Parts were orientated with the longest dimension along the X axis of the print bed, and were orientated 3mm above the bottom of the build volume to ensure there was sufficient powder below the part before printing to reduce the chance of parts lifting during sintering.

The five parts were spaced 23mm apart, centre to centre, from one another on the Y axis to ensure sufficient clearance from one another to enable removal from the powder cake after printing, as demonstrated in Figure 1 below. The intent in choosing this part was to be able to provide comment on the differences in tensile strength of parts from each trial, which was accounted for by selection of the ANSI standard part, and the number of parts printed in each trial. However, due to a reduced number of usable dog bones produced parts were only assessed by the density.

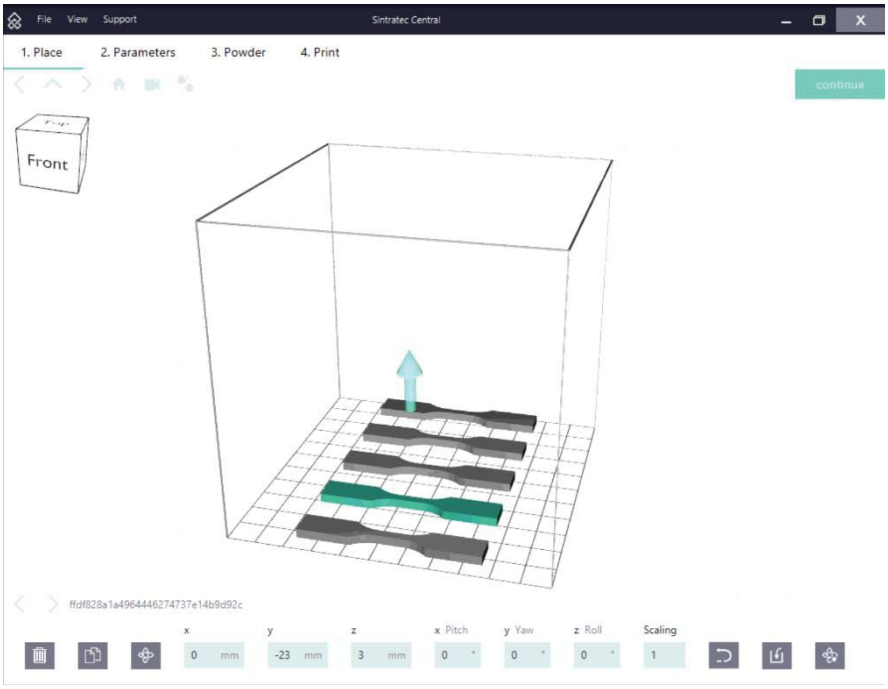

Figure 4.1: Part orientation and positions using Sintratec Central software.

4.2.3 Machine Print Parameter Selection

Printing parameters were chosen for this design of experiment (DoE) based on a combination of results from the powder characterisation in Chapter 3, and recommended printing parameters for the Sintratec PA12 Black powder for use with the Sintratec Kit printer. As determined by the SW identified in Chapter 3, the minimum temperature for the combined SW is 147.4°C, so a chamber temperature of 150°C was selected, the maximum the software will allow.

Three factors of the experiment will be independent: the powder, Print Bed Temperature, and Laser Scan Speed. The dependent measures are powder melt qualities, including qualitative assessment by the ability for a part to be removed successfully from the print bed powder cake, as well as visible assessment of particle coalescence using the SEM. Quantitative assessment of the parts was done by measurement of dimensions and mass, and calculation of density of produced parts.

Each of the independent factors will have two levels, giving 9 trials total for each powder, and 18 trials in total. The trial run order was determined using Minitab 17 (Minitab Inc, USA). A full factorial design was constructed, with 1 replicate for each level, as shown in table 1 below.

Table 4.1: Design of Experiment trial run order

Trial Number (Standard order)	Run Order	Bed Temperature (°C)	Laser Scan Speed (mm/s)	Powder
1	4	165	650	Precimid 1170
2	3	165	650	Sintratec PA12 Black
3	13	165	550	Precimid 1170
4	5	165	550	Sintratec PA12 Black
5	18	165	450	Precimid 1170
6	1	165	450	Sintratec PA12 Black
7	11	170	650	Precimid 1170
8	14	170	650	Sintratec PA12 Black
9	6	170	550	Precimid 1170
10	10	170	550	Sintratec PA12 Black
11	16	170	450	Precimid 1170
12	17	170	450	Sintratec PA12 Black
13	7	175	650	Precimid 1170
14	12	175	650	Sintratec PA12 Black
15	9	175	550	Precimid 1170
16	15	175	550	Sintratec PA12 Black
17	8	175	450	Precimid 1170
18	2	175	450	Sintratec PA12 Black

4.2.3.A Energy Melt Ratio

With the printing parameters for the trials selected, the EMR for each trial can be calculated. Specific heat capacity was taken as an average value calculated from the DSC results, as was the onset of melt temperature, and enthalpy of melting. A value for bulk density for each material was taken from their respective specification sheets, as provided by their manufacturers. The packing fraction was taken from the 'as deposited' packing fraction from Chapter 3, due to the nature of powder spreading in SLS processes involving minimal agitation of powders. Scan count, scan spacing, and layer thickness were all left at the recommended settings for Sintratec PA12 Black. Laser power is fixed at 2.3W. The value for the parameters are listed below in Table 3. The resulting EMR values for each trial are listed in Table 4.

Table 4.2: Energy Melt Ratio parameter values for the two powders.

Parameter Name	Parameter	Sintratec PA12 Black Value	Precimid 1170 Value
Specific Heat Capacity (kJ/g°C)	C_P	35.166074	46.59588
Print Bed Temperature (°C)	$T_{b1} - T_{b3}$	165, 170, 175	165, 170, 175
Onset of melt temperature (°C)	T_m	180.1	177.2
Enthalpy of melting (J)	H_f	105.6	110.0
Bulk Density (g/mm^3)	Q	0.001	0.00094
Packing Fraction	Φ	5.13E-01	5.25E-01
Scan Count	V_c	1	1
Scan Spacing (mm)	V_s	0.05	0.05
Laser Speed (mm/s)	V_1, V_2, V_3	450, 550, 650	450, 550, 650
Layer Thickness (mm)	Z	0.1	0.1
Laser Power (W)	P	2.3	2.3

Table 4.3: Energy Melt Ratio values for trial print parameters.

Print Bed Temperature (°C)	Laser Speed (mm/s)	Sintratec PA12 Black EMR	Precimid 1170 EMR
165	650	2.130	2.024
165	550	2.517	2.392
165	450	3.077	2.923
170	650	2.925	3.080
170	550	3.456	3.640
170	450	4.224	4.448
175	650	4.665	6.440
175	550	5.513	7.611
175	450	6.738	9.302

The EMR values for all trials are above a value of 1, indicating that sintering should occur in all trials. The EMR values also reflect the differences that the lower melting temperature makes for the Precimid powder, as it has higher EMR values across the board, despite having a greater specific heat capacity than the Sintratec powder.

4.3 Results

Across all trials it was used in, the Precimid 1170 failed to produce a successful print at any parameter combination, despite having a maximum EMR value of 9.302 at a powder bed temperature of 175°C and laser scan speed of 450mm/s**.** Further testing at higher energy density settings revealed that the machine itself would reach a point of overheating before any successful sintering could occur, however it was possible at 180°C to produce a solidified powder cake without addition of laser energy.

While a powder cake did form in all trials for the Precimid 1170, there was no evidence of any sintering having occurred, and clumps of powder would disintegrate upon handling. As such, there was no further examination of material from trials using the Precimid 1170 powder. For the trials the part in position 5, the part closest to the back wall of the print bed, failed to print successfully. In some trials it was noted to be partially sintered in some layers, however absent in others. It is believed that this was caused by a limitation of the machine itself, as it was difficult to replicate the effect in further testing.

4.3.1 Part Removal From Powder Cake

Several trials of the Sintratec PA12 did not result in complete dog bones that could be removed from the powder cake after printing. Of note were those with a Print Bed Temperature of 165ºC, the trials with Laser Speeds of 650 mm/s and 550 mm/s had very fragile parts, some of which broke during removal from the powder cake using a soft paintbrush. The trial with a Laser Speed of 450 mm/s suffered from curling during printing, and had parts swept off the print bed by the powder spreading blade. While there were partial parts made from a remainder of the part not swept off the bed, there were no complete dog bones produced.

Also of note were all trials with a Print Bed Temperature of 175ºC. These trials resulted in printed parts, but excess material was bonded to the print, as visible in Figure 4.1, and was difficult to remove without damaging the printed parts. The outcome of each trial is listed in Table 4 below.

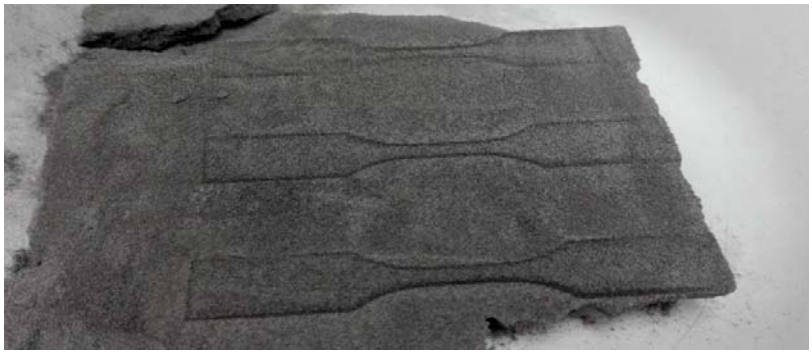

Figure 4.1: The powder cake that was produced during trial number 16, with a Print Bed Temperature of 175°C, and a laser scan speed of 550 mm/s using Sintratec PA12 Black.

Table 4.4: Trial notes from the experiment.

Print Bed Temperature	Laser Speed	Sintratec PA12 Black Print Comments	Precimid 1170 Print Comments
165	650	Print finished, loose powder cake formed, several dog bones broke upon removal from powder cake with fine paintbrush, dog bone in position 5 absent.	Print unsuccessful, no effect of powder evident
165	550	Print finished, loose powder cake formed, one dog bone crumbled on removal from powder cake with fine paintbrush	Print unsuccessful, no effect of powder evident
165	450	Print not successful, parts curled and were swept off bed several times. Partial dog bones remaining in bed after print of reduced thickness.	Print unsuccessful, occasional small loose clumps of powder
170	650	Print successful, all samples removed without issue.	Print unsuccessful, no effect of powder evident
170	550	Print successful, all samples removed without issue.	Print unsuccessful, occasional small loose clumps of powder
170	450	Print successful, some excess powder melting present on one sample, removal possible with wire brush.	Print unsuccessful, very loose powder cake formed
175	650	Print successful, excess powder bonded to several samples, rigid powder cake formed, removal possible with wire brush.	Print unsuccessful, very loose powder cake formed
175	550	Print successful, excess powder bonded to several samples, rigid powder cake formed, removal possible with wire brush.	Print unsuccessful, very loose powder cake formed
175	450	Print successful, excess powder bonded to all samples, rigid powder cake formed, removal possible with wire brush o	Print unsuccessful, very loose powder cake formed

4.3.2 Imaging by Scanning Electron Microscope

By examining sample cross sections with the SEM, it is possible to directly observe the bonding that has occurred between powder particles during printing, and to observe part porosity as the EMR increases. The full gallery of all images taken is available in Appendix B.

4.3.2.A Method of imaging using Scanning Electron Microscope

To prepare samples for examination, the end of the dog bone was cut off using a scalpel with a clean, fresh blade, cutting through the build layers with a slow, gentle pressure. The sample was then mounted to a specimen stub using conductive double-sided tape, with the 'external' side of the sample contacting the tape, and the 'internal' side of the samples facing up for examination. Samples were then sputter-coated with gold using a Desk Sputter Coater DSR1 (Nanostructured Coatings Co, Iran), operating at 10 mA, with a layer thickness of 20 Å.

All samples were imaged using a TM3030Plus Desktop SEM, and accompanying TM3030 Plus software (Hitachi, Japan), set to 'Secondary Electron' (SE) mode, with an accelerating voltage of 15, 000 Volts.

4.3.2.B Results

The samples produced in trial 2, at the lowest energy density settings with a print bed temperature of 165°C, and with a laser scan speed of 650 mm/s, do reveal large internal cavities visible, as shown in Figure 4.2. However, some necking between individual particles are visible despite most particles being well defined when viewed at 500 times magnification in Figure 4.3 below.

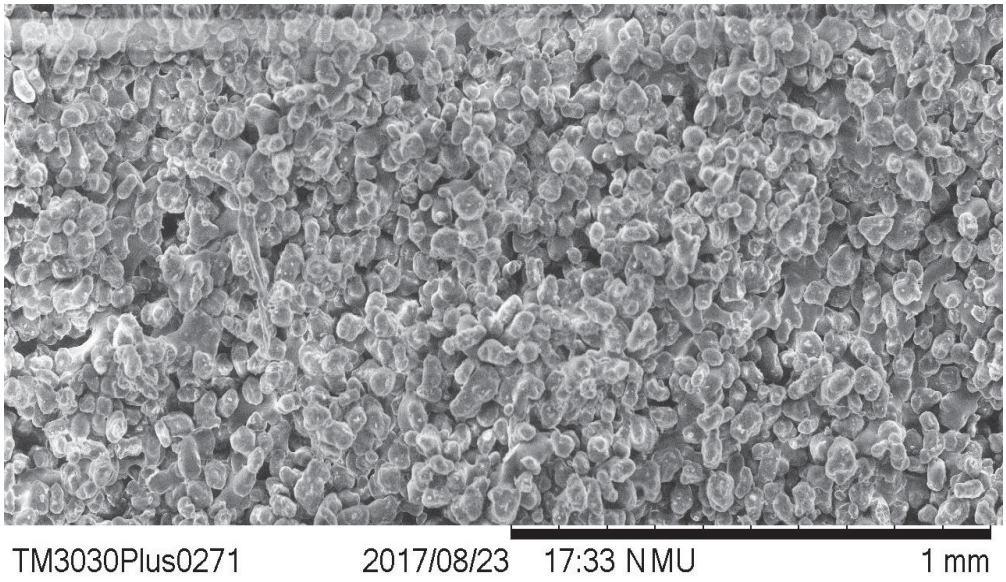

Figure 4.2: 100 x magnification SEM image of Sintratec PA12 Black powder with powder bed temperature of 165°C, and laser scan speed of 650 mm/s.

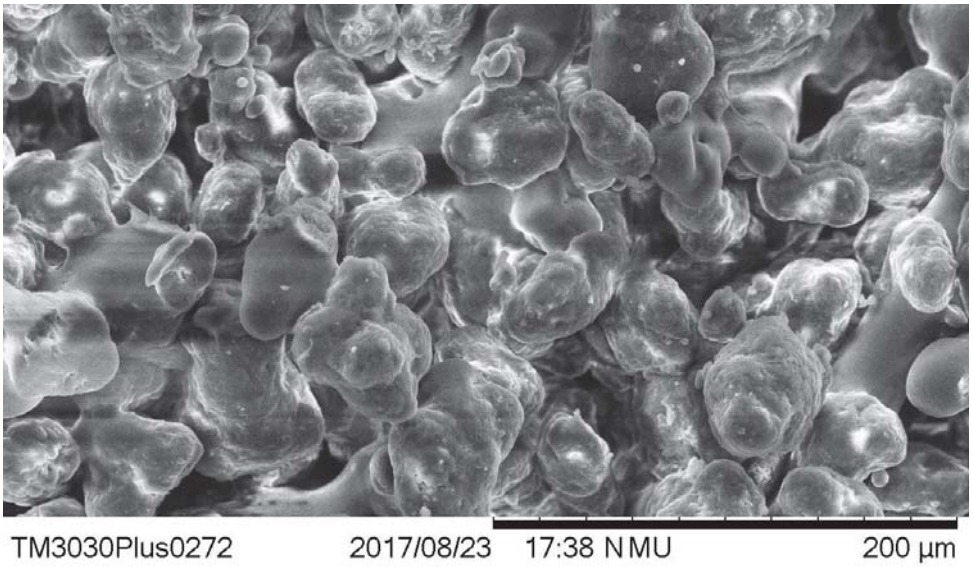

Figure 4.3: 500 x magnification SEM image of Sintratec PA12 Black powder with powder bed temperature of 165°C, and laser scan speed of 650 mm/s.

Trials 6 and 8 are of note, because they have very similar EMR values (3.077 and 2.925 respectively) but different processing parameters. SEM imaging shows that samples from both trials look similar, with areas of coalescence visible in large sections of the part, visible in Figures 4.4. Outside of the areas of coalescence, porous areas are still visible, but higher magnification imaging in Figures 4.5 reveals that necking is now pronounced between individual powder particles.

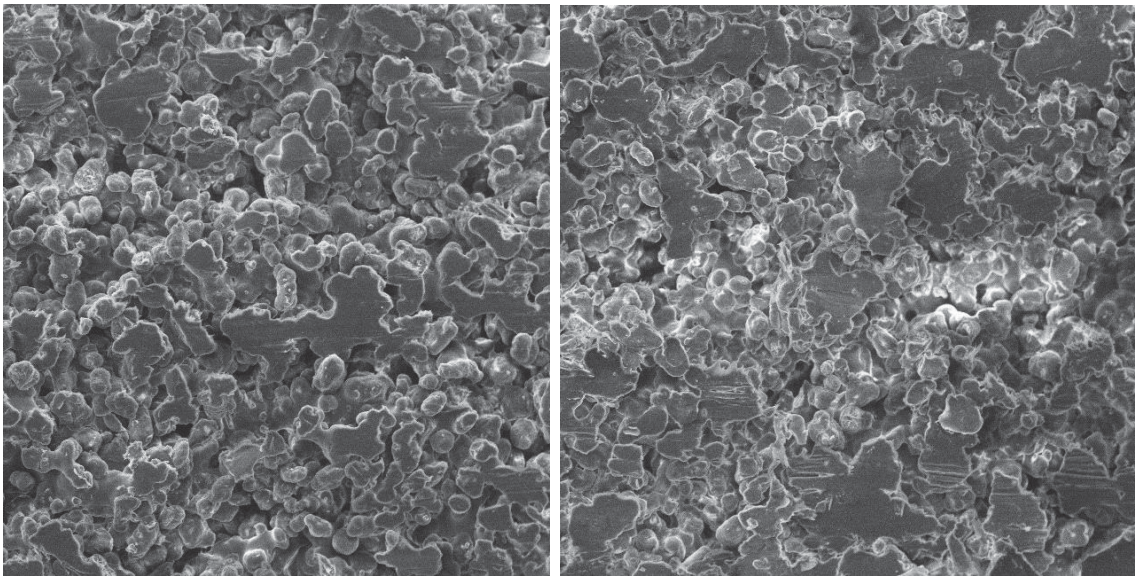

Figure 4.4: Comparison of SEM images taken at 100 times magnification of samples from trial 6 (left), with print bed temperature of 165°C, and laser scan speed of 450 mm/s, and trial 8 (right), with a print bed temperature of 170°C, and laser scan speed of 650 mm/

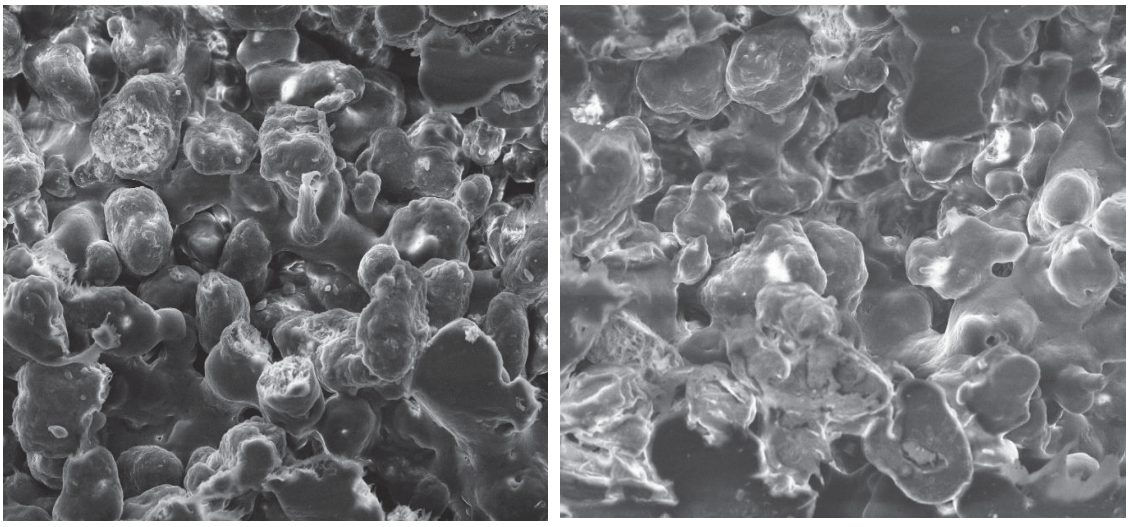

Figure 4.5: Comparison of SEM images taken at 500 x magnification of samples from trial 6 (left), and trial 8 (right).

Trial 12 was the trial with the highest EMR value that parts were removable from the powder cake without issue. One part did have excess material attached to it, but this was removable with a wire brush. Figure 4.6 shows that coalescence has happened across a majority of the sample, however porous areas are still common. Necking of particles has become so pronounced that under high magnification, identification of individual particles is difficult, as seen in Figure 4.7. The horizontal lines visible crossing the sample are likely from the cutting process used to prepare it.

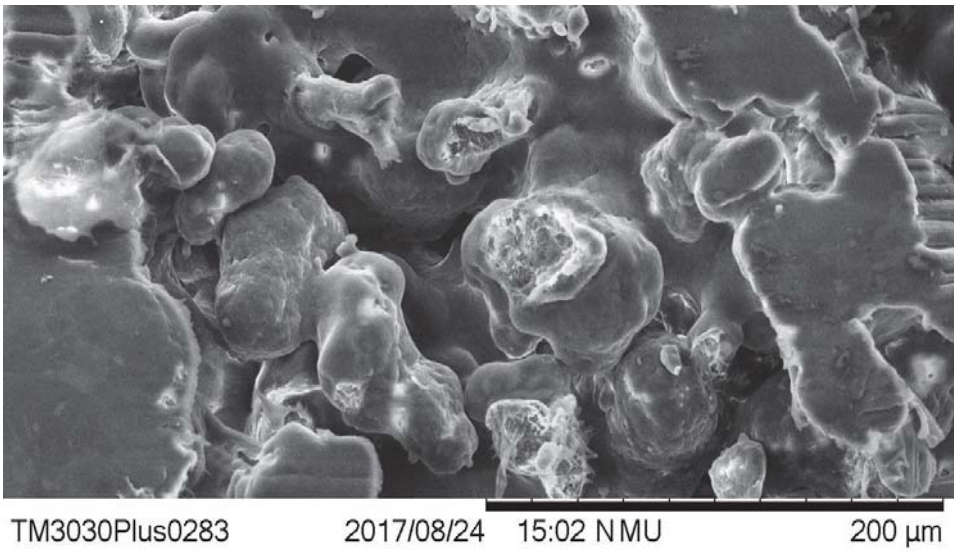

Figure 4.6: Image taken at 500 times magnification of a sample from trial 12, with print bed temperature of 170°C, and laser speed of 450 mm/s.

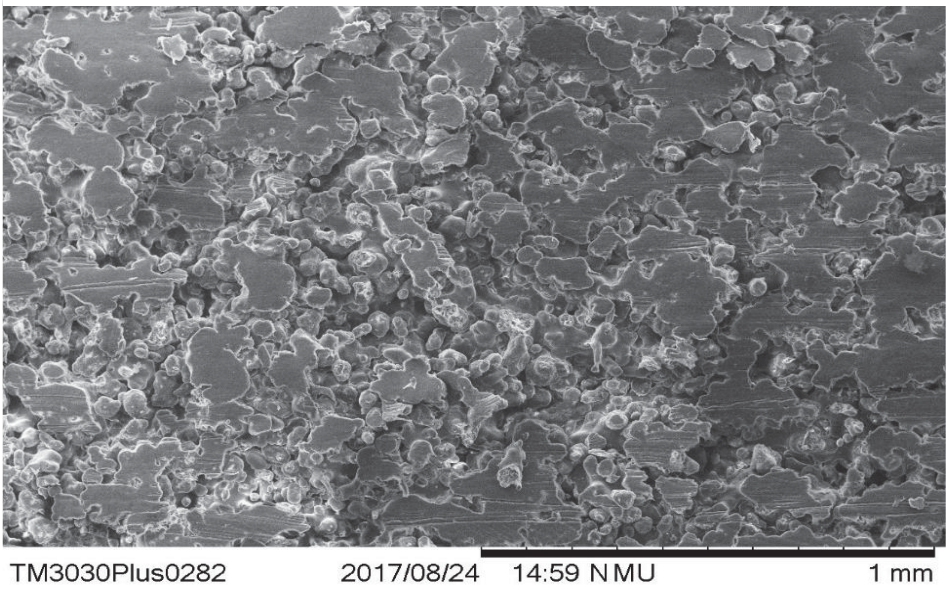

Figure 4.7: Image taken at 100 times magnification of a sample from trial 12, with print bed temperature of 170°C, and laser speed of 450 mm/s

Figure 4.8 shows the sample from the trial with the highest EMR value for Sintratec PA12 Black, trial 17. This sample has the most coalesced area visible of all the samples. Figure 4.9 shows a high magnification image, and individual particles are often difficult to discern due to necking with surrounding material.

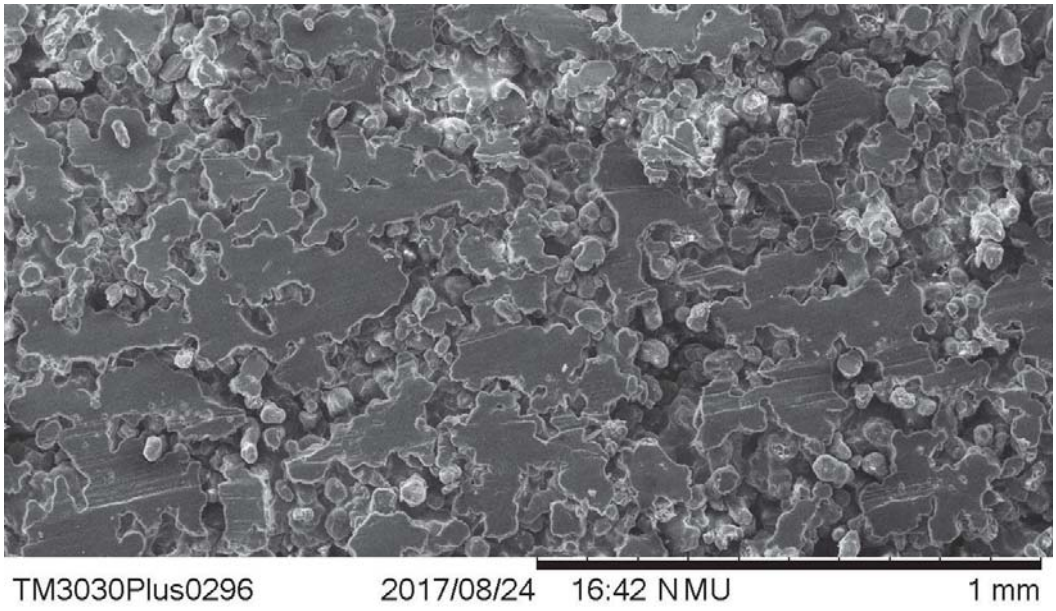

Figure 4.8: SEM image taken at 100 times magnification of the sample from trial 12, with a print bed temperature of 175°C, and a laser scan speed of 450 mm/s.

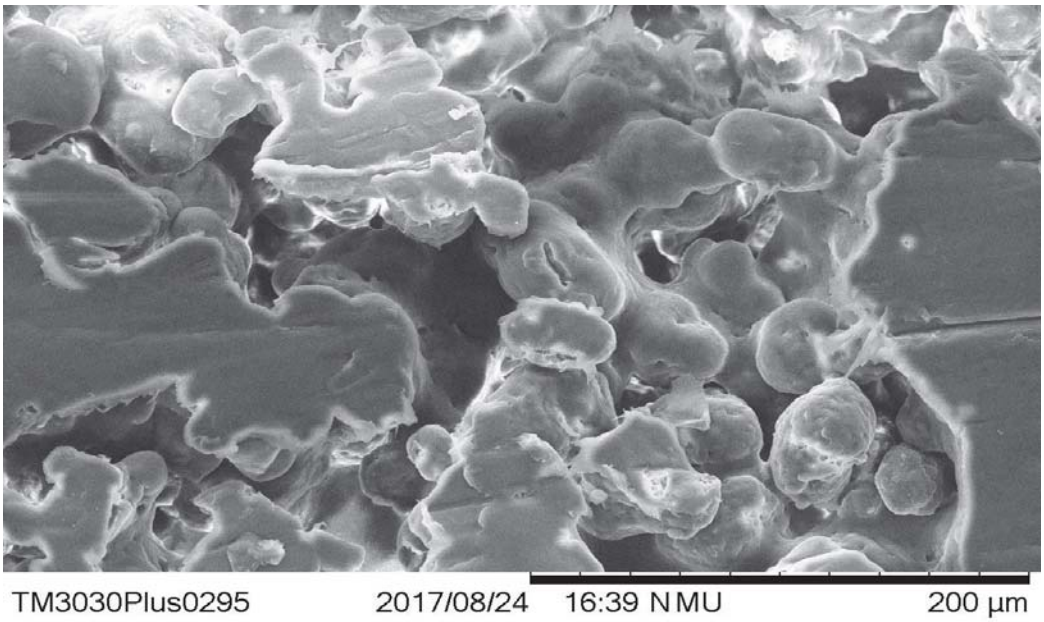

Figure 4.9: SEM image taken at 500 times magnification of the sample from trial 12. Most powder particles are coalesced, and very few are still distinguishable as individuals.

4.3.3 Part Density

The original intent was to conduct tensile testing of produced parts once removed from the powder bed. However, due to the number of parts that were not able to be successfully removed from the print bed without damage it was determined that these results would be of questionable reliability. It was therefore decided that an alternative form of quantitative comparison would be needed. There is an explored relationship between density and tensile strength of laser sintered parts in existing literature [65, 76], as well as flexural modulus [77], finding that denser parts have greater physical properties. This means that while tensile strength, often used as an indication of the functional usefulness of a part, is not able to be directly measured we are able to compare an alternative for the purposes of evaluating the print parameters, and values such as the EMR.

4.3.3.A Density Sample Preparation

In ideal circumstances a part of known size and therefore volume would be obtained to enable the most reliable means of calculating part density from measured mass. However, as visible below in Figure 4.10, some parts had defects, meaning part features were incomplete, and difficult to accurately measure. To remedy this, sections of the printed parts were chosen, trimmed to a rectangular shape, at which point the sizes and masses were measured.

Figure 4.10: A dog bone produced during trials. On the right-hand side a defect is visible.

The sections chosen for this were those identified to be the more complete sections of the part, with the intention of minimising the loss of material during handling caused by handling unsintered powder. The complete list of dimensions and masses measured for each part is available in Appendix C. Samples were trimmed using a sharp modelling knife, and by cutting slowly with light pressure. Samples were trimmed until edges were square and flat, ensuring measured dimensions would be accurate. Dimension measurements were taking using CD-6 ASX Digital Vernier Caliper set (Mitutoyo Corporation, Japan). Mass measurements were taken using a Entris2241-1S Electronic Balance (Sartorius Lab Instruments Gmbh & Co, Germany). Data was analysed in Excel 2016 (Microsoft Corporation, USA).

4.3.3.B Results from Sample Measurements

A complete set of measurements taken from all samples is available in Appendix C. From these dimensions a volume can be calculated for each sample, and when combined with the mass measurements a value for density can be calculated. These values were averaged across samples from each bed position of the experimental trial, giving Mean Density for each trial. This was done to ensure that the effect of the position of the part on the print bed had no effect on the density results. Shown below is a Surface Plot of these Mean Densities, against the independent variables for the experimental trials, Print Bed Temperature (°C) and Laser Scan Speed (mm/s).

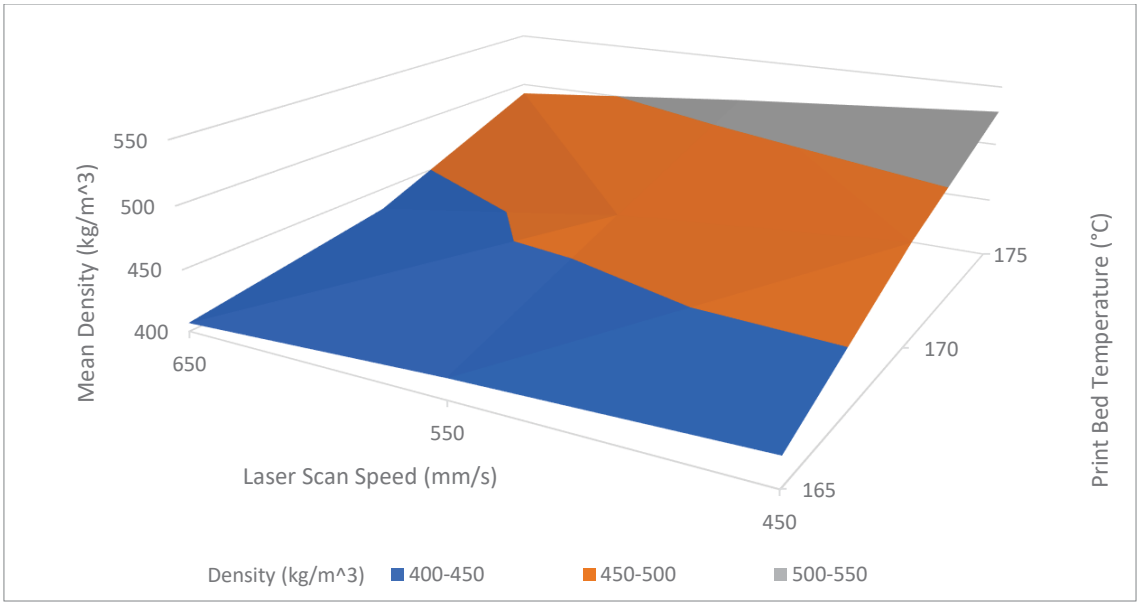

Figure 4.11: Surface Plot of Mean Density of each experimental trial.

As seen in the Surface Plot, the Mean Density of each experimental trial increased as the energy density of the print increases, which is caused by an increase in either Print Bed Temperature, or a decrease in Laser Scan Speed.

4.4 Discussion

The purpose of this chapter was to test the effectiveness of the existing modelling methods in their ability to predict print parameters which would lead to successful sintering, based on the methods of powder characterisation undertaken in Chapter 3. Following the trials undertaken in this chapter, successfully produced samples were assessed qualitatively, by the ability for the part to be removed from the powder cake, as well as their appearance during SEM imaging. Parts were also assessed quantitatively, by calculating the Mean Density of each experimental trial. These assessments allow for a balanced assessment on the models in the section on the ability to produce a successful part using the SW and EMR models.

4.4.1 Print Parameter Predictions

As discussed at the beginning of this chapter, the EMR calculations for all trials were above a value of 1, indicating that sintering should successfully occur at print parameters of all trials. When characterising the two powders in Chapter 3, there was no significant difference that was measured between the two powders.

All current methods of characterising the powders, such as the Sintering Window and the Energy Melt Ratio determined that the two powders should have successfully sintered. It was therefore unexpected that the Precimid 1170 powder failed to sinter even when exposed to 9 times the minimum amount of energy required for sintering to occur, as calculated with the EMR.

4.4.2 Removal From Powder Cake

None of the trials for the Precimid 1170 powder were successful in creating a part that could be removed from the powder cake. In additional, further testing to determine what settings would be required to attain a sintered part using Precimid 1170 powder resulted in the Sintratec kit overheating and switching off, which would indicate that the settings cannot be attained without potentially damaging the machine. This suggests that some of the energy being inputted into the powder is not being absorbed by the powder, which is reinforced by the fact that the machine was overheating during the printing process when further testing was conducted.

An exploration of published literature for possible reasons for this did not identify any previous published research that could explain this. In addition to this, the Sintratec PA12 Black did not successfully produce parts that could be removed from the powder cake in trial 2, where the EMR value was greater than 2. This suggests that there is a factor of energy loss present for the Sintratec PA12 Black powder, despite being recommended for this printer by the manufacturer.

The fact that the Sintratec PA12 Black parts produced with the highest EMR values required removal of excess powder with a wire brush instead of a paint brush suggests that bonding is excessive. Post-processing of this nature risks damaging finer details of some parts, and could be considered a failure to successfully process the material. However, there is means of indicating this behaviour with the EMR, posing a risk to operators who choose to print with higher EMR values as a means of avoiding insufficient energy density in parts.

4.4.3 Scanning Electron Microscope

Despite the SW and EMR not successfully predicting the print parameters required for the Precimid 1170 powder, there was an observable trend that necking between particles and general coalescence in the part, which increased as the EMR values increased. This suggests that while the EMR value still has limitations in predicting the minimum amount of energy required to successfully produce a part, it was useful for classifying the quantity of energy being put into the part. This is a result that matches results from previous literature [43], indicating that this situation is not unique to the Sintratec machine or this study.

4.4.4 Density

The relationship between energy density and part density has been reported to vary, and appears to be dependent on material properties. Some authors have reported that increased energy density leads to an increase in crystallinity [28], which in turn leads to greater physical properties like Tensile Strength. However, other authors have reported that after initial gains in part density, further increases in energy density have led to a decrease in party density [64], due to gas trapping by polymer degradation. While it is unclear in this instance if material degradation has occurred, there is certainly a clear positive relationship between part density and energy density of the print parameters.

It does not appear as if either of the two independent variables has a more significant effect than the other, as trials with similar energy densities, as calculated by the EMR value, have similar Mean Densities. This can be observed in data from the trial with a Laser Scan Speed of 450 mm/s and a Bed Temperature of 165 °C, and the trial with a Laser Scan Speed of 650 mm/s and a Bed Temperature of 170 °C. This does correlate with previous literature, where the effect of print parameters has more of a known effect on failure modes [78].

It may be possible with future work to classify a part density which correlates with the onset of excessive unintended melting, as seen with the higher EMR value builds. Looking at the Surface Plot, it does appear as if there is a region on the plot at which part feature definition becomes lost when the part is removed from the print bed due to unintended bonding of surrounding parts. It is difficult to obtain this level of detail from the results of this experimental set due to the small number of trials conducted limiting the data set available. With a larger number of trials, and a more varied set of EMR values this could be possible. If this data was correlated with other attempts at quantifying the degree of crystallinity of SLS prints, such as the work down with Degree of Particle Melt [79, 80] there could be another useful metric for the EMR equation that enables operators to better understand their print parameter selection, streamlining new material adoption processes.

One thing that is missing from existing methods of powder classification and modelling methods is accounting for potential losses than occur during the printing process. In addition to this, the absorption of the laser is not considered in the material properties, meaning that all laser energy emitted by the machine is assumed to be absorbed, and contribute towards the powder being heated. This may not always be the case, as laser energy may be reflected, or absorbed and re-emitted, as in fluorescence.

4.5 Chapter Summary

This chapter covered the experimental procedure undertaken to assess the current methods of characterising SLS powders are sufficient. After determining print parameters that predicted successful sintering for both powders during experimental trials, the trials were conducted. While no parameter combination tried resulted in successful production of a part using the Precimid 1170 powder, the Sintratec PA12 Black powder had trials that resulted in a range of parts that demonstrated insufficient bonding of material, successful bonding of material, and excess unintentional bonding. Further assessment of the Sintratec PA12 Black parts confirmed a likely relationship between EMR values and crystallisation of material in parts produced.

From these results it was determined that while the EMR and SW models have some use in quantifying the energy input into parts, it has some weakness for determining minimised print parameters for successful sintering. It has been noted that both the SW and the EMR models lack any sort of recognition of the fact that laser energy is reflected by the powder during sintering, and this represents a source of energy loss in the sintering process. To improve the accuracy of the current models a means of usefully quantifying these losses needs to be identified.

In Chapter 5, some possible ways of quantifying these losses will be assessed. These will be done with reference to the two powders already used in this study, and will reference to the results of Chapter 3 and 4, with the intent of better explaining the results of the experimental trials of Chapter 4.

Chapter 5 Investigation into Optical Properties of Sintering Powders

5.1 Chapter Overview

Additional experimentation is undertaken to identity contributors to the results seen in Chapter 4, namely the failure of the Sintering Window (SW) and Energy Melt Ratio (EMR) models to predict print parameters required for sintering to occur successfully within the two parts. The objective of this additional experimentation was to further characterise the properties of the two sintering powders using Spectrofluorophotometry, and Fourier Transform Infrared Spectroscopy (FTIR) analysis.

Trials in Chapter 3 focused on methods used in previous studies and classified powders based on thermal considerations, like the melting temperature, specific heat capacity, and powder flow considerations like packing fractions. In these categories the two powders showed many similarities, and existing models predicted that the two could be successfully sintered using a set of common printing parameters. However, none of these methods considered the colour of the two powders, and the effect this has on the energy requirements.

The common parameters tested in the design of experiment trials in Chapter 4 did not sinter the Precimid 1170 powder, while the Sintratec PA12 Black successfully sintered, provided the EMR value was greater than 2.925. Further testing indicated that the Sintratec Kit printer was unable to deliver enough energy to cause sintering before overheating.

While previous research has focused on the reflection of laser energy from the powder surface, studies found that powder size and packing fraction had a significant effect on levels of reflectance [56, 69]. Laumer *et al.* (2016) noted during a classification of optical properties of sintering powders that "another reason for the material behaviour needs to be considered: the optical material characterisation of the basic polymer" [67]. It is therefore important to classify optical properties, and investigate whether these properties may explain energy losses not reflected in the model. The work in this chapter will do this using Spectrofluorophotometry and Fourier Transform Infrared Spectroscopy (FTIR). Spectrofluorophotometry will identify differences in energy losses through fluorescence, while FTIR will give an absorption spectrum for the two powders across a range of wavelengths.

5.2 Spectrofluorophotometry

The spectrofluorophotometer will determine the amount of fluorescence that occurs across a spectrum when the material is excited by a focused input of a given wavelength. In the context of this study this is critical because it is important for determining the effect the input of the laser has during the Selective Laser Sintering (SLS) process. The greater the amount of fluorescence that occurs, the greater the proportion of energy not being converted to heat energy.

5.2.1 Machine Used for Testing

The machine used is the Shimadzu RF-600 Spectrofluorophotometer, operated using the LabSolutions RF software (Shimadzu Scientific Instruments, USA). Results were also processed within the LabSolutions RF software.

5.2.2 Method Used for Testing

Samples were placed into a clean, dry cuvette, which was then gently tamped to minimise transmission through the powder. The cuvette was then placed into the machine, and positioned at a 45-degree angle to the excitation beam. This was done due to the likely low transmittance of the excitation sources through the powder, therefore better enabling the emissions detector to absorb emissions from the surface of the sample facing the excitation beam.

An excitation versus emissions sweep was conducted from 350 nm to 800 nm, with the settings listed in table 1 below.

Table 5.1: Table of Machine Settings for Spectrofluorophotometry

Measurement Settings		Instrument Settings	
Parameter	Value	Light Source	Xenon Arc Lamp
Spectrum Type	3D	Signal Processing	Analogue
Excitation Wavelength Band	350 nm -800 nm	Excitation Bandwidth	3 nm
Emission Wavelength Band	350 nm – 800 nm	Emission Bandwidth	5 nm
Data Interval	5 nm	Sensitivity	High
Scan Speed	12000 nm/min		

5.2.3 Results

Results of the trials are displayed using the LabSolutions RF software in a contour plot, of excitation wavelength against emissions wavelengths, with intensity of emissions (measured in Fluorescence Intensity) signified by the colour of the contours. Some intense emission absorptions are visible at the excitation wavelengths, forming a diagonal line across the results. As emissions cannot be more energetic than their excitation wavelength, all values above this diagonal line can be ignored for the purposes of interpretation.

The Precimid 1170 powder shows some fluorescence when excited with the same wavelength light as the Sintratec Kit laser, at 445 nm. The emissions of this fluorescence start at around 750, and intensifies at the end of the emissions detection bandwidth, at 800 nm, as visible below in figure 1. The intensity of the fluorescence emissions is approximately 10% of the highest value emission.

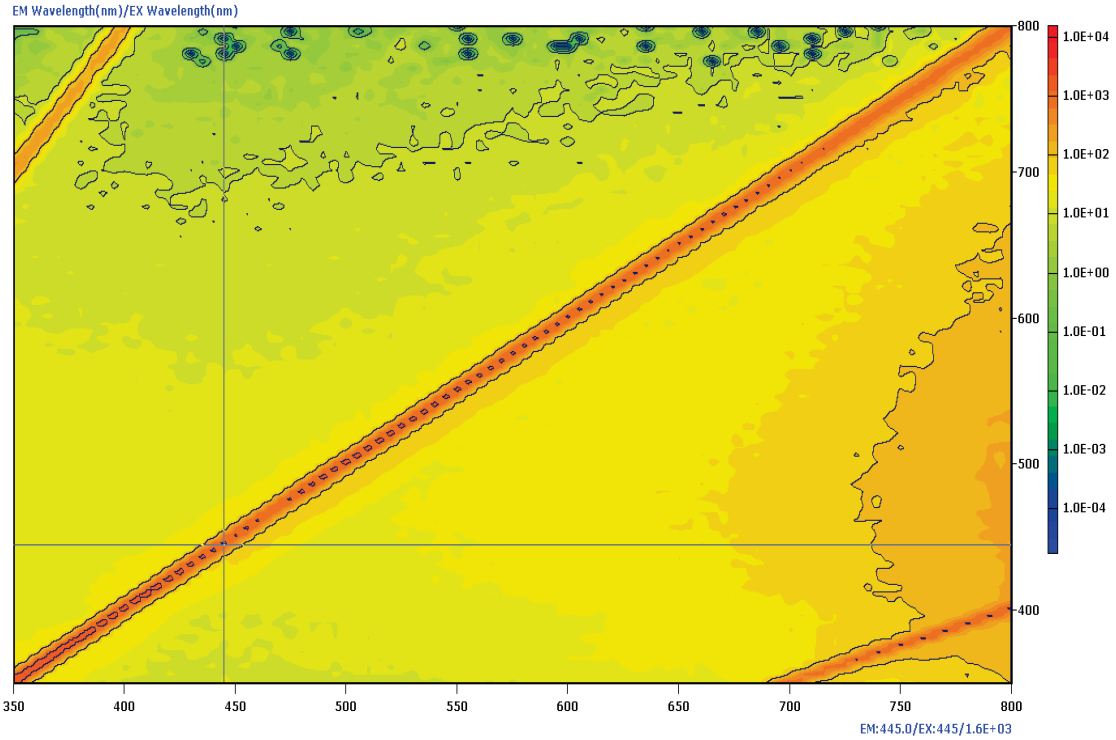

Figure 5.1: Contour plot of Excitation wavelength versus Emissions wavelength for the Precimid 1170 powder.

The Sintratec PA12 Black produced comparable results, but with lower intensity at the same wavelengths when compared to the Precimid 1170, with fluorescence emissions maximising at around 1%. The fluorescence also occurred at a much narrower wavelength than the Precimid 1170 as well, with the contour occurring above emission wavelengths of 780 nm.

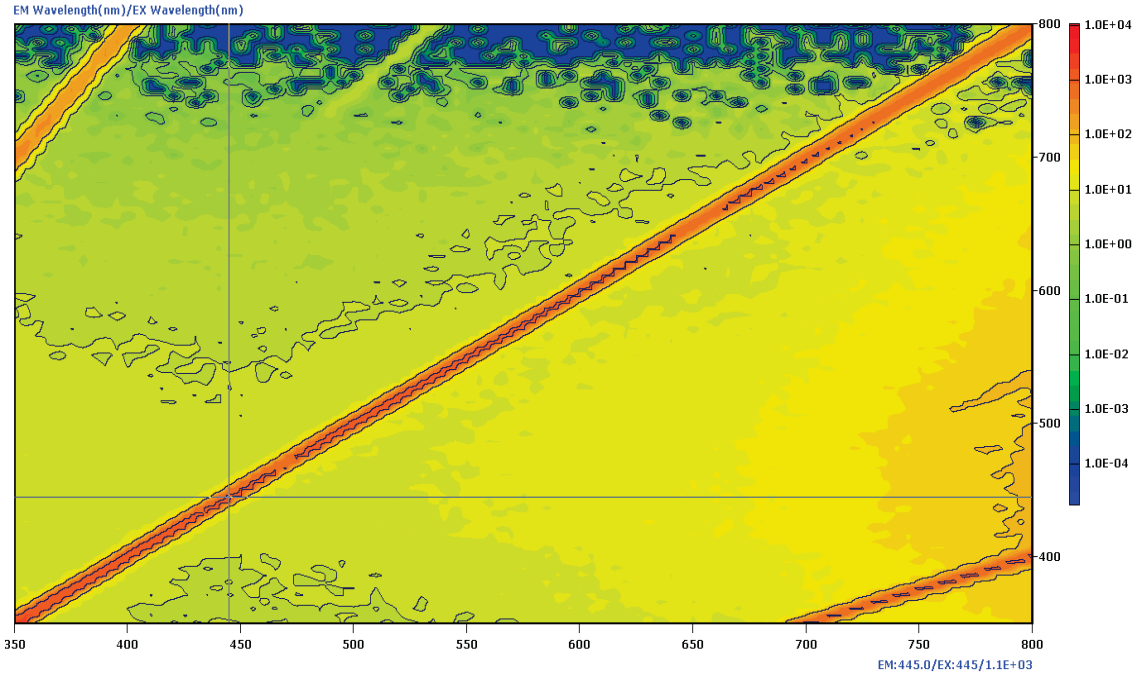

Figure 2: Contour plot of Excitation wavelength versus Emissions wavelength for the Sintratec PA12 Black.

5.3 Fourier Transform Infrared Spectroscopy

Fourier Transform Infrared Spectroscopy is used to gather a spectrum of absorption of a material when exposed to a broad range of wavelengths. As mentioned previously in Chapter 2, there is previous use of FTIR in literature as a means of classifying material absorbance of energy, in particular at the CO_2 laser wavelength [68]. By specifying a wide enough bandwidth of measurement, it should be possible to measure not only the absorption of the two materials at the bandwidth of the Sintratec Kit laser, at 445 nm, but also of the near and mid-range infrared wavelengths that would correlate to the heat lamps that the kit uses to heat the powder. This would enable a classifying of the absorption of the two key forms of energy input for the kit, which is key to explaining the results of the design of experiment seen in Chapter 4.

5.3.1 Machine used for Testing

The unit used for these experiments is a Bruker ALPHA Spectrometer, running on the Bruker OPUS software package (Bruker Optik GmbH., Germany). The machine fitted with a diamond attenuated total reflectance (ATR) crystal, which enables the direct measurement of powder without further preparation. The machine was calibrated with a background spectrum test before use, and was cleaned with acetone between samples.

5.3.2 Method used for Testing

Virgin samples of each powder were used, with a laboratory spatula used to spoon enough material onto the ATR crystal to cover it completely. The anvil was lowered until it applied firm pressure against the sample and the ATR crystal.

5.3.3 Results of Testing

The OPUS software displays the results of the trials using Absorbance Units (AU), as shown in Figure 5.2 below. This is done to provide a more easily visualized comparison of the absorbance of the two powders.

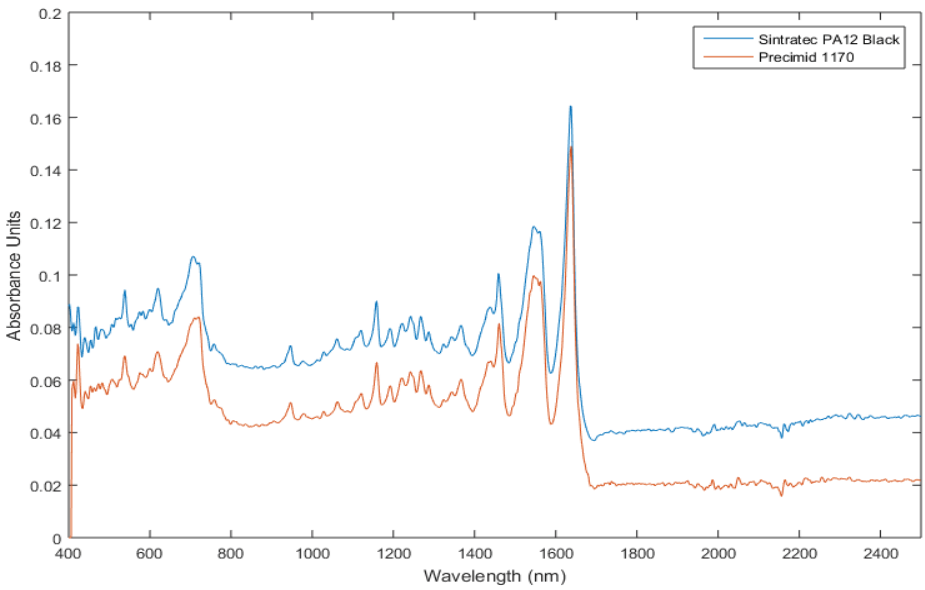

Figure 5.2 Absorbtance of the powders over Wavelength of light.:

To provide a method of comparison that enables classification of the powders by energy losses the data can be transformed to show powder energy transmittance as a percentage. The data is transformed according to the Beer-Lambert Law, shown below as Equation 5.1, where transmittance is described as the ratio of the intensity of the transmitted light (I) to the intensity if the incident light (I_o) where A is Absorbance, I is the transmitted light, and I_O is the incident light.

$$A = log_{10}\left(\frac{I_o}{I}\right) \tag{5.1}$$

The calculated transmittance is graphed below, in Figure Three. The transmission of the of the Sintratec PA12 black powder is lower at all points than the Precimid 1170 powder, indicating it absorbs more of the light. The characteristic absorption peaks are at the same wavelengths, and the differences in transmission is much smaller at these points. The OPUS software identified both powders as of the Polyamide-12 family. The measurements at the four lowest wavelengths for the Precimid 1170 are reported to be 100% transmission, which would appear to be an error. At the wavelength of the Sintratec Kit laser, 445 nm, the transmittance of the Sintratec PA12 Black powder is only 3.781 % lower than the Precimid 1170 (84.51% versus 88.29%). Removing the four lowest wavelength measurements to remove the error as a possible source of bias, the average transmittance across all remaining values is 87.23% for the Sintratec PA12, and 92.01% for the Precimid 1170.

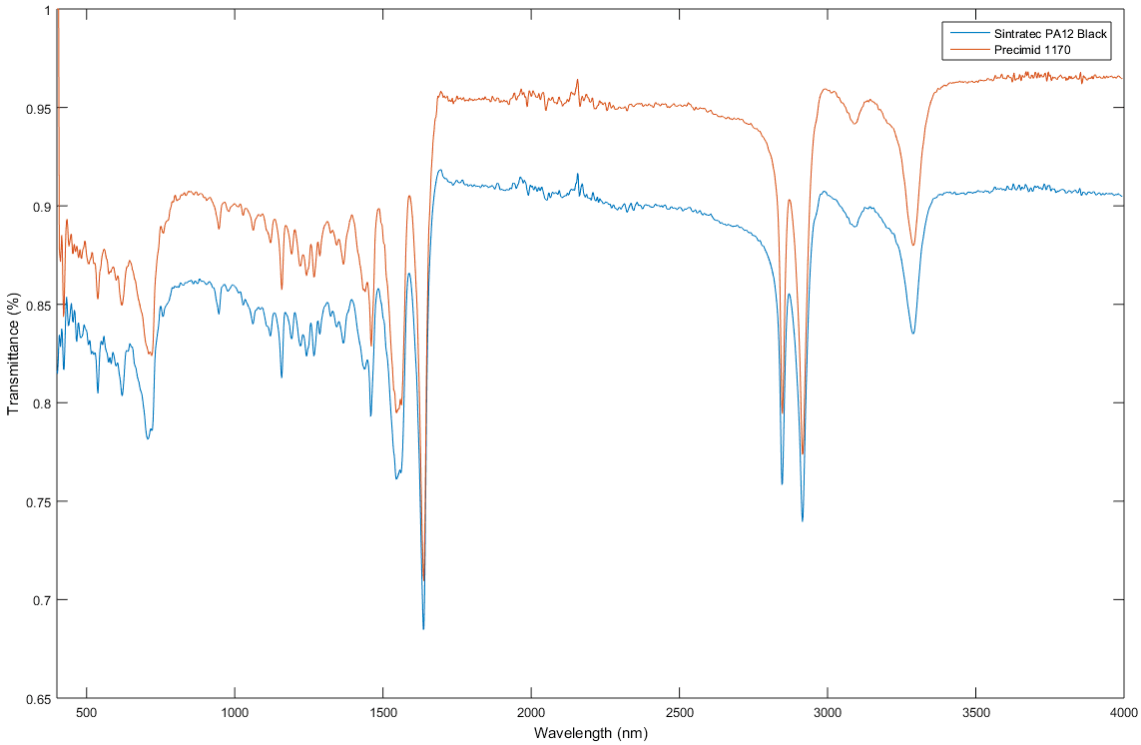

Figure 5.3: Transformed FTIR values to show transmittance of light through the sample against wavelength of light measured.

5.4 Discussion

While no literature exists on the use of the Spectrofluorophotometer as a means of classifying SLS powders currently, the nature of the material used in the powders make the results unsurprising. Nylon is chosen for use in sintering due to its stable nature, both in resistance to decomposition to heat, as well as many common solvents. This is due to strong molecular bonds, which would require significant energy to break. This means that the fact the material has minimal fluorescence is not surprising, however it must be noted that the Sintratec PA12 Black powder does emit less, not only in terms of intensity, but also in terms of wavelengths of emissions.

The samples were placed into the machine on a 45-degree angle, to increase the chance of emissions being successfully detected. This had an added effect on increasing the amount of scattering that occurred, which is visible as emissions detected at the excitation wavelength, shown as a diagonal line across the results graph. The effect of this is that it effectively scales the results according to the excitation source strength. We can see that the emissions at the 445-nm wavelength are much smaller than the excitation wavelength, suggesting that losses are minimal, although present. The fact that spectrofluorophotometry uses the arbitrary unit of Fluorescence-Intensity units makes such small emissions hard to quantify for the purposes of improved modelling, however the two powders do have an observable difference, which could contribute to energy losses during sintering.

The FTIR results show a clear difference between the two powders when the data is transformed to show transmittance. The results from the FTIR are similar to those found by previous authors [68], although the authors of previous work have shown the data as the complementary absorbance, as opposed to transmittance. The results also show that the Sintratec PA12 Black does absorb a greater percentage of the 445-nm wavelength energy, however only by less than 4%. This indicates that the results of these tests are indicative of the differences only, and do no show the differences in losses between the two powders that would be required to explain the results in Chapter 3.

The characteristic absorption wavelengths that identify both powders are Polyamide-12 also shows that there is a lack of any chemical contaminant that could have caused the differences in the results seen in Chapter 3. This is interesting given that the Sintratec PA12 Black was likely dyed to attain the black colour. Previous work does cover the use of black powders [68], noting that their colouring is likely used to improve laser absorption, however the effect of the colour on the powder is not examined in depth as done here. The results from this test have significance in showing the effect that colouring has on a powder, which is a material property that has otherwise been yet unexplored.

While the SW and EMR models do account for basic thermal and physical characteristics of the material, they fail to account for any optical properties of the material. The two tests do demonstrate there are measurable optical properties that can be classified by existing testing processes. This is significant because further classification of properties allows for more refined models that can account for potential energy losses, enabling greater accuracy. Given that the two materials are so similar, it is crucial that more methods are explored to model how the material will react during the sintering process.

5.5 *Chapter Summary*

In this chapter the aim was to conduct experimentation to classify previously unconsidered optical properties of the two SLS powders for the purposes of improving the existing models used to predict the minimum print parameters required for successful sintering.

To achieve this both powders were characterised by FTIR and Spectrofluorophotometry processes to determine their responses to a range of wavelength excitations, such as absorption, and fluorescence. There was an identifiable difference in the response of the two powders, which can partially be attributed to the difference in colour of the two powders.

However, the results do not provide sufficient explanation for the findings from in the experimental trials from Chapter 4, as the differences are not great enough to explain why sintering does not occur for the Precimid 1170 powder when the EMR predicts the energy being inputted is over nine times the required amount to cause sintering to occur.

In Chapter 6, the results of this will be discussed with implication for the effectiveness of the existing models, with respect to their ability to be improved upon in future research.

Chapter 6 Discussion

6.1 Chapter Overview

Selective Laser Sintering (SLS) has significant potential as an Additive Manufacturing (AM) process. However, to stimulate this growth, there needs to be an increase in the range of materials available for printing. Key to enabling this, is that operators can determine what printing parameters are required to process these new materials. This chapter aims to examine the results of this study with respect to the objectives outlined in Chapter 1.

These objectives are:

1. Identify the current existing models used to determine printing parameters for a new material
2. Identify weaknesses in current modelling processes
3. Conduct experimentation to explore the validity of these weaknesses.
4. Explore opportunities to improve the print parameter model to address these weaknesses

6.2 Existing Models

As identified in Chapter 2, there are several existing models that operators can use to predict the parameters required when printing with new materials. Between the Sintering Window (SW) and the Energy Melt Ratio (EMR) operators can identify most of the common temperature parameters, such as chamber and print bed temperatures [3, 11, 35], as well as laser scan settings, like scan speed and scan count [12, 56]. By providing the operator with models for identifying these parameters, one of the most difficult challenges when using a new material can be reduced. By having an accurate method of calculating what print parameter values will lead to successful prints, operators will require fewer failed prints to bring new powders into service. Reducing the barriers to operators being able to utilize new powders provides greater incentive for them to try new materials.

6.3 Identified Weaknesses

Both the SW and EMR models are useful because they offer operators a means of identifying parameter values for sintering, and they are also simple to implement. Both the SW and EMR primarily rely on values that are obtained through Differential Scanning Calorimetry (DSC), and can utilize an ASTM-standardized testing technique to obtain relevant values [45]. The material specification sheets provided by some manufacturers often contain these values as well [81]. This enables operators to easily obtain the values, either through the specification sheets, or by contracting out these testing processes. This frees operators from having to purchase expensive specialized testing equipment, thus reducing some of the barriers to printing using new materials.

However, part of the simplicity of these models comes from the fact that they are limited in their acknowledgement of material behaviours. They are sufficient at acknowledging energy requirements for sintering, but do not address the losses that can occur during sintering, especially with respect to the laser heating a powder bed. This means that existing models do not accurately predict the print parameters that will lead to a successful print. We see confirmation of these in the difference between the predictions of sintering seen in Chapter 3, and the results of the sintering in Chapter 4.

6.4 Validity of Identified Weaknesses

Despite the characterisation of the powders in Chapter 3 predicting that all trials would result in successful sintering, there were no successful print results for the white Precimid 1170 powder. Additionally, model predictions of success for the Sintratec PA12 Black powder for print parameter with the lowest EMR values were incorrect, despite them predicting twice as much energy required for sintering to occur. While previous studies have acknowledged limitations in the accuracy of the EMR model at low laser energy density values [43], there is little literature exploring this topic, and none with intent to explore the limitations of the model such as seen in this thesis research.

The models were not without value to operators, as they did see some success with the Sintratec PA12 Black powder, providing a useful indication of coalescence, as well as correlating EMR values with density, which in turn has been linked to mechanical properties such as strength. While the original intent was to provide tensile strength results, the limited success in printing complete parts that could be removed successfully from the powder cake without fracturing made this unfeasible. Future work could remedy this by increasing both the number of parts produced in a print, as well as increasing the number of trials for each printer setting to ensure the best chance of printing complete parts that are amenable for tensile testing. As it was the parts produced in this research were still able to be classified by the density of the parts produced, and by using Scanning Electron Microscope to observe particle coalescence.

Another limitation of the two print parameter prediction models used (SW and EMR) was the inability to determine when an excess of energy was being inputted to the print bed during printing, causing solidification of the powder cake, with excess powder melting to the part. While previous studies have discussed an EMR value related to material degrading thermally [56], there has not yet been a means of classifying when a part achieves a full melt. Classification of this would enable operators to narrow the energy window the machine operates in to reduce the chance of this excess melting occurring. Some literature exists classifying parts according to degree of particle melt [79], so a means of correlating this concept and EMR to provide operators with a means of classifying the state of coalescence numerically would enable operators to set a more useful upper bound for the energy input of the printing process.

6.5 Improvements To The Models

Previous work on the EMR model has been conducted using commercial-grade CO_2-laser machines [43, 45, 56]. This is important because there is existing knowledge in literature about the reflectance of a powder material having a dependence on the wavelength of the laser used [69, 70]. No previous research has been conducted with a SLS printer with a laser with a wavelength of 445 nm, such as the one used in the Sintratec Kit, so no direct comparisons can be drawn.

Previous studies have established the absorptance of similar polyamide powders at values around 90% of energy emitted from CO_2 lasers, with a wavelength of 10.6µm [67, 82]. This means that a relatively small amount of energy is being lost to reflection, which could have contributed to a lack of further research as to possible improvements to the model. Laumer *et al.* (2016) established that changing wavelengths from 10.6µm to 1.94 reduces the absorptance of a polyamide from above 90% of energy emitted to below 50% of energy emitted, a significant amount of energy now being wasted.

The results of Chapter 4 indicate that energy losses may be around this number, as sintering did not successfully occur when using the Sintratec PA12 Black in trials with an EMR values of 2.517, but sintering was observed at the next greatest energy density, 3.077. There is mention in existing literature about the EMR failing to predict the necessary energy required to achieve sintering, even with a CO_2 laser [43].

Ideally a measure of reflectance would be conducted using the experimental setup shown by Laumer *et al.* (2016), however, as noted in Chapter 3 this experimental setup is a specialized one not found commonly in laboratories. The resources required to recreate such a setup were beyond the scope of this project, and attempts to find similar laboratory setups were unsuccessful. While integrating spheres do find use in existing laboratories, the physical arrangement of these setups is often unsuitable, with specimen holders being mounted in the horizontal position, meaning pure loose powder cannot being easily measured. The prospect of purchasing specialised equipment such as this would represent a barrier for an operator considering trialling new materials, and as such alternative methods of measuring optical properties were explored in Chapter 5.

Previously literature measuring reflectance of SLS powders has noted that there is a relationship between reflectance and mean particle size, and consequently powder packing fraction [67, 82]. As noted in Chapter 3, packing fractions for the two materials used in this study were very similar, indicating similar particle size and packing efficiencies between the two powders. This is backed up by observations made using Scanning Electron Microscope of both powders, showing both powders to have similar particle sizes and morphologies, as well as particle surfaces. Laumer *et al.* (2016) explores this relationship further, noting that absorption behaviours of powders are dependent on absorption behaviours of single particles, and thus of the material behaviours. This shows the need for further powder classification of powders by their material behaviours rather than solely by powder behaviours, such as powder flow measurements.

There is a lack of literature on the differences between two similar powders of different colours in a larger context, however again the relationship between wavelength and absorption could play a key part in explaining this. Because the losses through reflection as so minimal, as mentioned earlier, any changes in absorption due to colour may have been so minimal that they did not attract researchers' attention before. This study appears to be the first time the colour of a powder plays a significant part in the ability for a powder to be sintered in a SLS printer.

Fourier Transform Infrared Spectroscopy (FTIR) has been utilized in previous works as a classifying the material absorption of SLS powders [35]. It has been used previously to show the differences in absorption between powders of different composition [69], including a black powder , but never to show the differences between to similar powders of different colours [68]. The results in Chapter 5 indicate that FTIR can be used as a method of exploring the difference in material absorption properties between the two different coloured powders. The black powder absorbed more than the white powder across all wavelengths, which fits with the results seen within Chapter 4 of the white powder not sintering at EMR values that the black powder successfully sintered at.

The biggest limitation of using FTIR as a means of classifying the absorption of the materials is that while it is useful for indicating differences in absorption of materials it does not provide a true representative value of the amount of energy being absorbed during the sintering process, unlike processes such as those using integration spheres [70]. Therefore, while FTIR does provide the ability to confirm suspicions about the difference in material absorption of the two powders due to the difference in colour, it does not provide a method of quantifying the difference in a way that would enable refining of the model.

Another aspect of material behaviour that is not well explored in literature is the fluorescence behaviour of SLS materials. As mentioned previously, much of the existing literature surrounding energy density of SLS powders was conducted using CO_2 lasers. However, by changing wavelengths of laser it is possible that the interactions occurring between laser energy and powder particles has changed. In the presence of 10.6µm wavelength laser the material undergoes heating by excitation of the induced oscillations of the molecule chain, however when exposed to near-range infrared the behaviours change. Molecules instead undergo electronic excitation of electrons, leading to indirect excitation [67]. The Sintratec Kit uses a 445-nm wavelength laser, which has even more energetic photons than near-range infrared, which could cause energy to be re-emitted as photons rather than converted to phonons. There is no previous literature examining the fluorescence of powders, so the data has little comparative use. The re-emittance of fluorescent energy in this case appeared to be minimal, but could be subjective to material and wavelength, meaning that it may not be insignificant in all cases, as other powders may react differently.

Chapter 7 Conclusion

For Selective Laser Sintering (SLS) to experience growth in markets previously serviced by other methods of Additive Manufacture (AM) it must expand the range of materials that can be processed into useful products. Today only a small number of materials are available when compared to other AM technologies, limiting the applications that can utilize this technology. One of the biggest barriers to adoption of materials is the danger inherent to high-energy processes such as SLS. The aim of this research was to identify opportunities to improve current methods for modelling the relationship between material specifications, and printing parameters.

This aim was achieved though completion of 4 objectives, including:

1. Identifying current existing models used to determine printing parameters for a new material
2. Identify weaknesses in current modelling processes
3. Conduct experimentation to explore the validity of these weaknesses, and
4. Explore opportunities to improve the model to address these weaknesses

The current models to determine printer parameters to achieve successful sintering include both the Sintering Window (SW) and the Energy Melt Ratio (EMR). These two models are complementary, and the two are both required to establish all common print parameters. They include both thermal and physical powder properties, but do not include any optical properties. This is significant because the nature of the SLS printing process relies on concentrated delivery of laser energy to achieve successful sintering.

Experimental trials using two similar polyamide powders, one black and one white, identified that the two powders were similar thermally and physically, meaning that the models predicted that they should both sinter successfully utilizing the same set of print parameters. Results of the experiments were, that none of the trials involving the white powder sintered successfully, and trials involving the black powder suffered from issues with either insufficient energy to successfully remove them without disintegrating, or excessive energy causing excess powder to bond to the part.

Further experimentation was carried out to investigate the differences in optical properties using Fourier Transform Infrared Spectroscopy (FTIR) and Spectrofluorophotometry. FTIR revealed that there was a difference in absorption as a material property, despite similar particle size and shapes, indicating that differences in laser energy absorption could explain the results seen in the trials. Spectrofluorophotometry revealed minimal differences in fluorescence of the powders, suggesting it an unlikely source of energy loss within the sintering process.

Future work is recommended to include finding some standardized form of testing setup that can be used to categorize the reflectance of a material, as current work relies on proprietary experimental setups. Finding methods of classifying the laser absorption that would avoid these setups would remove another barrier for operators, and enable refinement of the EMR equation to reflect the energy losses during printing.

In addition to this, further work is also recommended in establishing the relationship between the EMR and Degree of Particle Melt to provide a more concise energy envelope for operators to select parameters for. This would reduce the chance of operators fusing parts into the powder cake with unintentional powder melting due to excess energy.

Bibliography

[1] J. Kruth, G. Levy, and R. Schindel, "Consolidation of Polymer Powders by Selective Laser Sintering, PMI 2008," in *International Conference*, 2008, pp. 17-19.

[2] J. Gardan, "Additive manufacturing technologies: State of the art and trends," *International Journal of Production Research,* vol. 54, pp. 3118-3132, 2016.

[3] M. Schmid, A. Amado, and K. Wegener, "Materials perspective of polymers for additive manufacturing with selective laser sintering," *Journal of Materials Research,* vol. 29, pp. 1824-1832, 2014.

[4] J.-H. Zhu, W.-H. Zhang, and L. Xia, "Topology optimization in aircraft and aerospace structures design," *Archives of Computational Methods in Engineering,* vol. 23, pp. 595-622, 2016.

[5] A. Standard, "ISO/ASTM 52900: 2015 Additive manufacturing-General principles-terminology," *ASTM F2792-10e1,* 2012.

[6] B. Wendel, D. Rietzel, F. Kühnlein, R. Feulner, G. Hülder, and E. Schmachtenberg, "Additive processing of polymers," *Macromolecular materials and engineering,* vol. 293, pp. 799-809, 2008.

[7] C. W. Hull, "Apparatus for production of three-dimensional objects by stereolithography," ed: Google Patents, 1986.

[8] D. Gu, W. Meiners, K. Wissenbach, and R. Poprawe, "Laser additive manufacturing of metallic components: materials, processes and mechanisms," *International materials reviews,* vol. 57, pp. 133-164, 2012.

[9] B. Derby, "Additive Manufacture of Ceramics Components by Inkjet Printing," *Engineering,* vol. 1, pp. 113-123, 2015.

[10] R. Goodridge, C. Tuck, and R. Hague, "Laser sintering of polyamides and other polymers," *Progress in Materials Science,* vol. 57, pp. 229-267, 2012.

[11] M. Schmid, A. Amado, and K. Wegener, "Polymer powders for selective laser sintering (SLS)," vol. 1664, p. 160009, 2015.

[12] G. Vasquez, C. Majewski, B. Haworth, and N. Hopkinson, "A targeted material selection process for polymers in laser sintering," *Additive Manufacturing,* vol. 1, pp. 127-138, 2014.

[13] ASTM, "ASTM Additive Manufacturing Committee Approves Terminology Standard," ed: ASTM, 2009, p. 1.

[14] A. C. F. o. A. M. Technologies and A. C. F. o. A. M. T. S. F. o. Terminology, *Standard Terminology for Additive Manufacturing Technologies*: ASTM International, 2012.

[15] B. Berman, "3-D printing: The new industrial revolution," *Business horizons,* vol. 55, pp. 155-162, 2012.

[16] R. Van Noort, "The future of dental devices is digital," *Dental materials,* vol. 28, pp. 3-12, 2012.

[17] R. Jamieson and H. Hacker, "Direct slicing of CAD models for rapid prototyping," *Rapid Prototyping Journal,* vol. 1, pp. 4-12, 1995.

[18] H. Bikas, P. Stavropoulos, and G. Chryssolouris, "Additive manufacturing methods and modelling approaches: a critical review," *The International Journal of Advanced Manufacturing Technology,* vol. 83, pp. 389-405, 2016.

[19] J. W. Stansbury and M. J. Idacavage, "3D printing with polymers: Challenges among expanding options and opportunities," *Dental Materials,* vol. 32, pp. 54-64, 2016.

[20] M. Cotteleer, J. Holdowsky, and M. Mahto, "The 3D opportunity primer: The basics of additive manufacturing," *Retreived from http://d2mtr37y39tpbu. cloudfront. net/wp-content/uploads/2014/03/DUP_718-Additive-Manufacturing-Overview_MASTER1. pdf,* 2013.

[21] J.-P. Kruth, P. Mercelis, J. Van Vaerenbergh, L. Froyen, and M. Rombouts, "Binding mechanisms in selective laser sintering and selective laser melting," *Rapid prototyping journal,* vol. 11, pp. 26-36, 2005.

[22] M. Core-Baillais, H. Bensoussan, A. Richardot, and H. Kusnadi, "State of 3D Printing 2017," p. 32, 24 May 2017 2017.

[23] F. P. Melchels, J. Feijen, and D. W. Grijpma, "A review on stereolithography and its applications in biomedical engineering," *Biomaterials,* vol. 31, pp. 6121-6130, 2010.
[24] G. Goh, S. Agarwala, G. Goh, V. Dikshit, and W. Yeong, "Additive manufacturing in unmanned aerial vehicles (UAVs): Challenges and potential," *Aerospace Science and Technology,* 2016.
[25] T. Wohlers and T. Gornet, "History of additive manufacturing," *Wohlers report,* vol. 24, p. 118, 2014.
[26] B. J. Brooks, K. M. Arif, S. Dirven, and J. Potgieter, "Robot-assisted 3D printing of biopolymer thin shells," *The International Journal of Advanced Manufacturing Technology,* pp. 1-12, 2016.
[27] D. Roberson, C. M. Shemelya, E. MacDonald, and R. Wicker, "Expanding the applicability of FDM-type technologies through materials development," *Rapid Prototyping Journal,* vol. 21, pp. 137-143, 2015.
[28] D. L. Bourell, T. J. Watt, D. K. Leigh, and B. Fulcher, "Performance Limitations in Polymer Laser Sintering," *Physics Procedia,* vol. 56, pp. 147-156, 2014.
[29] P. Fischer, V. Romano, H.-P. Weber, N. Karapatis, E. Boillat, and R. Glardon, "Sintering of commercially pure titanium powder with a Nd: YAG laser source," *Acta Materialia,* vol. 51, pp. 1651-1662, 2003.
[30] N. Gardan and A. Schneider, "Topological optimization of internal patterns and support in additive manufacturing," *Journal of Manufacturing Systems,* vol. 37, pp. 417-425, 2015.
[31] D. Brackett, I. Ashcroft, and R. Hague, "Topology optimization for additive manufacturing," in *Proceedings of the solid freeform fabrication symposium, Austin, TX*, 2011, pp. 348-362.
[32] T. Zegard and G. H. Paulino, "Bridging topology optimization and additive manufacturing," *Structural and Multidisciplinary Optimization,* vol. 53, pp. 175-192, 2016.
[33] M. Tomlin and J. Meyer, "Topology optimization of an additive layer manufactured (ALM) aerospace part," in *Proceeding of the 7th Altair CAE technology conference*, 2011, pp. 1-9.
[34] K. V. Wong and A. Hernandez, "A review of additive manufacturing," *ISRN Mechanical Engineering,* vol. 2012, 2012.
[35] A. F. A. Becker, "Characterization and prediction of SLS processability of polymer powders with respect to powder flow and part warpage," Pontificia Universidad Católica de Chile, 2016.
[36] M. M. Tseng, J. Jiao, and M. E. Merchant, "Design for mass customization," *CIRP Annals-Manufacturing Technology,* vol. 45, pp. 153-156, 1996.
[37] J. H. Pallari, K. W. Dalgarno, and J. Woodburn, "Mass customization of foot orthoses for rheumatoid arthritis using selective laser sintering," *IEEE Transactions on Biomedical Engineering,* vol. 57, pp. 1750-1756, 2010.
[38] O. Diegel, S. Singamneni, S. Reay, and A. Withell, "Tools for sustainable product design: additive manufacturing," 2010.
[39] D. Eyers and K. Dotchev, "Technology review for mass customisation using rapid manufacturing," *Assembly Automation,* vol. 30, pp. 39-46, 2010.
[40] S. Rüsenberg, S. Josupeit, and H.-J. Schmid, "A Method to Characterize the Quality of a Polymer Laser Sintering Process," *Advances in Mechanical Engineering,* vol. 6, p. 185374, 2014.
[41] W. Zeng, Y. Guo, K. Jiang, Z. Yu, Y. Liu, Y. Shen, *et al.*, "Laser intensity effect on mechanical properties of wood-plastic composite parts fabricated by selective laser sintering," *Journal of Thermoplastic Composite Materials,* vol. 26, pp. 125-136, 2012.
[42] L. Verbelen, S. Dadbakhsh, M. Van den Eynde, J. P. Kruth, B. Goderis, and P. Van Puyvelde, "Characterization of polyamide powders for determination of laser sintering processability," *European Polymer Journal,* vol. 75, pp. 163-174, Feb 2016.
[43] S. Berretta, K. Evans, and O. Ghita, "Predicting processing parameters in high temperature laser sintering (HT-LS) from powder properties," *Materials & Design,* vol. 105, pp. 301-314, 2016.
[44] A. Amado, M. Schmid, G. Levy, and K. Wegener, "Advances in SLS powder characterization," *Group,* vol. 7, p. 12, 2011.
[45] M. Vasquez, "Analysis and development of new materials for polymer laser sintering," © Mike Vasquez, 2012.

[46] S. Ziegelmeier, P. Christou, F. Wöllecke, C. Tuck, R. Goodridge, R. Hague, *et al.*, "An experimental study into the effects of bulk and flow behaviour of laser sintering polymer powders on resulting part properties," *Journal of Materials Processing Technology,* vol. 215, pp. 239-250, 2015.

[47] S. Dadbakhsh, L. Verbelen, T. Vandeputte, D. Strobbe, P. Van Puyvelde, and J.-P. Kruth, "Effect of powder size and shape on the SLS processability and mechanical properties of a TPU elastomer," *Physics Procedia,* vol. 83, pp. 971-980, 2016.

[48] S. Berretta, O. Ghita, and K. E. Evans, "Morphology of polymeric powders in laser sintering (LS): from polyamide to new PEEK powders," *European Polymer Journal,* vol. 59, pp. 218-229, 2014.

[49] Y. Guo, W. Zeng, and K. Jiang, "Preparation and selective laser sintering of wood–plastic composite powers and post processing," *Digest Journal of Nanomaterials and Biostructures,* vol. 6, pp. 1435-1444, 2011.

[50] B. Liu, R. Wildman, C. Tuck, I. Ashcroft, and R. Hague, "Investigation the effect of particle size distribution on processing parameters optimisation in selective laser melting process," in *International solid freeform fabrication symposium: an additive manufacturing conference. University of Texas at Austin, Austin*, 2011, pp. 227-238.

[51] H. Mazhar, J. Bollmann, E. Forti, T. Osswald, and D. Negrut, "Studying the effect of powder geometry on the selective laser sintering process," 2014.

[52] M. Schmid, F. Amado, G. Levy, and K. Wegener, "Flowability of powders for selective laser sintering (SLS) investigated by round robin test," in *High Value Manufacturing: Advanced Research in Virtual and Rapid Prototyping: Proceedings of the 6th International Conference on Advanced Research in Virtual and Rapid Prototyping, Leiria, Portugal, 1-5 October, 2013*, 2013, p. 95.

[53] M. Van den Eynde, L. Verbelen, and P. Van Puyvelde, "Assessing polymer powder flow for the application of laser sintering," *Powder Technology,* vol. 286, pp. 151-155, 2015.

[54] W. L. Zeng, Y. L. Guo, and K. Y. Jiang, "Research on Powder Spreading Property Improvement of Wood-Plastic Composite SLS Rapid Prototyping Process," in *Applied Mechanics and Materials*, 2010, pp. 616-619.

[55] M. Krantz, H. Zhang, and J. Zhu, "Characterization of powder flow: Static and dynamic testing," *Powder Technology,* vol. 194, pp. 239-245, 2009.

[56] M. Vasquez, B. Haworth, and N. Hopkinson, "Methods for quantifying the stable sintering region in laser sintered polyamide-12," *Polymer Engineering & Science,* vol. 53, pp. 1230-1240, 2013.

[57] J. Schmidt, M. Sachs, C. Blümel, B. Winzer, F. Toni, K.-E. Wirth, *et al.*, "A novel process route for the production of spherical LBM polymer powders with small size and good flowability," *Powder Technology,* vol. 261, pp. 78-86, 2014.

[58] J. Schultz, J. Martin, R. Kander, and C. Suchicital, "Selective Laser Sintering of Nylon 12-PEEK Blends Formed by Cryogenic Mechanical Alloying," in *Proceedings SFF Symposium, Austin (TX), USA*, 2000, pp. 119-124.

[59] T. Vítěz and P. Trávníček, "Particle size distribution of sawdust and wood shavings mixtures," *Research in agricultural engineering,* vol. 56, pp. 154-158, 2010.

[60] M. Salemane and A. Luyt, "Thermal and mechanical properties of polypropylene–wood powder composites," *Journal of Applied Polymer Science,* vol. 100, pp. 4173-4180, 2006.

[61] S. Ziegelmeier, F. Wöllecke, C. Tuck, R. Goodridge, and R. Hague, "Characterizing the bulk & flow behaviour of LS polymer powders," in *Proceedings SFF Symposium, Austin (TX), USA*, 2013.

[62] W. Zeng, Y. Guo, K. Jiang, Z. Yu, and Y. Liu, "Preparation and selective laser sintering of rice husk-plastic composite powder and post processing," *Digest Journal of Nanomaterials and Biostructures,* vol. 7, pp. 1063-1070, 2012.

[63] D. Drummer, M. Drexler, and K. Wudy, "Impact of heating rate during exposure of laser molten parts on the processing window of PA12 powder," *Physics Procedia,* vol. 56, pp. 184-192, 2014.

[64] Y. Khalil, A. Kowalski, and N. Hopkinson, "Influence of energy density on flexural properties of laser-sintered UHMWPE," *Additive Manufacturing,* vol. 10, pp. 67-75, 2016.

[65] B. Caulfield, P. McHugh, and S. Lohfeld, "Dependence of mechanical properties of polyamide components on build parameters in the SLS process," *Journal of Materials Processing Technology,* vol. 182, pp. 477-488, 2007.

[66] V. S. Sharma, S. Singh, A. Sachdeva, and P. Kumar, "Influence of sintering parameters on dynamic mechanical

properties of selective laser sintered parts," *International Journal of Material Forming,* vol. 8, pp. 157-166, 2015.

[67] T. Laumer, T. Stichel, K. Nagulin, and M. Schmidt, "Optical analysis of polymer powder materials for Selective Laser Sintering," *Polymer Testing,* vol. 56, pp. 207-213, 2016.

[68] L. Fielder, "Evaluation of Polypropylene powder grades in consideration of the laser sintering process ability," *Journal of Plastics Technology,* vol. 3, pp. 34-39, 2007.

[69] K. Fan, K. Wong, W. Cheung, and I. Gibson, "Reflectance and transmittance of TrueFormTM powder and its composites to CO2 laser," *Rapid Prototyping Journal,* vol. 13, pp. 175-181, 2007.

[70] N. K. Tolochko, Y. V. Khlopkov, S. E. Mozzharov, M. B. Ignatiev, T. Laoui, and V. I. Titov, "Absorptance of powder materials suitable for laser sintering," *Rapid Prototyping Journal,* vol. 6, pp. 155-161, 2000.

[71] H. H. Sait, A. Hussain, A. A. Salema, and F. N. Ani, "Pyrolysis and combustion kinetics of date palm biomass using thermogravimetric analysis," *Bioresource Technology,* vol. 118, pp. 382-389, Aug 2012.

[72] R. Velu, A. Fernyhough, D. Smith, M. GUEN, and S. Singamneni, "Selective Laser Sintering of Biocomposite Materials," *Lasers in Engineering (Old City Publishing),* vol. 35, 2016.

[73] X. Zongsheng, G. Yanling, Y. Ping, and Z. Weiliang, "A study on the properties of rapidly prototyped wood-plastic composites based on selective laser sintering," 2009.

[74] W. Zhu, C. Yan, Y. Shi, S. Wen, J. Liu, and Y. Shi, "Investigation into mechanical and microstructural properties of polypropylene manufactured by selective laser sintering in comparison with injection molding counterparts," *Materials & Design,* vol. 82, pp. 37-45, 2015.

[75] T. L. Starr, T. J. Gornet, and J. S. Usher, "The effect of process conditions on mechanical properties of laser-sintered nylon," *Rapid Prototyping Journal,* vol. 17, pp. 418-423, 2011.

[76] I. Gibson and D. Shi, "Material properties and fabrication parameters in selective laser sintering process," *Rapid Prototyping Journal,* vol. 3, pp. 129-136, 1997.

[77] S. Akande, K. Dalgarno, J. Munguia, and J. Pallari, "Assessment of tests for use in process and quality control systems for selective laser sintering of polyamide powders," *Journal of Materials Processing Technology,* vol. 229, pp. 549-561, 2016.

[78] V. Beal, R. Paggi, G. Salmoria, and A. Lago, "Statistical evaluation of laser energy density effect on mechanical properties of polyamide parts manufactured by selective laser sintering," *Journal of Applied Polymer Science,* vol. 113, pp. 2910-2919, 2009.

[79] H. Zarringhalam, C. Majewski, and N. Hopkinson, "Degree of particle melt in Nylon-12 selective laser-sintered parts," *Rapid Prototyping Journal,* vol. 15, pp. 126-132, 2009.

[80] N. Hopkinson, C. Majewski, and H. Zarringhalam, "Quantifying the degree of particle melt in Selective Laser Sintering®," *CIRP Annals-Manufacturing Technology,* vol. 58, pp. 197-200, 2009.

[81] A. M. Solutions, *Precimid 1170 Data Sheet*, 2017.

[82] T. Laumer, K. Wudy, M. Drexler, P. Amend, S. Roth, D. Drummer, *et al.*, "Fundamental investigation of laser beam melting of polymers for additive manufacture," *Journal of Laser Applications,* vol. 26, p. 042003, 2014.

Appendices

Appendix A: Powder Manufacturer's Material Data Sheets

Appendix B: Scanning Electron Microscope Images from Chapter 3

Appendix C: Measurements from Density calculations

Appendix D: Conference Paper

Appendix A

Precimid 1170

Precimid ®1170
AMS Precimid

Precimid ®1170

Precimid ® 1170 is a proven ultramicro powder with high-performance application for laser sintering system. Laser sintering part can be used as functional model, vacuum casting prototype, and even final plastic part/product. According to different purposes, users can select different laser energy and in the most economical way to apply this material to plastic model and direct part.

Key Performance:

- Low temperature impact resistance
- Ultra-low water absorption
- High deflection
- Forming efficiency
- Heat and corrosion resistance
- Precise tolerance and almost non deformation

Applicable Systems:

- DTM
  - SINTERSTATION 2000
  - SINTERSTATION 2500
  - SINTERSTATION 2500PLUS
- 3DSYSTEMS
  - VANGUARD SERIES
- EOS GmbH
  - EOSINT P350
  - EOSINT P360
  - EOSINT P380
  - EOSINT P700
- TPM ELITE
  - P 3500
  - P 5000

High Tolerance
High Efficiency
High Performance

Precimid ®1170
AMS Precimid

Part Applications

- Plastic direct parts for automobile and motorcycle
- Gas collection tubes or air headers of different type
- Household/electrical appliance and toys
- Air and electric tools
- Underwater tools
- Sports equipment
- Medical equipment

Precimid ®1170 Property Sheet

		Test method	Unit	State	Precimid ® 1170
General properties					
Density			Kg/dm^3	Dry	0.94
Water absorption	(23°C/sat.)	DIN 53495	%		1.5
Moisture absorption	(23°C/50% r.h.)	Acc. DIN 53495	%		0.7
Mechanical properties					
Tensile strength		ISO527	MPa	Cond.	40
Elongation at break		ISO527	%	Cond.	18
Tensile E modulus		ISO 527	MPa	Cond.	1100
Impact strength	Izod, 23°C	ISO 180/1C	MPa	Cond.	N.B.
	Izod, -30°C	ISO 180/1C	MPa	Cond.	N.B.
Notched impact strength	Izod, 23°C	ISO 180/1A	J/m	Cond.	8
	Izod, -30°C	ISO 180/1A	J/m	Cond.	4
Thermal properties					
Heat distortion temperature					
HDT B 0.46 N/mm2	DSC	DIN 53461	°C	Dry	110
HDT A 1.82 N/mm2	DSC	DIN 53461	°C	Dry	62

- Parameters of sintering energy may vary according to different laser sintering system;
- Parameters of sintering energy may also vary according to different usage;

High Tolerance
High Efficiency
High Performance

NO.2610050045

CNAS IB0071

MATERIAL SAFETY DATA SHEET

Product Name: Precimid 1170

Revision Date: 2010-06-12

Compiler: Liu Linlin

Checker: Yangyi

Approver: Zhangxiaojin

Shanghai Research Institute of Chemical Industry Testing Centre
Shanghai Classification and Testing Centre of Dangerous Chemicals for State Work Safety

NO.2610050045

Advance Molding Solution Co., Ltd.

MATERIAL SAFETY DATA SHEET

Precimid 1170

SECTION1 PRODUCT AND COMPANY IDENTIFICATION

Product name:	Precimid 1170
Company:	Advance Molding Solution Co., Ltd.
Address:	Room 1206, 12th Floor, Ryan Plaza, No. 333 Huaihai Middle Road, Shanghai City, 200021, P. R. China
Email:	contact@amstek.info
Fax:	86-21-51160555
Emergency Phone:	86-13611799910
MSDS Number:	2610050045
MSDS Date:	2010-06-12

SECTION2 INFORMATION ON INGREDIENTS

Product name: Precimid 1170

Ingredient	Concentration	CAS No.	EC No.
Polyamide	100%	63428-84-2	/

SECTION3 HAZARDS IDENTIFICATION

Hazards Identification:
This substance is considered to be non-hazardous for transport.

Emergency Overview:
May cause irritation to eyes, respiratory system and skin.

NO.2610050044

SECTION4 FIRST-AID MEASURES

Skin Exposure:

In case of contact, immediately wash skin with soap and copious amounts of water. If irritation persists, call a physician.

Eye Exposure:

In case of contact with eyes, flush with copious amounts of water for at least 15 minutes. Assure adequate flushing by separating the eyelids with fingers. If irritation persists, call a physician.

Inhalation Exposure:

If inhaled, remove to fresh air. If necessary, get medical attention.

Oral Exposure:

If swallowed, immediately wash out mouth with water provided person is conscious. Call a physician.

SECTION5 FIRE FIGHTING MEASURES

Extinguishing Media:

Suitable: Water spray, Dry chemical, Carbon dioxide or appropriate foam.

Firefighting:

Protective Equipment: Wear self-contained breathing apparatus and protective clothing to prevent contact with skin and eyes.

SECTION6 ACCIDENTAL RELEASE MEASURES

Procedure of Personal Precaution:

Exercise appropriate precautions to minimize direct contact with skin or eyes and prevent inhalation of dust.

Methods for Cleaning up:

Sweep up with spade and transfer to a dry, clean, lidded container for disposal. Avoid raising dust. Ventilate area and wash spill site after material pickup is complete.

SECTION7 HANDLING AND STORAGE

Handling:

Wear appropriate protective clothing and safety gloves. Do not breathe dust. Avoid contact with eyes, skin and clothing. Avoid prolonged or repeated exposure. Mechanical exhaust required. Keep away from ignition sources, heat and flame. Incompatibilities: strong oxidizing agents and foods. No smoking at working site.

Storage:

Store in a cool, well-ventilated area. Keep away from ignition sources, heat and flame. Store in a tightly closed container. Incompatibilities: strong oxidizing agents and foods.

2/4

NO.2610050044

SECTION8 EXPLOSURE CONTROL/PPE

Engineering Controls:
Mechanical exhaust required. Safety shower and eye bath.

Personal Protective Equipment:
Respiratory: Government approved respirator.
Eye: Chemical safety goggles.
Clothing: Wear appropriate protective clothing.
Hand: Protective gloves.

Other Protect:
No smoking, drinking and eating at working site. Wash thoroughly after handling.

SECTION9 PHYSICAL/CHEMICAL PROPERTIES

Appearance:	White powder
Odor:	Weak odor
Melting Point/℃:	>350℃
pH Value:	5.8 (25℃, 50.0g/L) 6.3 (25℃, 10.0g/L)
Solubility:	Weak soluble in water

SECTION10 STABILITY AND REACTIVITY

Stability:
Stable under normal temperatures and pressures.

Materials to Avoid:
Strong oxidizing agents and foods.

Hazardous Polymerization:
Will not occur.

Hazardous Decomposition Products:
Carbon monoxide, Carbon dioxide, Nitrogen oxides.

SECTION11 TOXICOLOGICAL INFORMATION

Toxicity Data:
No data available.

Irritation Data:
May cause irritation to eyes, respiratory system and skin.

SECTION12 ECOLOGICAL INFORMATION

No data available.

SECTION13 DISPOSAL CONSIDERATION

Appropriate Method of Disposal of Substance:
Contact a licensed professional waste disposal service to dispose of this material. Dissolve or mix the material with a combustible solvent and burn in a chemical incinerator equipped with and afterburner and scrubber. Observe all federal, state, and local environmental regulations.

NO.2610050044

SECTION14 TRANSPORT INFORMATION

DOT:	Non-Hazardous for Transport: This substance is considered to be non-hazardous for transport.
RID/ADR:	Non-Hazardous for Transport: This substance is considered to be non-hazardous for transport.
IATA:	Non-Hazardous for Air Transport: Non-hazardous for air transport.
IMO:	Non-Hazardous for Sea Transport: Non-hazardous for sea transport.

SECTION15 REGULATORY INFORMATION

EU Additional Classification:
S: 2 26
Safety Statements: Keep out of the reach of children. In case of contact with eyes, rinse immediately with plenty of water and seek medical.

SECTION16 OTHER INFORMATION

Date:	2010-06-11
Department:	Shanghai Research Institute of Chemical Industry Testing Centre Shanghai Classification and Testing Centre of Dangerous Chemicals for State Administration of Work Safety Tel(Fax):8621-52815377/52800971/52807275/52811034/52569800
Revision:	0
Other	The above information is believed to be correct but does not purport to be all inclusive and shall be used only as a guide. We make no warranty of merchantability or any other warranty, express or implied, with respect to such information, and we assume no liability resulting from its use. Users should make their own investigation to determine the suitability of the information for their particular purposes. In no way shall we be liable for any claims, losses, or damages of any third party or for lost profits or any special, indirect, incidental, consequential or exemplary damages, howsoever arising from using the above information.

Sintratec PA12 Black

Sintratec

Safety Data Sheet

Product name: Sintratec PA12 black

Version 1 Region: GB Issue Date 01.06.16

SECTION 1: Identification of the substance/mixture and of the company/undertaking

1.1 Product identifier

Trade name	Sintratec PA12 black
Product name	Sintratec PA12 black

1.2 Relevant identified uses of the substance or mixture and uses advised against

Relevant identified uses of the substance or mixture
Laser sintering

Uses advised against
No data available.

1.3 Details of the supplier of the safety data sheet

Adress:	
Company name	Sintratec AG
Street	Badenerstrasse 13
Postal Code	5200
City	Brugg
Country	Switzerland
Phone number	+41 56 552 00 22
Mail	info@sintratec.com

1.4 Emergency telephone number

+41 56 552 00 22 (Mo – Fr 9am -12pm & 13pm – 17pm) (CET)

SECTION 2: Hazards identification

2.1 Classification of the substance or mixture

Classification information
Classification and labelling criteria given in the Regulation (EC) No 1272/2008 (CLP) and Dangerous Substances Directive 67/548/EC (DSD) are not met by the product.

2.2 Label elements

Not relevant

Labelling information
A hazard-warning label in accordance with EC Directives is not needed.

2.3 Other hazards

No information available.

SECTION 3: Composition and information on ingredients

3.1 Substances

Chemical characterization
Polylaurolactam (polyamide 12) (Cas-No. 25038-74-8), modified, polymer

3.2 Mixtures

The product is not a mixture.

SECTION 4: First aid measures

4.1 Description of first aid measures

General information
In case of continuing adverse effects, see a physician. Change contaminated clothing immediately.

After inhalation
IF INHALED: The affected person has to be removed to an area with fresh air and placed in a comfortable position for breathing.

After skin contact
If product gets in contact with skin it is recommended to wash of with water and soap. When in contact with molten product, cool quickly with fresh water. It is recommended to not pull solidified product from the skin and seek medical attention. Seek for medical attention.

After eye contact
Clean right after with enough water, also under eyelids, for a minimum of 15 minutes.

After ingestion
Rinse mouth carefully with water. Get medical advice immediately. An unconscious person should never be given anything by mouth.

4.2 Most important symptoms and effects, both acute and delayed

No data available.

4.3 Indication of any immediate medical attention and special treatment needed

Treat symptomatically.

SECTION 5: Firefighting measures

5.1 Extinguishing media

Suitable extinguishing media
Foam; Water spray jet; Carbon dioxide; extinguishing powder

Unsuitable extinguishing media
No data available.

5.2 Special hazards arising from the substance or mixture

In case of fire, the following can be set free: Carbon dioxide (CO2); Carbon monoxide (CO); Nitrogen oxides (NOx); Combustion materials of this product have to be classified invariably as respiratory poison.

5.3 Advise for firefighters

As in any fire, wear self-contained breathing apparatus and wear full protective gear.

SECTION 6: Accidental release measures

6.1 Personal precautions, protective equipment and emergency procedures

For non-emergency personnel
Ensure the existence of adequate ventilation. Avoid contact with skin, eyes or clothing and the formation of dust. Sources of ignition should be kept away. Refer to protective measures listed in sections 7 and 8.

For emergency responders
Personal protective equipment (PPE) - see Section 8.

6.2 Environmental precautions

Releasing into groundwater/surface waters/drains is not permitted.

6.3 Methods and material for containment and cleaning up

Treat the material as prescribed under the heading "Disposal considerations" when picked up. Take up mechanically.

6.4 Reference to other sections
No data available

SECTION 7: Handling and storage

7.1 Precautions for safe handling

Advice on safe handling
There are no measures necessary if stored and handled as instructed. Avoid dust formations and depositions. Good ventilation is needed (local exhaust ventilation, if necessary)

General protective and hygiene measures
Washing hands before breaks and after work is recommended. Foodstuff and beverages should be kept away. Eating, drinking or smoking is not aloud during work time. Provide eye wash fountain in work area. No dust inhalation. Areas of the skin touched by dust are to be washed with soap and water immediately, as the powder takes the natural moisture from the skin.

Advice on protection against fire and explosion
Sources of heat and ignition should be kept away. Together with air dust can create an explosive mixture.
To avoid static charges any possible precautionary measures should be taken.

7.2 Conditions for safe storage, including any incompatibilities

Technical measures and storage conditions
The containers should be stored dry, tightly closed, at temperatures around 5 and 35°C and relative air moisture of 20 – 70%.

Requirements for storage rooms and vessels
The product has to be stored in closed containers.

7.3 Specific end use(s)
No data available.

SECTION 8: Exposure controls/personal protection

8.1 Control parameters

Dust	
List of approved workplace exposure limits (WELs) / EH4	
Total inhalable dust	
TWA	10 mg/ m³
List of approved workplace exposure limits (WELs) / EH40	
Respirable dust	
TWA	4 mg/ m³

8.2 Exposure controls

Appropriate engineering controls
No data available.

Personal protective equipment

Respiratory protection
If dust formations do happen, take appropriate measures for a breathing protection in the event workplace threshold values are not clarified. As soon as workplace exposure limits are exceeded, a respiration protection necessary for this job must be worn. Respirator with particulate filter (filter cat. P 3)

Eye / face protection

Safety glasses (EN 166)

Hand protection
During intensive contact, use protective gloves (EN 374). Before wearing, the protective gloves should be tested for its specific work-station suitability (i.e. mechanical resistance , product compatibility, and antistatic properties). Design operations to avoid constant usage use of the gloves. Read the manufacturer's instructions and information of the use, storage, care and replacement of protective gloves. After being damaged or worn, the gloves have to be replaced. At room temperature no protective gloves are needed. Thermally insulating protective gloves are worn when thermal processing.

Other
Always fully closed clothing.

Environmental exposure controls
No data available.

SECTION 9: Physical and chemical properties

9.1 Information on basic physical and chemical properties

Appearance	Powder
Color	Dark Grey
Odor	Odorless
Odor Threshold	Not determined
pH	Not applicable
Melting point/freezing point	185 °C
Method	EN ISO 11357-1
Boiling point / boiling range	Not applicable
Flash point	Not applicable
Evaporation rate	Not determined
Flammability (solid, gas)	Not flammable
Lower flammability or explosive limits	Not determined
Upper flammability or explosive limits	Not determined
Vapor Pressure	Not applicable
Vapor density	Not determined
Density	1.0 – 1.1 g/cm³
Reference temperature	20°C
Relative density	Not determined
Water solubility	Insoluble
Partition coefficient: n-octagonol/water	Not determined
Ignition temperature	>350 °C
Method	DIN 51794
Auto-Ignition temperature	No data available
Decomposition temperature	>300 °C
Viscosity	Not determined
Explosive properties	Product is explosive
Oxidizing properties	No oxidizing properties

SECTION 10: Stability and reactivity

10.1 Reactivity
No data available.

10.2 Chemical stability
No data available.

10.3 Possibility of hazardous reactions
No data available.

10.4 Conditions to avoid
None, when handled according to its intended use.

10.5 Incompatible materials
None, if handled according to order

10.6 Hazardous decomposition products
No hazardous decomposition products known.

SECTION 11: Information on Toxicology

11.1 Information on toxicological effects

Acute oral toxicity
No data available.
Acute dermal toxicity
No data available.
Acute inhalation toxicity
No data available.

Skin corrosion/irritation
Not classified
Serious eye damage/eye irritation
Eye contact may cause mechanical irritation through dust particles
Reproductive toxicity
Not classified
Germ cell mutagenicity
Not classified
Reproductive toxicity
Not classified
Carcinogenicity
Not classified
STOT – single exposure
Not classified
STOT – repeated exposure
Not classified
Aspiration hazard
Not classified
Symptoms related to the physical, chemical and toxicological characteristics
Eye Contact In case of eye contact, it is possible to cause mechanical irritation through dust particles.
Delayed and immediate effects as well as chronic effects from short and long-term exposure
Dust inhalation can irritate the respiratory tract.

SECTION 12: Ecological information

12.1 Toxicity

Toxicity to fish (acute)	No data available
Toxicity to fish (chronic)	No data available
Toxicity to Daphnia (acute)	No data available
Toxicity to Daphnia (chronic)	No data available
Toxicity to algae (acute)	No data available
Toxicity to algae (chronic)	No data available
Bacteria toxicity	No data available

12.2 Persistence and degradability
If used as intended, this product causes no problems, on the strength of previous experience.

12.3 Bioaccumulative potential
No data available.

12.4 Mobility in soil
No data available.

12.5 Results of PBT and vPvB assessment
No data available.

12.6 Other adverse effects
No data available.

12.7 Other information
No unmonitored discharge into environment.

SECTION 13: Disposal considerations

13 Waste treatment methods
Product
The disposal of the product should be accordingly with applicable regional, national, local laws and regulations and be according to the European Waste Catalogue.

Packaging
All the residuals have to be removed from packaging and when emptied totally disposed of in accordance with the regulations for waste removal. If not completely emptied, packages have to be disposed of as requested by the regional disposer.

SECTION 14: Transport Information

14.1 Transport ADR/RID/ADN
The product is not subject to ADR/RID/ADN regulations.

14.2 Transport IMDG
The product is not subject to IMDG regulations.

14.3 Transport ICAO-TI / IATA
The product is not subject to ICAO-TI / IATA regulations.

14.4 Other information
No data available.

14.5 Environmental hazards
Information on environmental hazards, if relevant, please see 14.1 - 14.3.

14.6 Special precautions for user
No data available.

14.7 Transport in bulk according to Annex II of MARPOL 73/78 and the IBC Code
Not relevant

SECTION 15: Regulatory information

15.1 Safety, health and environmental regulations/legislation specific for the substance or mixture

EU regulations:

Regulation (EC) No 1907/2006 (REACH) Annex XIV (List of substances subject to authorization)
In accordance with the Reach regulation (EC) 1907/2006, the product does not contain any substances that are considered as subject to listing in annex XIV, inventory of substances requiring authorization.

REACH candidate list of substances of very high concern (SVHC) for authorization
In accordance with article 57 and article 59 of the Reach regulation (EC) 1907/2006, this substance is not considered as subject to listing in annex XIV, inventory of substances requiring authorization ("Authorization list").

Regulation (EC) No 1907/2006 (REACH) Annex XVII: RESTRICTIONS ON THE MANUFACTURE, PLACING ON THE MARKET AND USE OF CERTAIN DANGEROUS SUBSTANCES, PREPARATIONS AND ARTICLES
The substance is not subject to the provisions of annex XVII (restriction entries) of the Reach regulation (EC) 1997/2006.

Council Directive 96/82/EC on the control of major-accident hazards involving dangerous substances
Annex I, part 1 + 2: not mentioned. With regard to possibly appropriate decomposition products see Chapter 10.

15.2 Chemical safety assessment
No data available.

SECTION 16: Other information

16.1 Revision Note

Issue Date	01-Jun-2016
Revision Date	01-Jun-2016

Appendix B

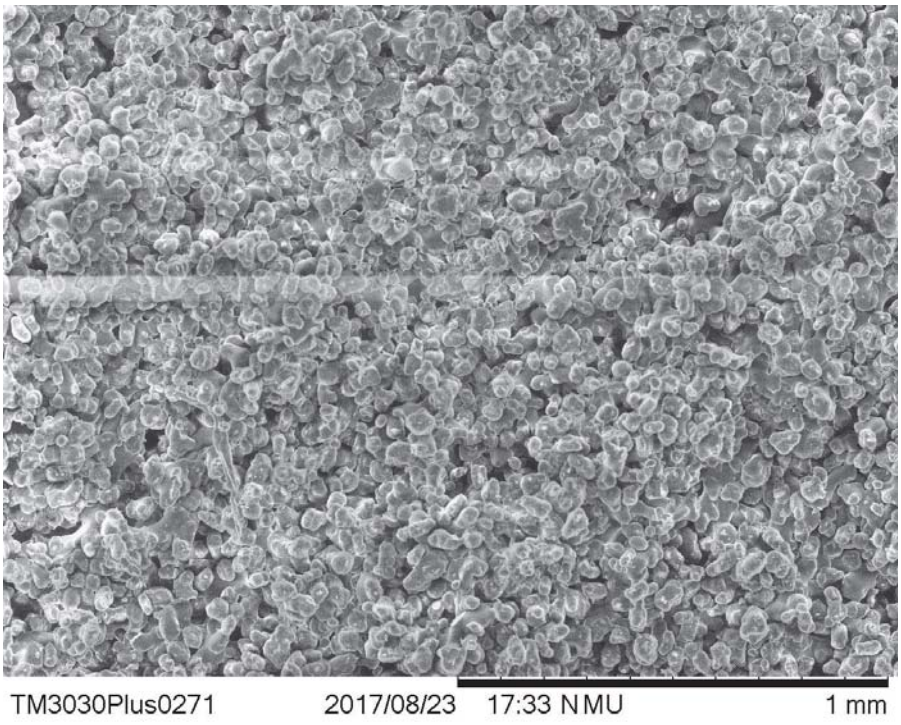

Figure B1: Sample printed at Print Bed Temperature of 165°C, and Laser Scan Speed of 650mm/s, at 100 x magnification

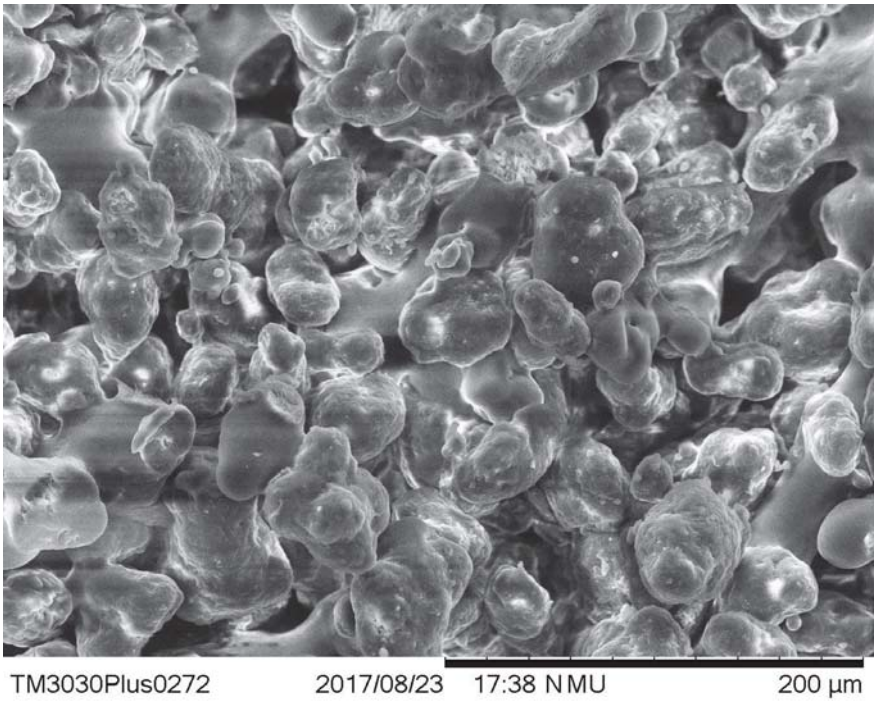

Figure B2: Sample printed at Print Bed Temperature of 165°C, and Laser Scan Speed of 650mm/s, at 500 x magnification

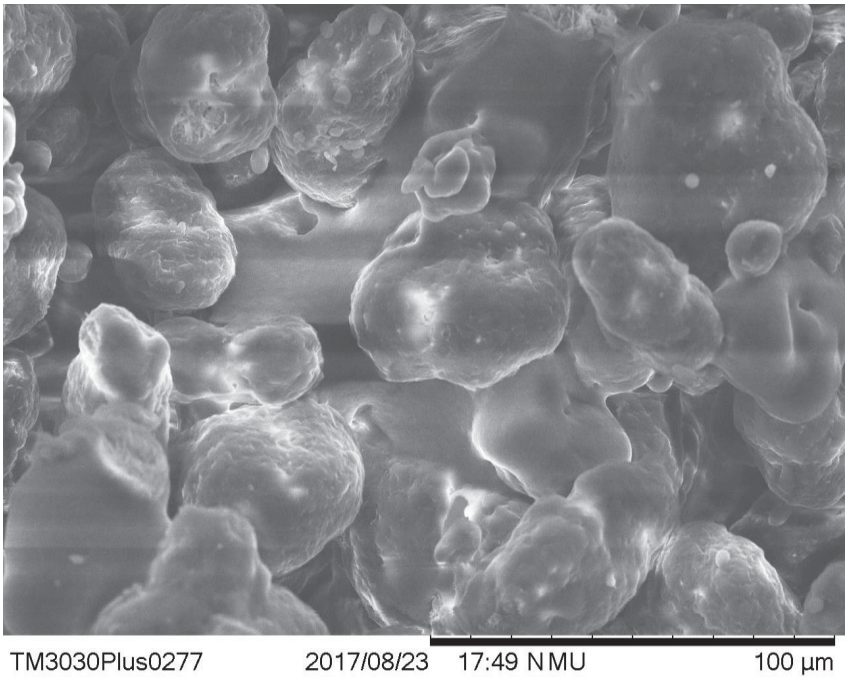

Figure B3: Sample printed at Print Bed Temperature of 165°C, and Laser Scan Speed of 650mm/s, at 1000 x magnification

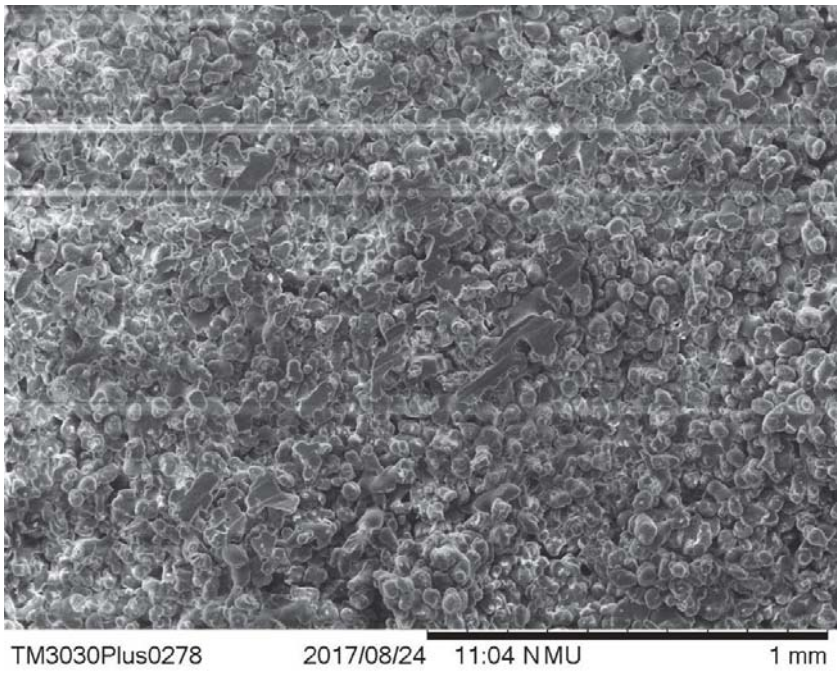

Figure B4: Sample printed at Print Bed Temperature of 165°C, and Laser Scan Speed of 550mm/s, at 100 x magnification

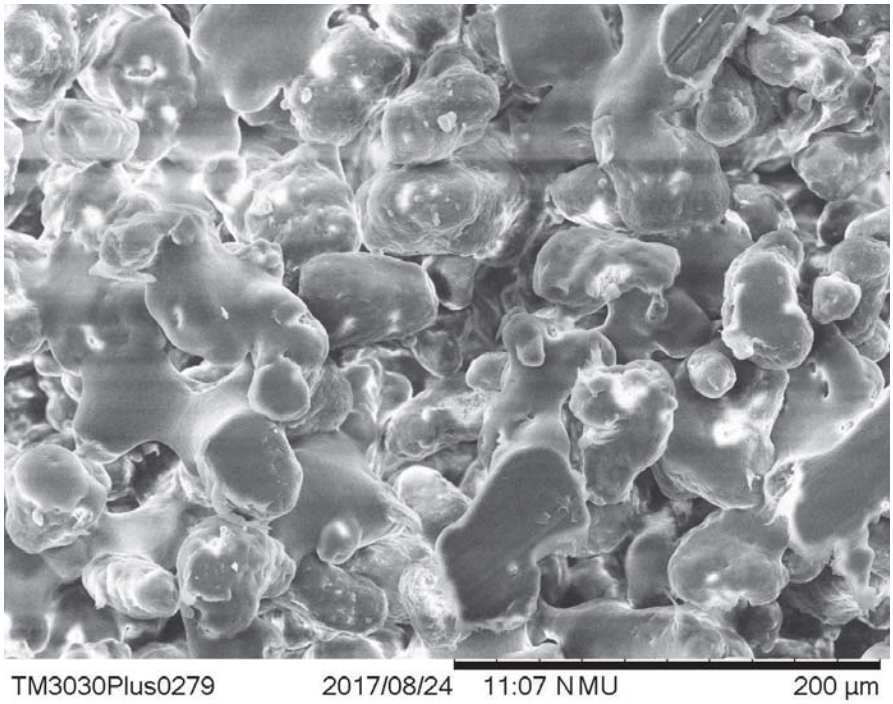

Figure B5: Sample printed at Print Bed Temperature of 165°C, and Laser Scan Speed of 550mm/s, at 500 x magnification

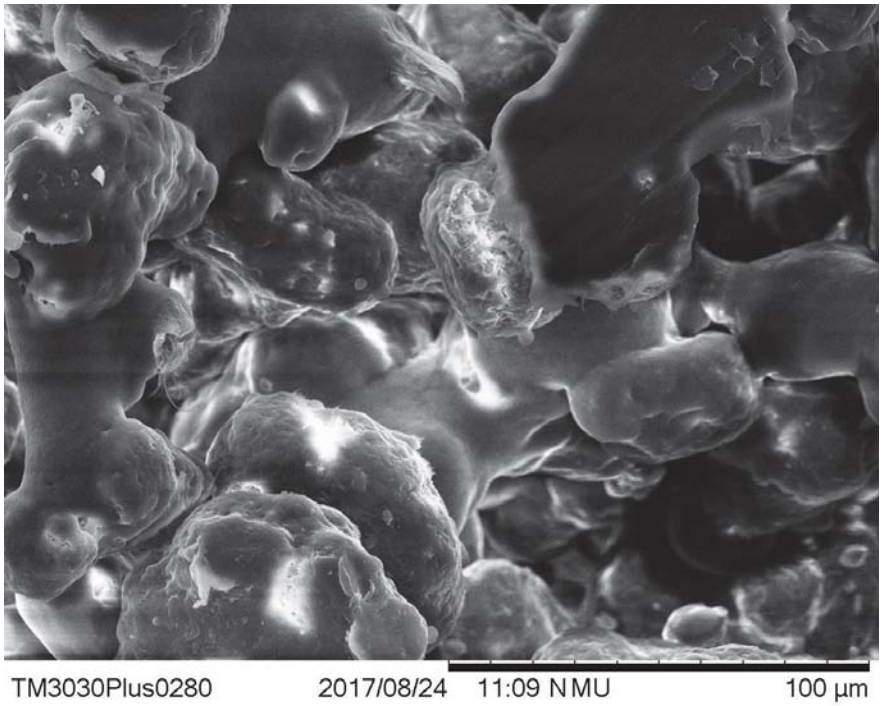

Figure B6: Sample printed at Print Bed Temperature of 165°C, and Laser Scan Speed of 550mm/s, at 1000 x magnification

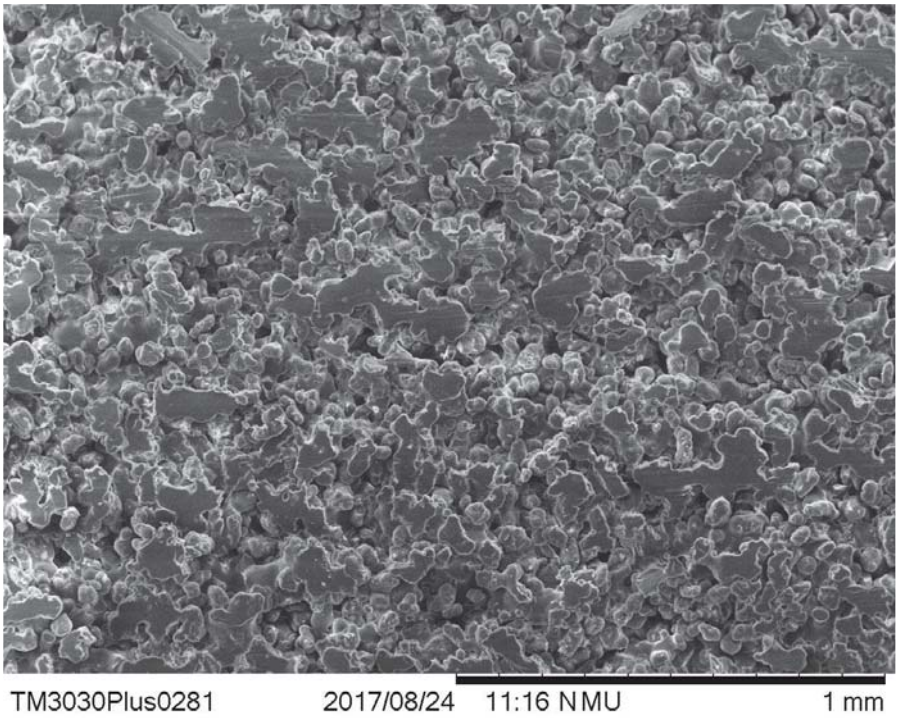

Figure B7: Sample printed at Print Bed Temperature of 165°C, and Laser Scan Speed of 450mm/s, at 100 x magnification

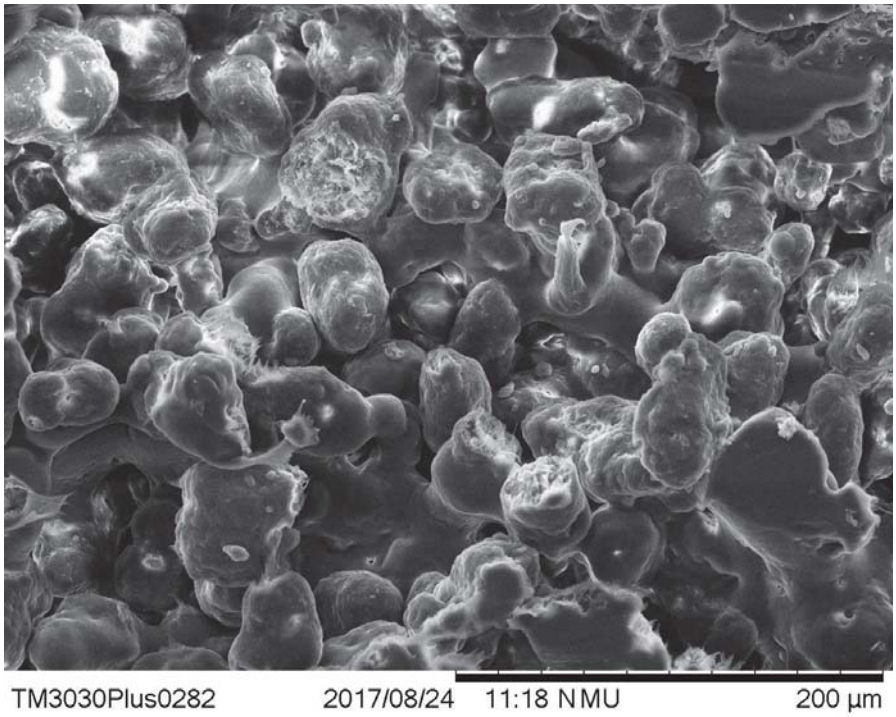

Figure B8: Sample printed at Print Bed Temperature of 165°C, and Laser Scan Speed of 450mm/s, at 500 x magnification

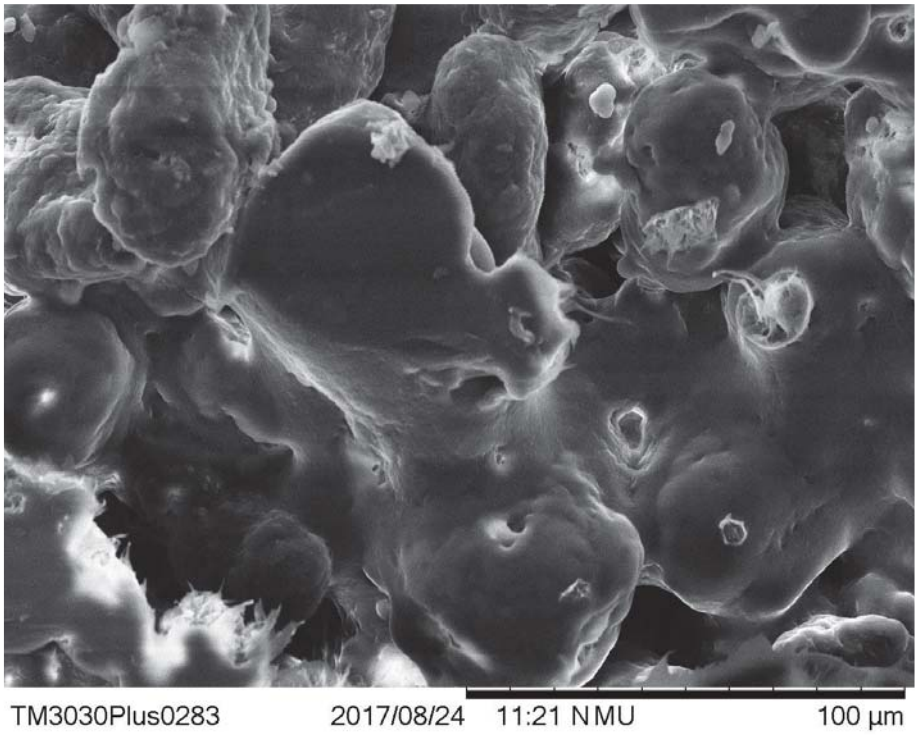

Figure B9: Sample printed at Print Bed Temperature of 165°C, and Laser Scan Speed of 450mm/s, at 1000 x magnification

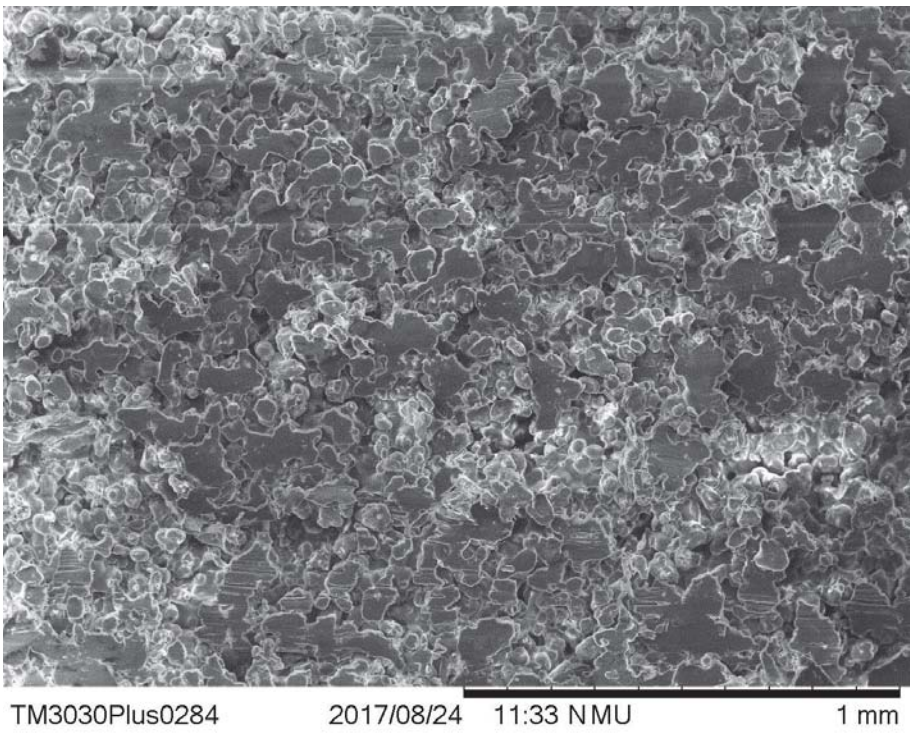

Figure B20: Sample printed at Print Bed Temperature of 170°C, and Laser Scan Speed of 650mm/s, at 100 x magnification

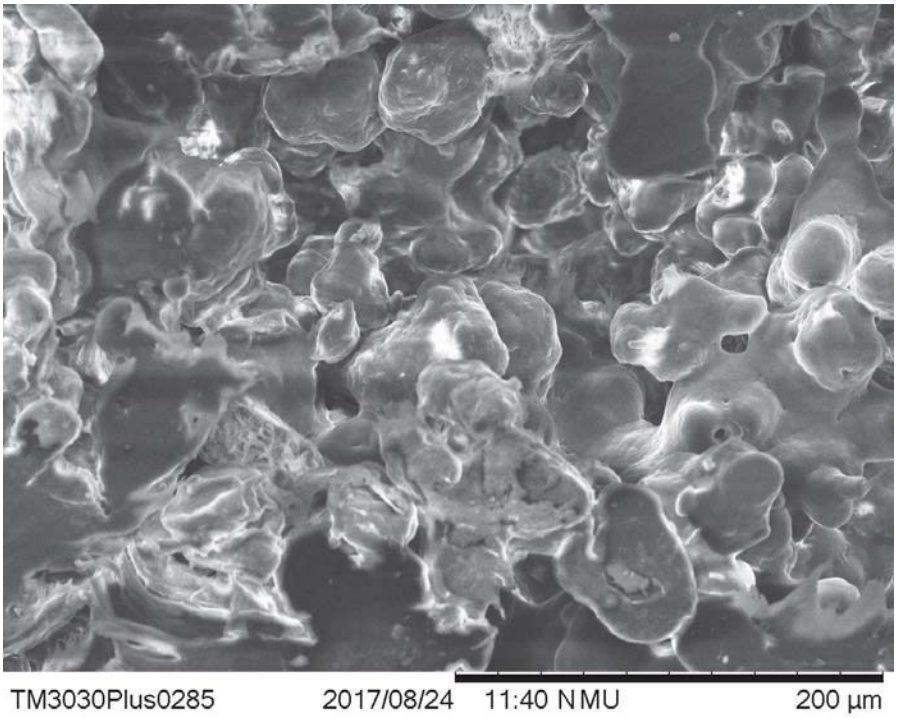

Figure B14: Sample printed at Print Bed Temperature of 170°C, and Laser Scan Speed of 650mm/s, at 500 x magnification

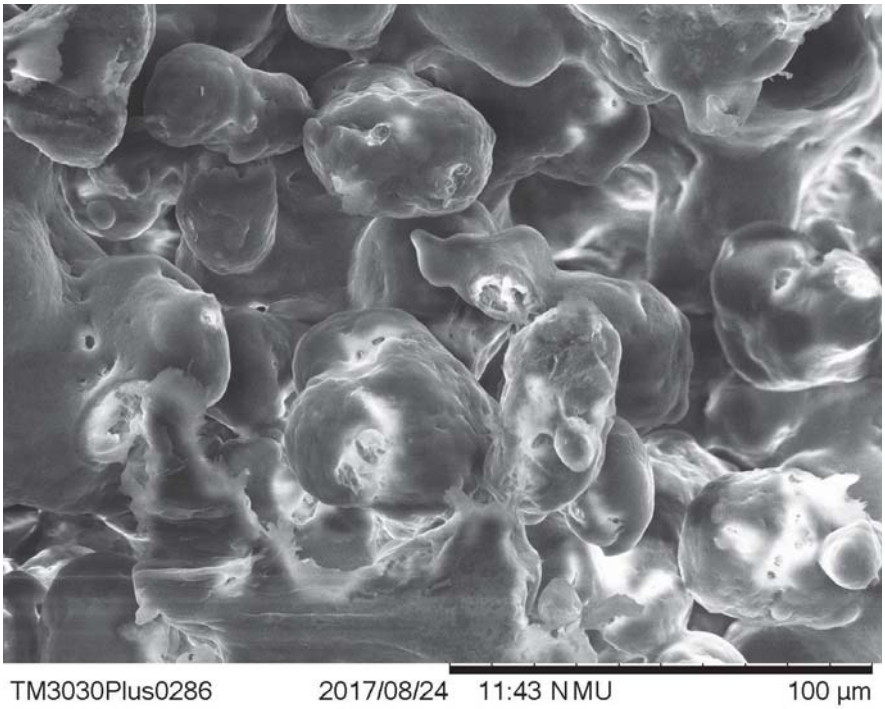

Figure B32: Sample printed at Print Bed Temperature of 170°C, and Laser Scan Speed of 650mm/s, at 1000 x magnification

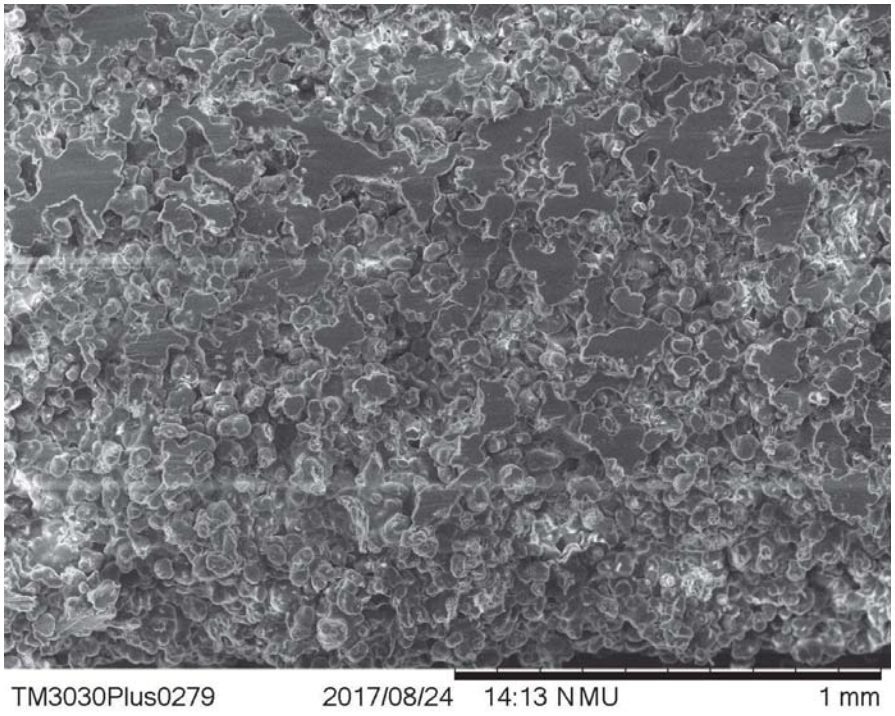

Figure B63: Sample printed at Print Bed Temperature of 170°C, and Laser Scan Speed of 550mm/s, at 100 x magnification

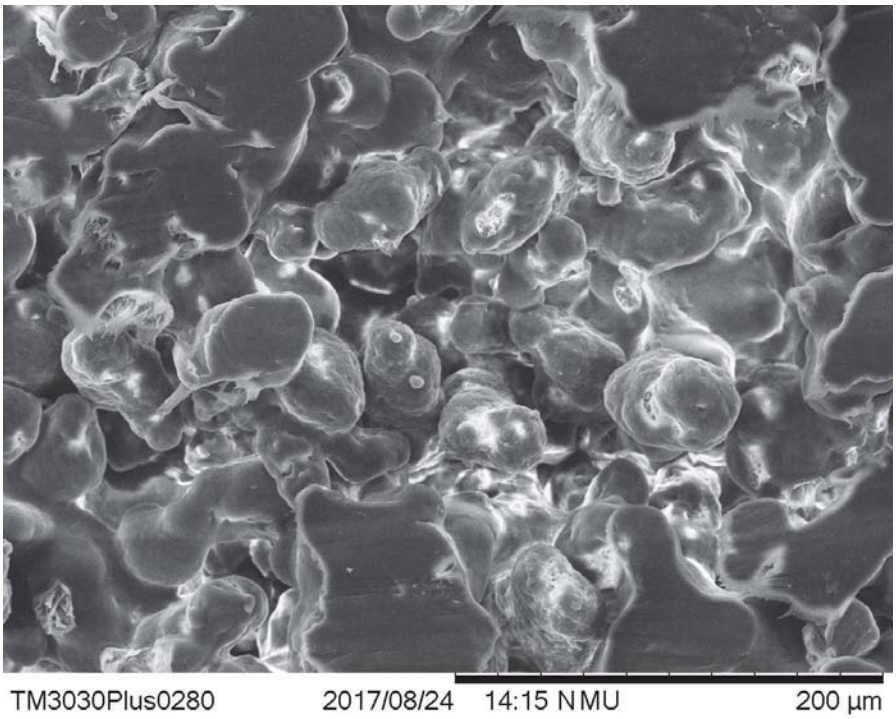

Figure B54: Sample printed at Print Bed Temperature of 170°C, and Laser Scan Speed of 550mm/s, at 500 x magnification

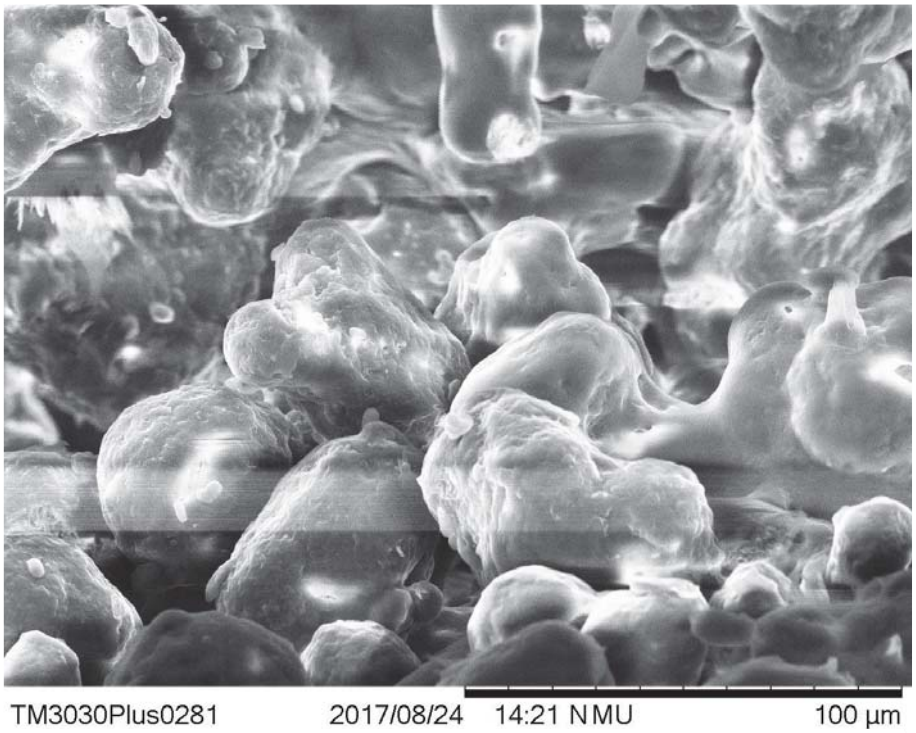

Figure B75: Sample printed at Print Bed Temperature of 170°C, and Laser Scan Speed of 550mm/s, at 1000 x magnification

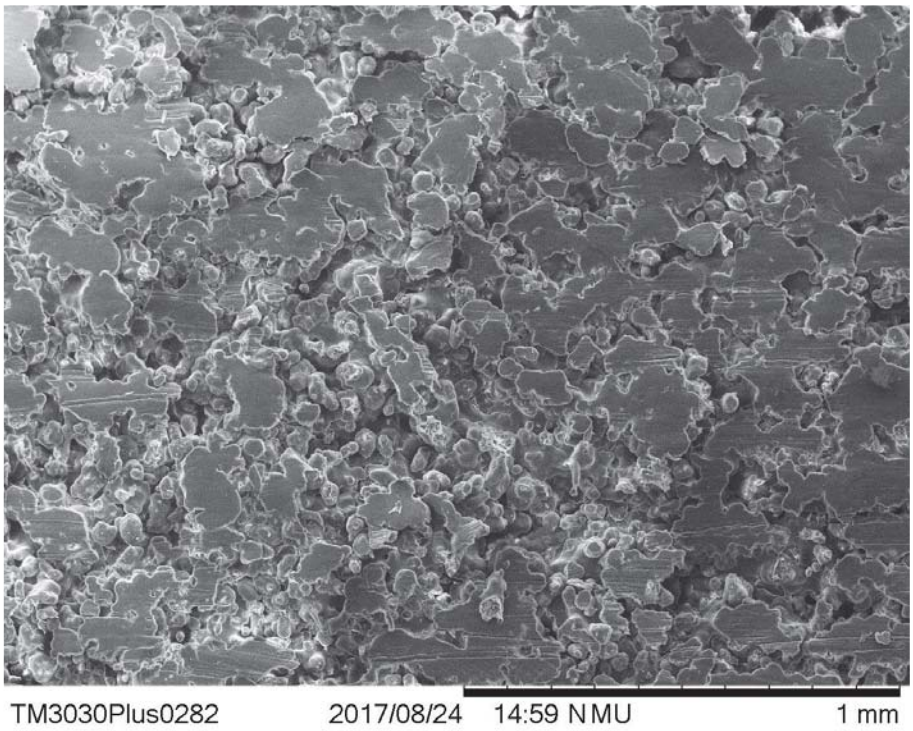

Figure B86: Sample printed at Print Bed Temperature of 170°C, and Laser Scan Speed of 450mm/s, at 100 x magnification

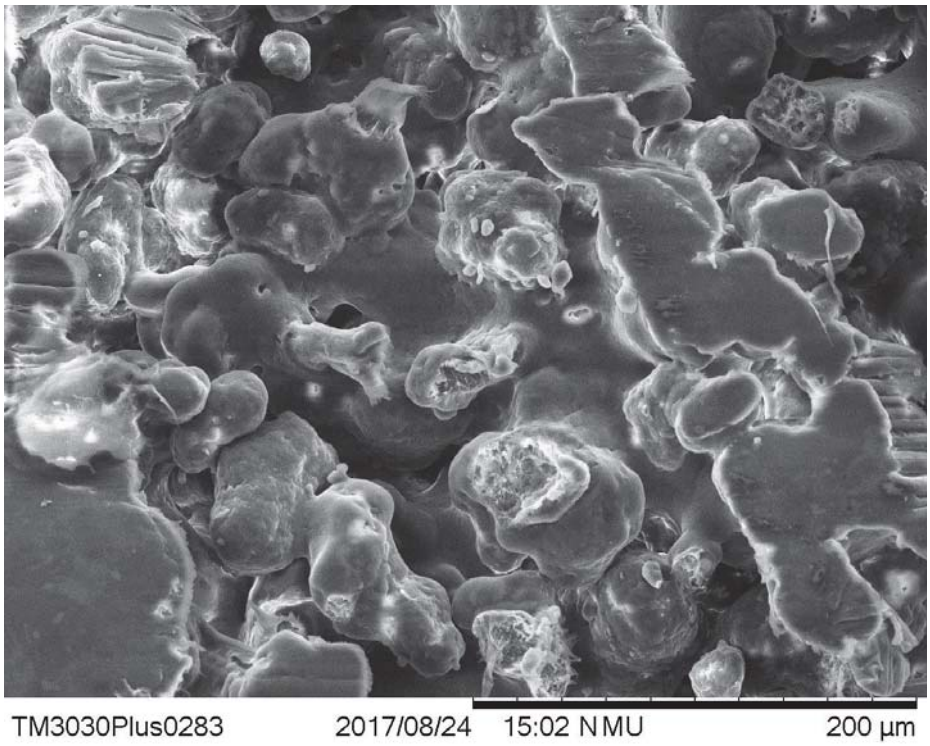

Figure B107: Sample printed at Print Bed Temperature of 170°C, and Laser Scan Speed of 450mm/s, at 500 x magnification

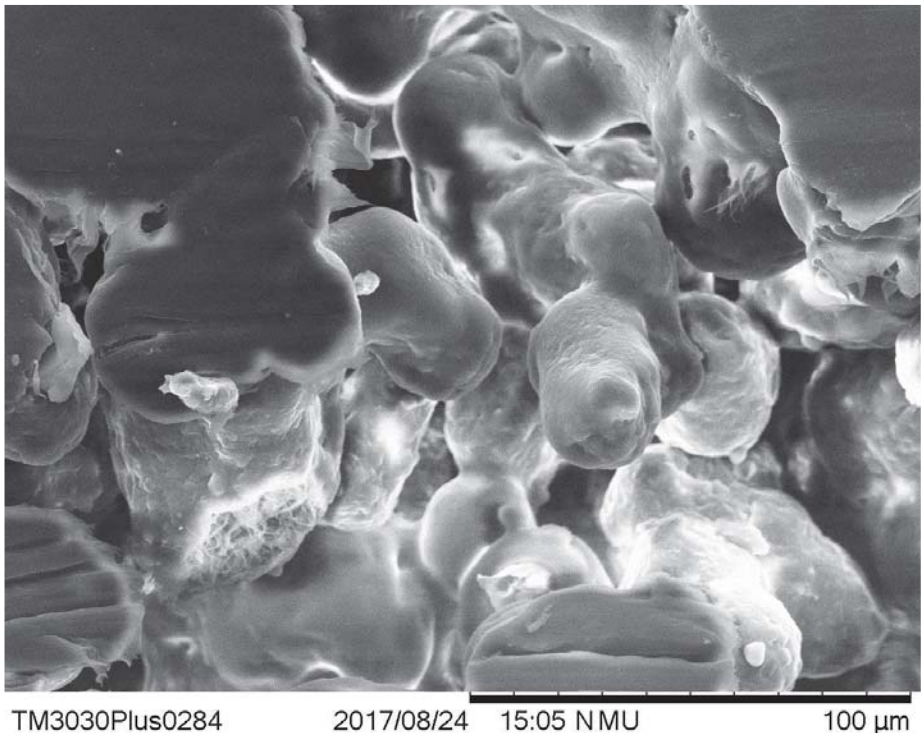

Figure B98: Sample printed at Print Bed Temperature of 170°C, and Laser Scan Speed of 450mm/s, at 1000 x magnification

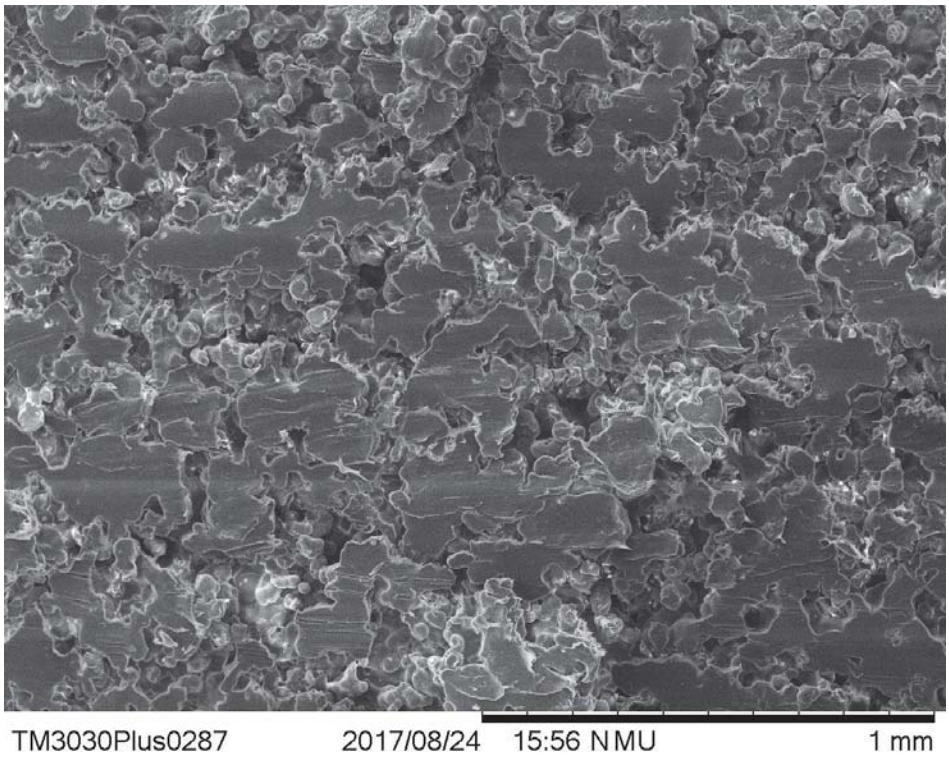

Figure B119: Sample printed at Print Bed Temperature of 175°C, and Laser Scan Speed of 650mm/s, at 100 x magnification

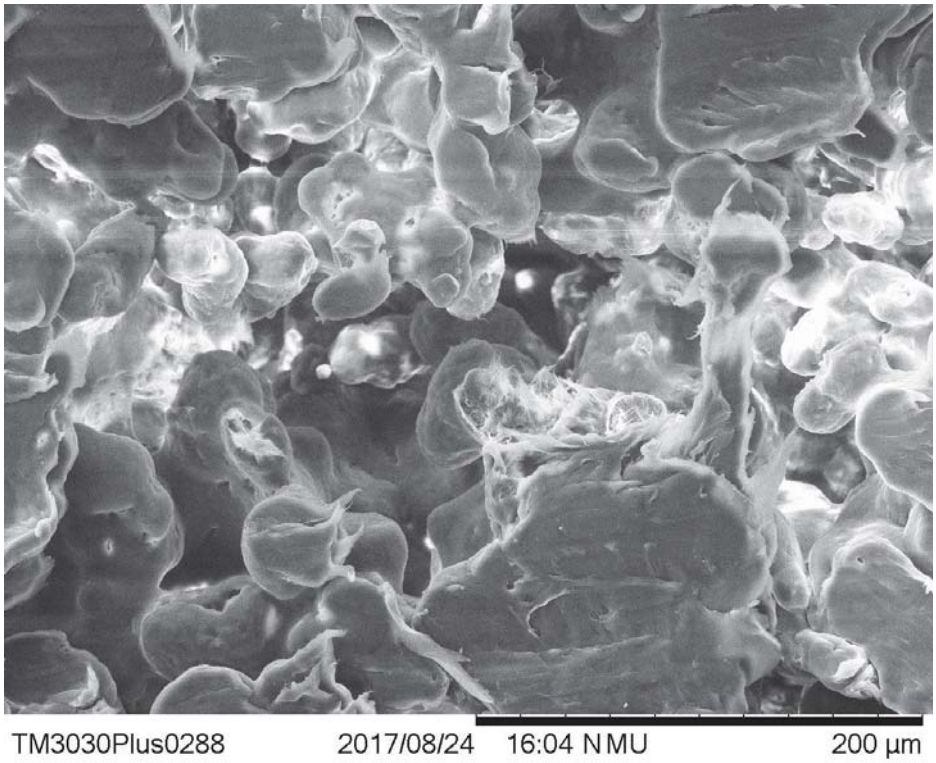

Figure B20: Sample printed at Print Bed Temperature of 175°C, and Laser Scan Speed of 650mm/s, at 500 x magnification

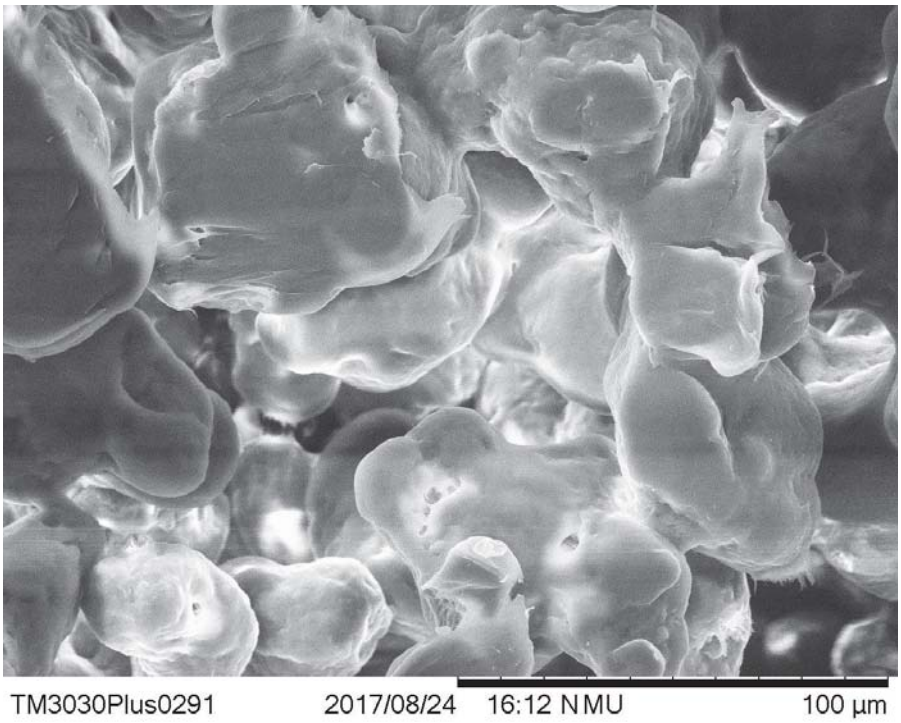

Figure B21: Sample printed at Print Bed Temperature of 175°C, and Laser Scan Speed of 650mm/s, at 1000 x magnification

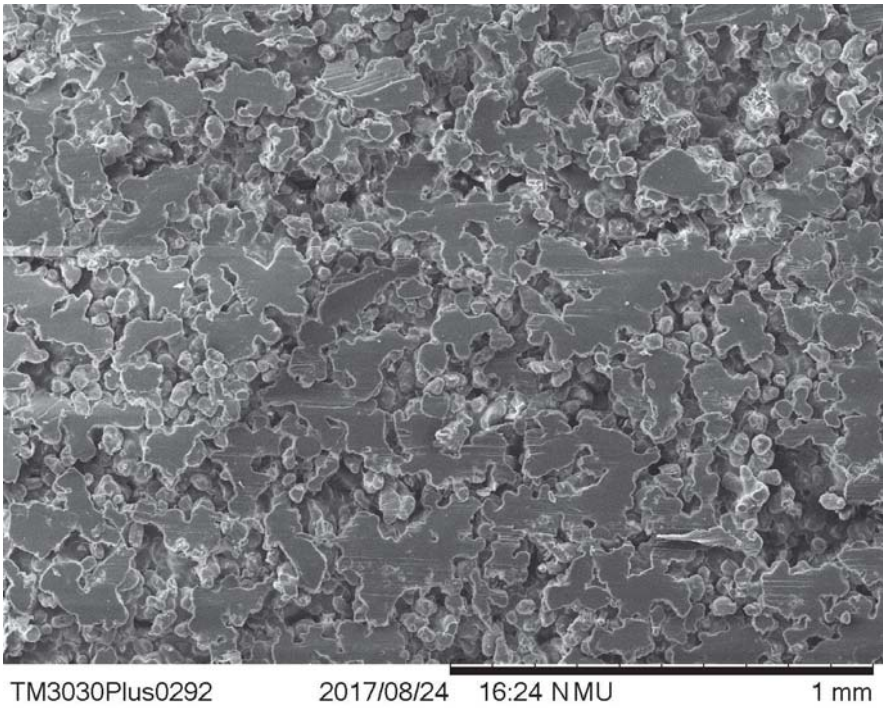

Figure B22: Sample printed at Print Bed Temperature of 175°C, and Laser Scan Speed of 550mm/s, at 100 x magnification

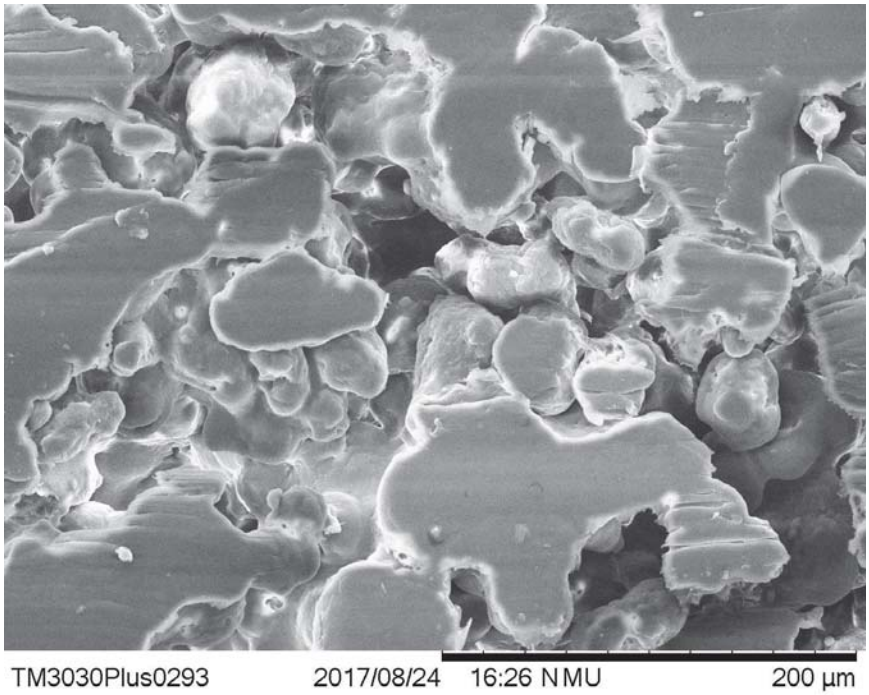

Figure B23: Sample printed at Print Bed Temperature of 175°C, and Laser Scan Speed of 550mm/s, at 500 x magnification

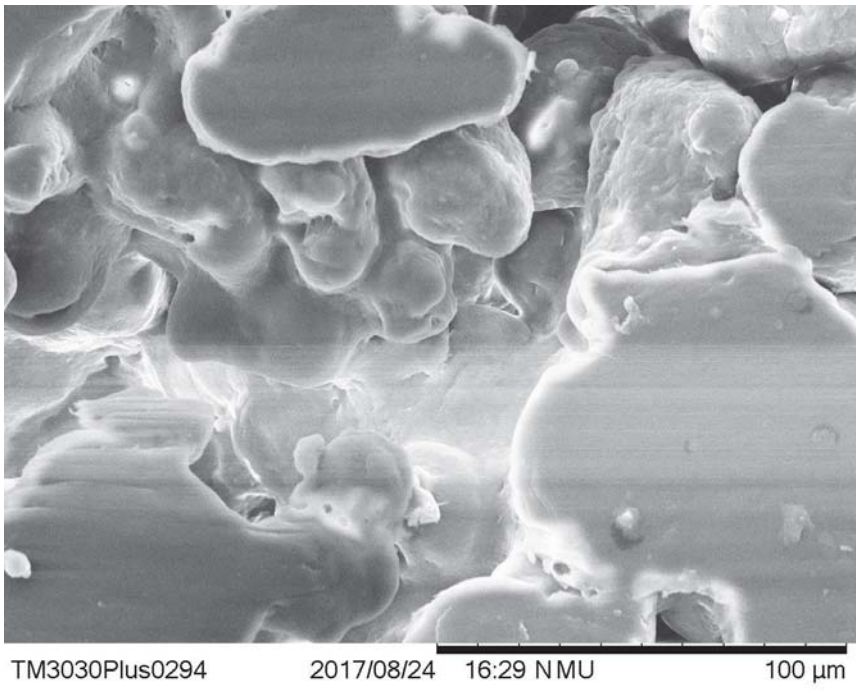

Figure B24: Sample printed at Print Bed Temperature of 175°C, and Laser Scan Speed of 550mm/s, at 1000 x magnification

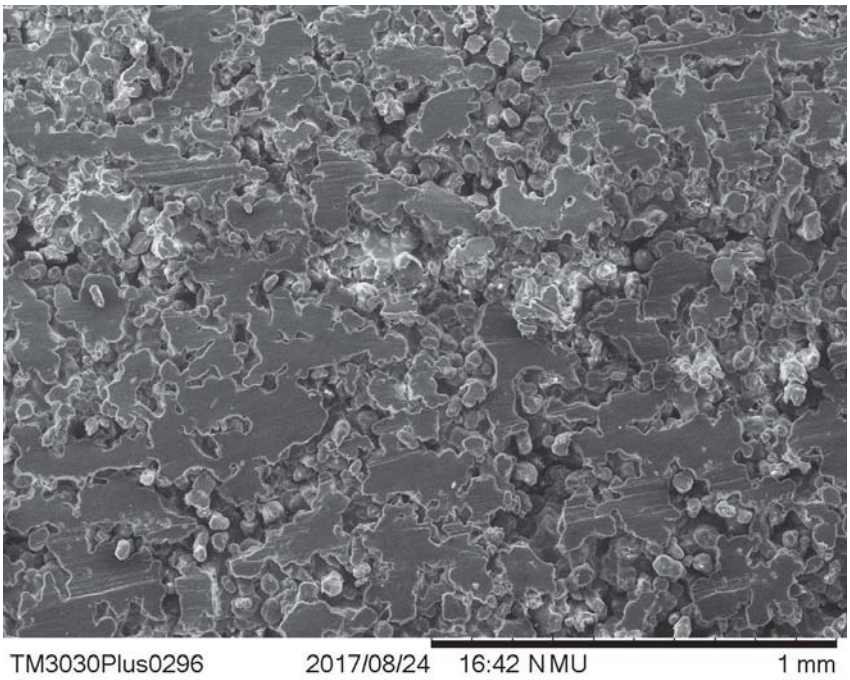

Figure B25: Sample printed at Print Bed Temperature of 175°C, and Laser Scan Speed of 450mm/s, at 100 x magnification

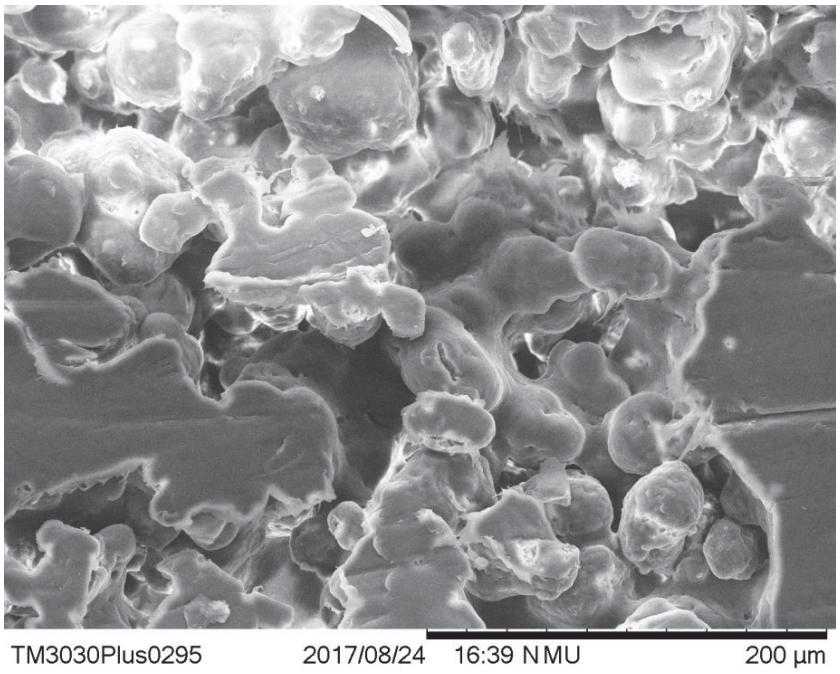

Figure B26: Sample printed at Print Bed Temperature of 175°C, and Laser Scan Speed of 450mm/s, at 500 x magnification

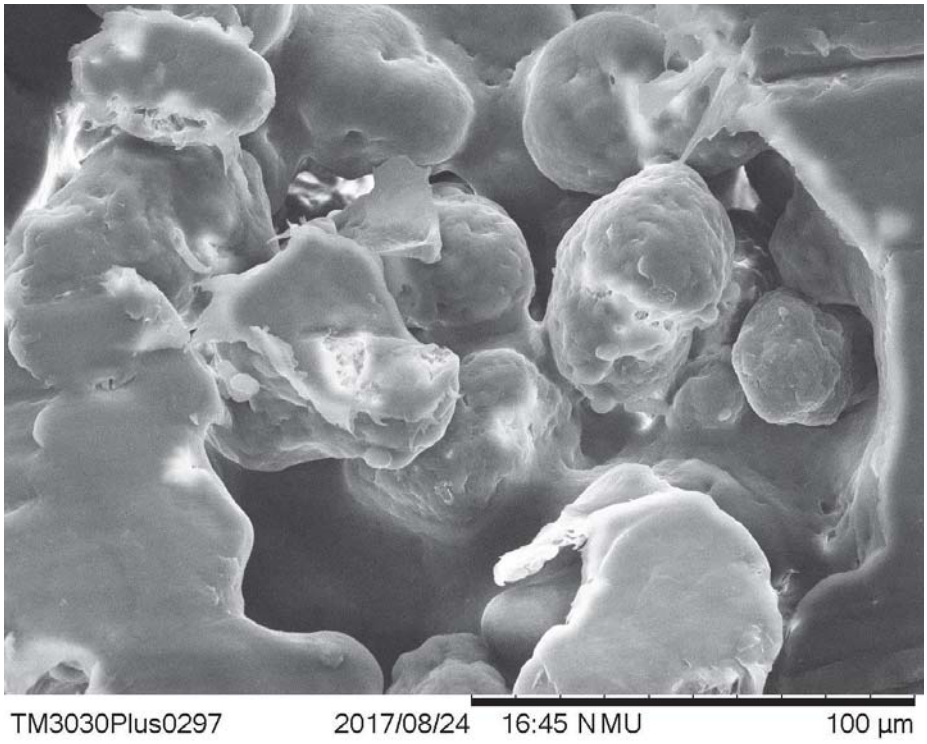

Figure B27: Sample printed at Print Bed Temperature of 175°C, and Laser Scan Speed of 450mm/s, at 1000 x magnification

Appendix C

SLS Part Density Measurements												
Print Bed Temperature	Laser Scan Speed	Bed Location	Comments	Length (mm)	Width (mm)	Height (mm)	Volume (mm^3)	Volume (m^3)	Mass (g)	Mass (kg)	Density (g/mm^3)	Density (kg/m^3)	Mean Density of Trial
165	650	1		18.95	10.15	3.75	721.284375	7.21284E-07	0.2804	0.0002804	0.0003887	388.7509694	
165	650	2		19.12	9.88	3.52	664.947712	6.64948E-07	0.2762	0.0002762	0.0004157	415.3710059	
165	650	3		18.6	9.55	3.35	595.0605	5.95061E-07	0.2552	0.0002552	0.0004288	428.8639558	
165	650	4		19.85	10.28	3.79	773.37982	7.7338E-07	0.305	0.000305	0.0003943	394.3728452	
165	650	5	Not present										406.8396941
165	550	1		19.31	10.22	3.58	706.506556	7.06507E-07	0.3065	0.0003065	0.0004338	433.8247075	
165	550	2		18.43	9.92	3.59	656.343904	6.56344E-07	0.2808	0.0002808	0.0004278	427.8244961	
165	550	3		18.54	9.83	3.61	657.916002	6.57916E-07	0.2906	0.0002906	0.0004417	441.6977723	
165	550	4		18.43	9.96	3.75	688.3605	6.88361E-07	0.2676	0.0002676	0.0003887	388.7497903	
165	550	5		19.1	10.06	3.85	739.7621	7.39762E-07	0.2889	0.0002889	0.0003905	390.5309558	416.5255345
165	450	1		19.8	10.56	3.65	763.1712	7.63171E-07	0.3026	0.0003026	0.0003965	396.503432	
165	450	2		19.9	10.02	3.67	731.79066	7.31791E-07	0.3401	0.0003401	0.0004647	464.7503973	
165	450	3		19.7	9.84	3.59	695.91432	6.95914E-07	0.3014	0.0003014	0.0004331	433.0992293	
165	450	4		20.08	10.08	3.85	780.6096	7.80961E-07	0.3193	0.0003193	0.0004091	409.1199916	
165	450	5		19.65	10.41	3.85	787.542525	7.87543E-07	0.3344	0.0003344	0.0004246	424.6119916	422.3807881
170	650	1		20.74	10.9	3.53	798.01298	7.98013E-07	0.3712	0.0003712	0.0004651	465.1553412	
170	650	2		19.05	10.5	3.68	736.092	7.36092E-07	0.3392	0.0003392	0.0004608	460.8119637	
170	650	3		19.21	10.22	3.55	696.95801	6.96958E-07	0.3154	0.0003154	0.0004525	452.5380231	
170	650	4		19.45	10.32	3.58	718.59192	7.18592E-07	0.3305	0.0003305	0.0004599	459.9272422	
170	650	5		18.94	10.36	3.6	706.38624	7.06386E-07	0.2975	0.0002975	0.0004211	421.1576941	451.9180529
170	550	1		19.03	10.81	3.45	709.714335	7.09714E-07	0.3468	0.0003468	0.0004886	488.6473091	
170	550	2		19.5	10.23	3.35	668.27475	6.68275E-07	0.3567	0.0003567	0.0005337	533.7624981	
170	550	3		18.84	9.84	3.23	598.795488	5.98795E-07	0.2955	0.0002955	0.0004935	493.4906924	
170	550	4		19.94	10.12	3.53	712.328584	7.12329E-07	0.3422	0.0003422	0.0004804	480.3961773	
170	550	5		20.05	7.52	3.73	562.39448	5.62394E-07	0.1995	0.0001995	0.0003547	354.7332115	470.2059977
170	450	1		18.81	10.28	3.52	680.851136	6.80651E-07	0.336	0.000336	0.0004936	493.6449559	
170	450	2		19.4	10.51	3.72	758.48568	7.58486E-07	0.378	0.000378	0.0004984	498.3614193	
170	450	3		19.12	10.11	3.53	682.360296	6.8236E-07	0.3421	0.0003421	0.0005013	501.3480444	
170	450	4		18.6	10.06	3.53	660.51948	6.60519E-07	0.3176	0.0003176	0.0004808	480.8336614	
170	450	5		18.85	10.26	3.55	686.57355	6.86574E-07	0.3012	0.0003012	0.0004387	438.7002674	482.5776697
175	650	1		19.4	10.45	3.38	685.2274	6.85227E-07	0.3485	0.0003485	0.0005085	508.5902087	
175	650	2		19.84	10.37	3.45	709.80576	7.09806E-07	0.3556	0.0003556	0.0005009	500.9821278	
175	650	3		19.54	10.22	3.61	720.912668	7.20913E-07	0.3421	0.0003421	0.0004753	474.537368	
175	650	4		19.2	10.07	3.43	663.16992	6.6317E-07	0.3098	0.0003098	0.0004671	467.1502592	
175	650	5		19.16	10.18	3.45	672.91836	6.72918E-07	0.3156	0.0003156	0.0004690	469.0019158	484.0523915
175	550	1		20.44	10.84	3.7	819.80752	8.19808E-07	0.4248	0.0004248	0.0005181	518.1704115	
175	550	2		19.93	10.53	3.46	726.125634	7.26126E-07	0.4181	0.0004181	0.0005758	575.7956756	
175	550	3		18.92	10.41	3.47	683.441484	6.83441E-07	0.3814	0.0003814	0.0005585	558.058018	
175	550	4		19.37	10.25	3.56	706.8113	7.06811E-07	0.3238	0.0003238	0.0004581	458.1137851	
175	550	5		18.77	10.28	3.63	700.426828	7.00429E-07	0.3123	0.0003123	0.0004458	445.8697123	511.2015205
175	450	1		9.48	9.91	3.14	294.992952	2.94993E-07	0.1604	0.0001604	0.0005437	543.7418044	
175	450	2		19.63	10.1	3.28	650.30264	6.50303E-07	0.3578	0.0003578	0.0005502	550.2053628	
175	450	3		18.91	10.08	3.34	636.646752	6.36647E-07	0.3612	0.0003612	0.0005673	567.3475893	
175	450	4		18.6	10.11	3.43	644.99778	6.44998E-07	0.3345	0.0003345	0.0005186	518.6064361	
175	450	5		19.68	9.14	3.63	652.946976	6.52947E-07	0.3023	0.0003023	0.0004629	462.9778697	528.5758125

Appendix D

Experimental Analysis of the Effectiveness of Current Modelling Methods for SLS Parameter Determination.

Cameron Mearns*, Dr. Johan Potgieter*, Dr. Steven Dirven*, and Dr. Marie Joo Le Guen†
*School of Engineering and Advanced Technology
Massey University, Auckland, New Zealand 0632
j.potgieter@massey.ac.nz
†Manufacturing and Bioproducts Group, Scion, Rotorua, New Zealand, 3010

***Abstract*—Selective Laser Sintering (SLS) is a powder-bed Additive Manufacturing process that has a large amount of potential for future growth. Historically SLS has been limited to a narrow selection of polymers, although there have been recent advances in working with composite powders, such as Alumide. One of the biggest limitations to developing new materials for sintering is the elevated risk involved in testing to determine their suitability. In recent years, models of powder behaviour have largely focused on thermal characteristics. Models such as the Sintering Window and Energy Melt Ratio demonstrate how methodologies such as Differential Scanning Calorimetry can be used to determine suitability of materials. Testing of two Nylon powders with similar physical and thermal properties reveals limitations in the models when accounting for the colour of material and therefore the absorption of laser energy. Thus, it was identified that existing models require further investigation of laser energy inputs. This paper contributes a framework upon which new models can be tested in order to characterize their effectiveness.**

***Index Terms*—Selective Laser Sintering, material selection, Differential Scanning Calorimetry, Energy Melt Ratio, Sintering Window, powder characterisation**

I. Introduction

Additive Manufacturing (AM) is the name given to a series of processes used to create solids from 3 Dimensional (3D) models [1]. It is also known as Free Form Modelling, and 3D Printing [2]. Initially AM was developed to produce solids using polymers [3], however as new technologies and methods have been developed this has expanded to include metals [4], and ceramics [5] [6]. One such technology is Selective Laser Sintering (SLS), which is a process that involves the progressive processing of thin slices of powder into formed solids by means of a heated chamber, and a focused laser beam [7].

As AM processes, including SLS, increase in popularity one of the areas of growth identified is the diversification of printing materials [8]. Due to the elevated risk of combustion caused by the SLS process many operators are unwilling to test new powders unless it can be shown they can be processed safely by SLS. This means that the number of materials available is currently limited by the understanding of powder properties, and the ability to determine printing parameters from powder specifications [9].

Of importance for SLS printing is the thermal qualities of a material. The elevated temperatures of the SLS process increase the risk of material combustion, which puts greater importance of the precise and controlled application of energy into the powder. This can occur both in the form of convection, from the heated chamber of the printer, and in the form of radiation, from the laser. To be able to predict the energy required, to successfully print a material, it is important to understand the properties of the material.

One of the methods of determining sintering parameters from physical properties is the use of the Sintering Window. The Sintering Window (SW) is a method of defining the temperature range that the SLS machine must operate within, as defined by data collected using Differential Scanning Calorimetry (DSC). The SW is defined as the temperature region between the onset of crystallisation (T_c) and the onset of melting (T_m) for a given polymer [10]. This information provides the operator with a window to set the temperature for the machine, with a minimum chamber temperature above the crystallisation temperature, and a maximum of below the melting point. While this information is valuable this still does not provide the operator with the amount of energy required from the laser to cause the powder to sinter. It is advantageous to have as much energy input from the laser as possible in order to increase tensile strength of parts [11]. However, too much can cause a loss of accuracy in both dimension and feature definition, as well as warpage [12].

This is beneficial when combined with the concept of Energy Melt Ratio (EMR). The EMR is a volumetric metric for quantifying the amount of energy being put in by the system, as compared to the amount of energy required to melt the material. If the ratio is less than 1, then there is insufficient energy to sinter the layer [10]. Through a combination of these methods many variables can be established for SLS printing. Chamber temperatures, which are important for reduction of shrinkage and curling [12], can be established using the SW methods [8]. Once these temperatures have been established the chamber temperature can be used to establish the remain-

ing energy input required from the laser. Using EMR equations this can be converted to parameters such as laser scan speed, and laser power.

To verify this model two different powders were tested utilizing these models. A framework for assessing the effectiveness of the models is demonstrated with reference to identifying new powders, and recommendations on improvements for the models are given.

II. Methodology

Initially a material characterisation is undertaken to identify the similarity of the powders before the Design of Experiment (DoE) is run on an SLS printer. Once the materials have been characterised, a multifactorial experiment is performed to test the effectiveness of the model, and identify any limitations it may have. The first powder tested was dark grey nylon (Sintratec PA12 Black), and the second is a white nylon (Precimid 1170). The Sintratec PA12 Black come with the Sintratec printer, and has known print parameter values (Chamber Temperature of 150°C, Print Bed Temperature of 170°C, and Laser Scan Speed of 550 mm/s) that result in successful parts. The DoE was designed from these values to test the ability of the models to predict sintering in a similar powder, the Precimid 1170.

The characterisation involved conducting a DSC analysis of the powder to identify the crystallisation temperature, and the temperature of the melt. These were used to compare the two powders, and evaluate the likelihood of sintering using the same values by using the SW and EMR. In addition to the two temperatures, several values needed for the EMR can be gathered, from both the DSC software, and from calculations of the data gathered. The DoE will then be run to test the effectiveness of these parameters, and thus the SW and EMR models. A print's effectiveness is evaluated by whether the part printed and was removable from the powder cake, and porosity as visible by Scanning Electron Microscope (SEM).

The physical similarities of the two powders will be compared using examination of unprinted powder with an SEM to determine similarity of particle size, and morphology. Particle size and morphology has been shown to have an effect of the ability to spread a powder for each layer of sintering, and thus the print itself [13].

A. Differential Scanning Calorimetry

To establish the sintering window, a thermal analysis was conducted using a Discovery DSC in accordance with ASTM D3418. Samples of virgin material were subjected to a heating ramp from 20C to 250°C, at 5°C/min, before being cooled again to 20°C at 5°C/min. The data was recorded with the Discovery TRIOS software package, and analyzed with MATLAB 2015. Two experimental runs were run and recorded for each powder.

As stated, the Sintering Window exists between the onset of crystallization, and onset of melting for a material. As per the results of the DSC, a Sintering Window for the Sintratec PA12 Black exists between 151°C and 180.1°C, while the

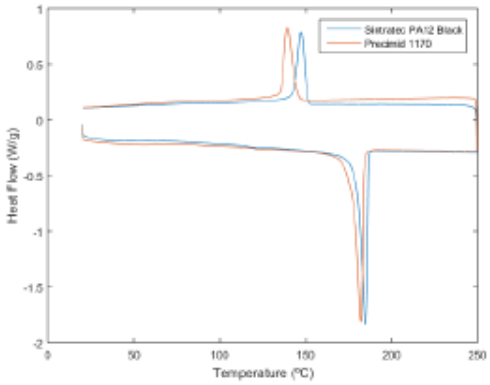

Fig. 1. DSC measurements of Heat Flow against Temperature, showing melting point (the lower spike) and crystallization point (upper spike) of both Sintratec PA12 Black, and Precimid 1170, both virgin powders

TABLE I
Powder properties as determined by Differential Scanning Calorimetry.

Property	Sintratec PA12 Black	Precimid 1170
Onset of melting (°C)	180.1	177.2
Melting point (°C)	184.7	181.9
Onset of crystallization (°C)	151.0	144.5
Crystallization point(°C)	147.4	139.1
Melt Enthalpy (J/g)	105.6	111.0
Crystallisation Enthalpy (J/g)	51.1	51.2
Specific Heat Capacity (J/g°C)	35.166	46.560

Sintering Window for Precimid 1170 exists between 144.5°C and 177.2°C. The similarity in these powders thermally means they should be able to be processed under identical conditions, provided the machine chamber and print bed temperatures are set with both powders in mind, such as between 144.5°C and 180.1°C. As the models are being used to predict sintering of the material, and not the overall process ability of the material, the focus will be on the surface of the powder during the sintering phase. This means that the upper range of the SW will be tested, by varying the Powder Surface temperature.

Furthermore, additional insight can be drawn from the DSC results. The Discovery TRIOS package can derive the melt and crystallization enthalpies from the tests (Table 2). The specific heat capacity for each powder can be derived from the temperature change of the known sample weights in each case. Values for Laser Speed were based on known values used for the Sintratec PA12 Black, given by Sintratec for the printer. A value for Packing Fraction was gathered by measuring tapped

TABLE II
VALUES USED TO CALCULATE ENERGY MELT RATIO VALUES.

Parameter Name	Symbol	Sintratec PA12 Black	Precimid 1170
Specific Heat Capacity (kJ/g.°C)	C_P	35.166	46.560
Print Bed Temperature (°C)	T_b	165, 170, 175	165, 170, 175
Onset of melt temperature (°C)	T_m	180.1	177.2
Enthalpy of melting (J)	H_f	105.6	110.0
Bulk Density (g/mm^3)	Q	0.001	0.00094
Packing Fraction	θ	5.13E-01	5.25E-01
Scan Count	Vc	1	1
Scan Spacing (mm)	Vs	0.05	0.05
Laser Speed (mm/s)	V	450, 550, 650	450, 550, 650
Layer Thickness (mm)	Z	0.1	0.1
Laser Power (W)	P	2.3	2.3

densities. These figures enable the Energy Melt Ratio to be calculated using the figures in Table 2.

B. Scanning Electron Microscope

Samples of fresh powder were prepared for examination by Gold Sputter Coating using a PVD DSR1, operating at 10 mA, with a layer thickness of 20Å. Samples were imaged using a Hitachi TM3030 Plus, and accompanying TM3030 Plus software.

Both powders appear to be very similar physically. While the Precimid 1170 appears to have slightly smaller particle sizes on average, and more spherical morphologies, the differences are minor enough that the physical properties should have no significant effect [14].

C. Sintering Methodology

These tests were conducted with a Sintratec Kit SLS printer, equipped with a 2.3W 445nm diode laser. The print was 5 ANSI D638 Type 5 Dog bones orientated parallel to the X axis. Chamber temperature was set at 150°C, the highest the machine allows.

Based on the values gathered in the characterisation, the two factors for the experiment will be the Print Bed Temperature, and the Laser Speed, each with 3 levels. The Energy Melt Ratio for each trial of both powders is visible below (Table 3).

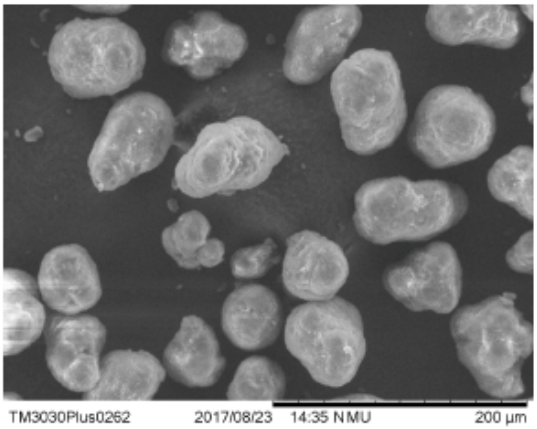

Fig. 2. SEM Images of the Precimid 1170 at 500 times magnification

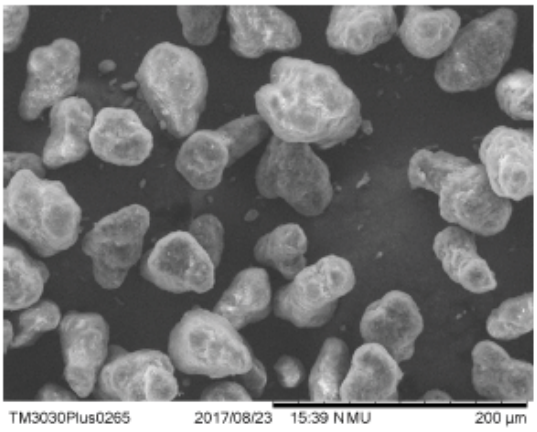

Fig. 3. SEM Images of the Sintratec PA12 Black at 500 times magnification

III. RESULTS

The Sintratec PA12 Black printed successfully for the settings which are recommended for it with this machine. Behaviour for the black powder was roughly consistent with the SW and EMR models. However, none of the trials using white powder resulted in a successful print. While a loose powder cake did form in all prints, there was no evidence of any sintering having occurred, and clumps of powder would disintegrate upon handling. As such, there was no further examination of material from trials using the Precimid 1170 powder.

Several prints of the Sintratec PA12 Black also had irregularities, including prints that crumbled when being removed from the powder cake, lifting of prints from the powder bed during spreading, and melting of excess material to the print.

TABLE III
ENERGY MELT RATIO VALUES FOR DESIGN OF EXPERIMENT TRIALS.

Print Bed Temperature (°C)	Laser Speed (mm/s)	Sintratec PA12 Black EMR	Precimid 1170 EMR
165	650	2.130	2.024
165	550	2.517	2.392
165	450	3.077	2.923
170	650	2.925	3.080
170	550	3.456	3.640
170	450	4.224	4.448
175	650	4.665	6.440
175	550	5.513	7.611
175	450	6.738	9.302

A. Removal from powder cake

Several trials did not result in complete dog bones that could be removed from the powder cake after printing. Of note were those with a Print Bed Temperature of 165°C, the trials with Laser Speeds of 650 mm/s and 550 mm/s had very fragile parts, some of which broke during removal from the powder cake using a soft paintbrush. The trial with a Laser Speed of 450 mm/s suffered from curling during printing, and had parts swept off the print bed by the powder spreading blade. While there were partial dog bones made from the remainder of the part not swept off the bed, there were no complete dog bones produced.

Also of note were all trials with a Print Bed Temperature of 175°C. These trials resulted in printed parts, but excess material was bonded to the print, and was difficult to remove without damaging the part.

B. Scanning Electron Microscope

The advantage of using the SEM to examine cross sectional slices of the samples printed is that the necking between particles is visible. As expected, the necking that occurred between particles grew in frequency as both Print Bed Temperature and EMR increased. The images also show that EMR alone is not a sufficient estimate of the likelihood of printing, as shown with the trials with laser speeds of 650 mm/s. Necking was observed to increase with an increase in EMR, with porosity being reduced as necking increased. This is as expected, however the trial with a Print Bed Temperature of 165°C and Laser Scan Speed of 650 mm/s had an EMR of 2.130, which the model predicts should be sufficient to induce sintering. Prints from this trial were very fragile, and many dog bones did not survive removal from the powder cake, demonstrating that low EMR numbers may not produce parts of adequate quality, despite indicating they will be successful.

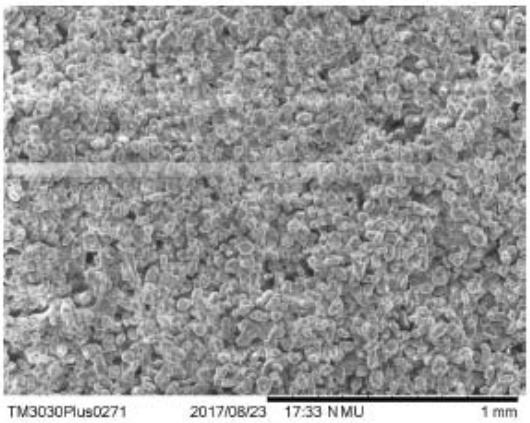

Fig. 4. SEM Image of Sintratec PA12 Black printed at 165°C, with a Laser Scan speed of 650 mm/s at 100 times magnification. The resultant Energy Melt Ratio value is 2.130. Note that there is necking present between particles, however areas of coalescence are rare.

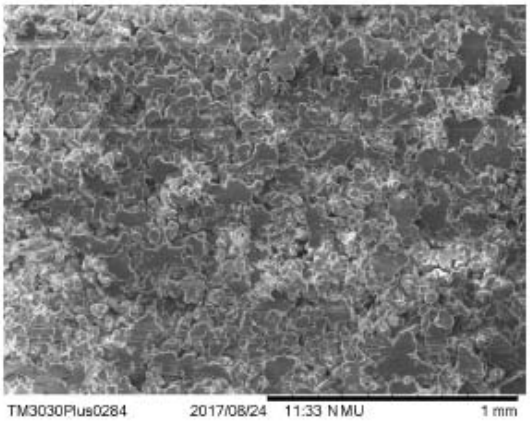

Fig. 5. SEM image of Sintratec PA12 Black, printed at 170C, with a Laser Scan Speed of 650 mm/s at 100 times magnification . The resultant Energy Melt Ratio is 2.925. Areas of coalescence are far more common, but partial necking and areas of porosity are still frequent.

At the other end of the temperature range, the samples printed at 175°C display large areas of particles which have coalesced, with occasional pores visible. The presence of these pores indicates that the sample is unlikely to have undergone a full physical transition to the molten state, however there was clearly enough energy being put into the material to undergo sintering.

IV. DISCUSSION

The Energy Melt Ratio and Sintering Window did predict a set of printing parameters that would result in successful prints. However, the biggest limitation identified in these tests

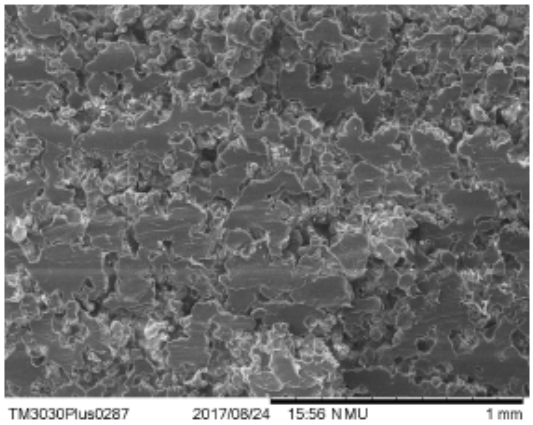

Fig. 6. Figure 5: SEM image of Sintratec PA12 Black, printed at 175°C, with a Laser Scan Speed of 650 mm/s at 100 times magnification. The resultant Energy Melt Ratio is 4.665. Areas of necking and porous areas are less common, and much of the part is coalesced.

was that neither the Sintering Window or Energy Melt Ratio models predicted that the white Precimid 1170 powder would not sinter. This is not a unexpected, as the white powder would reflect a larger amount of laser energy than black powder would. It is surprising that no melting occurred at the higher EMR values, given that it was over 9 times the amount required to cause sintering.

Authors of previous work have neglected to mention their assumptions on laser energy absorption [15]. There has been some work in identifying the reflectance of powders to lasers of varying wavelengths [16], but there has not been further work in implementing these findings into any models. This work does demonstrate that wavelength is a critical factor in the reflectance of laser energy. For the purposes of identifying and testing new materials for SLS further work should be done to improve these models, particularly finding a method of quantifying the proportion of laser energy being absorbed versus being reflected. While it be ideal to have a method of calculating these values for a given material across a range of laser wavelengths it may be feasible to gather these values experimentally.

V. Conclusion

The current methods of identifying printing parameters for Selective Laser Sintering include the use of the Sintering Window, and the Energy Melt Ratio. These two methods utilize data from Differential Scanning Calorimetry and the material data sheet to provide suitable values for both temperature settings, and for laser settings. These values are not exact, and will indicate values for the minimum energy to sinter material.

Experiments on two similar polyamide powders revealed some limitations in the use of the models, particularly for the Energy Melt Ratio. The EMR model does not take into account the reflectance of the laser energy of the powder during sintering, assuming that all light energy emitted from the laser is absorbed. This can lead to partial failures to print, such as porous parts which crumble on removal from the powder cake, or total failure, as seen with the failure to sinter white powder under any of the experimental conditions.

Future work will focus on identifying a revised EMR calculation featuring a factor to better represent the proportion of laser energy absorbed by the power.

References

[1] K. V. Wong and A. Hernandez, "A review of additive manufacturing," *ISRN Mechanical Engineering*, vol. 2012, 2012.

[2] B. Wendel, D. Rietzel, F. Khnlein, R. Feulner, G. Hlder, and E. Schmachtenberg, "Additive processing of polymers," *Macromolecular materials and engineering*, vol. 293, no. 10, pp. 799–809, 2008.

[3] C. W. Hull, "Apparatus for production of three-dimensional objects by stereolithography," Mar. 11 1986, uS Patent 4,575,330.

[4] D. Gu, W. Meiners, K. Wissenbach, and R. Poprawe, "Laser additive manufacturing of metallic components: materials, processes and mechanisms," *International materials reviews*, vol. 57, no. 3, pp. 133–164, 2012.

[5] B. Derby, "Additive manufacture of ceramics components by inkjet printing," *Engineering*, vol. 1, no. 1, pp. 113–123, 2015.

[6] J. Gardan, "Additive manufacturing technologies: State of the art and trends," *International Journal of Production Research*, vol. 54, no. 10, pp. 3118–3132, 2016.

[7] R. Goodridge, C. Tuck, and R. Hague, "Laser sintering of polyamides and other polymers," *Progress in Materials Science*, vol. 57, no. 2, pp. 229–267, 2012.

[8] M. Schmid, A. Amado, and K. Wegener, "Polymer powders for selective laser sintering (sls)," vol. 1664, p. 160009, 2015.

[9] G. Vasquez, C. Majewski, B. Haworth, and N. Hopkinson, "A targeted material selection process for polymers in laser sintering," *Additive Manufacturing*, vol. 1, pp. 127–138, 2014.

[10] M. Vasquez, B. Haworth, and N. Hopkinson, "Methods for quantifying the stable sintering region in laser sintered polyamide12," *Polymer Engineering Science*, vol. 53, no. 6, pp. 1230–1240, 2013.

[11] T. L. Starr, T. J. Gornet, and J. S. Usher, "The effect of process conditions on mechanical properties of laser-sintered nylon," *Rapid Prototyping Journal*, vol. 17, no. 6, pp. 418–423, 2011.

[12] V. Beal, R. Paggi, G. Salmoria, and A. Lago, "Statistical evaluation of laser energy density effect on mechanical properties of polyamide parts manufactured by selective laser sintering," *Journal of Applied Polymer Science*, vol. 113, no. 5, pp. 2910–2919, 2009.

[13] S. Berretta, O. Ghita, and K. E. Evans, "Morphology of polymeric powders in laser sintering (ls): from polyamide to new peek powders," *European Polymer Journal*, vol. 59, pp. 218–229, 2014.

[14] S. Ziegelmeier, P. Christou, F. Wilecke, C. Tuck, R. Goodridge, R. Hague, E. Krampe, and E. Wintermantel, "An experimental study into the effects of bulk and flow behaviour of laser sintering polymer powders on resulting part properties," *Journal of Materials Processing Technology*, vol. 215, pp. 239–250, 2015.

[15] S. Berretta, K. Evans, and O. Ghita, "Predicting processing parameters in high temperature laser sintering (ht-ls) from powder properties," *Materials Design*, vol. 105, pp. 301–314, 2016.

[16] N. K. Tolochko, Y. V. Khlopkov, S. E. Mozzharov, M. B. Ignatiev, T. Laoui, and V. I. Titov, "Absorptance of powder materials suitable for laser sintering," *Rapid Prototyping Journal*, vol. 6, no. 3, pp. 155–161, 2000.